IDŐJÁRÁS

QUARTERLY JOURNAL
OF THE HUNGARIAN METEOROLOGICAL SERVICE

CONTENTS

Ildikó Mesterházy, Róbert Mészáros, Rita Pongrácz, Péter Bodor, and *Márta Ladányi:* The analysis of climatic indicators using different growing season calculation methods – an application to grapevine grown in Hungary 217

Hristo Hristov and *Andrey Bogatchev:* An assessment of daily extreme temperature forecasts – stations average view 237

Danijela Vukoičić, Saša Milosavljević, Ivana Penjišević, Nikola Bačević, Milena Nikolić, Radomir Ivanović, and *Bojana Jandžiković:* Spatial analysis of air temperature and its impact on the sustainable development of mountain tourism in Central and Western Serbia..... 259

Károly Tar and *István Lázár:* Statistical structure of day by day alteration of daily average wind speeds 285

Hristo Chervenkov, Valentin Kazandjiev, and *Veska Gorgieva:* Application of the crop model WOFOST in grid using meteorological input data from reanalysis and objective analysis 305

Biljana Basarin, Tin Lukić, Dajana Bjelajac, Tanja Micić, Goran Stojićević, Igor Stamenković, Jasmina Đorđević, Tijana Đorđević, and *Andreas Matzarakis:* Bioclimatic and climatic tourism conditions at Zlatibor Mountain (Western Serbia) 321

Zoltán Kapros: A dynamic data-driven forecast prediction methodology for photovoltaic power systems..... 345

VOL. 122 ∗ NO. 3 ∗ JULY – SEPTEMBER 2018

IDŐJÁRÁS

Quarterly Journal of the Hungarian Meteorological Service

Editorial Office: Kitaibel P.u. 1, H-1024 Budapest, Hungary
P.O. Box 38, H-1525 Budapest, Hungary
E-mail: journal.idojaras@met.hu
Fax: (36-1) 346-4669

Indexed and abstracted in Science Citation Index Expanded™ and Journal Citation Reports/Science Edition
Covered in the abstract and citation database SCOPUS®
Included in EBSCO's databases

Subscription by mail:
IDŐJÁRÁS, P.O. Box 38, H-1525 Budapest, Hungary
E-mail: journal.idojaras@met.hu

DOI:10.28974/idojaras.2018.3.1

IDŐJÁRÁS

Quarterly Journal of the Hungarian Meteorological Service
Vol. 122, No. 3, July – September, 2018, pp. 217–235

The analysis of climatic indicators using different growing season calculation methods – an application to grapevine grown in Hungary

Ildikó Mesterházy[1]*, **Róbert Mészáros**[2], **Rita Pongrácz**[2,3], **Péter Bodor**[4], and **Márta Ladányi**[1]

[1]*Department of Biometrics and Agricultural Informatics, Szent István University, Villányi út 29-43., H-1118 Budapest, Hungary*

[2]*Department of Meteorology, Eötvös Loránd University, Pázmány P. sétány 1/A, H-1117 Budapest, Hungary*

[3]*Excellence Center, Faculty of Science, Eötvös Loránd University, Brunszvik u. 2., H-2462 Martonvásár, Hungary*

[4]*Department of Viticulture, Szent István University, Villányi út 29-43., H-1118 Budapest, Hungary*

**Corresponding author E-mail: Mesterhazy.Ildiko@kertk.szie.hu*

(Manuscript received in final form August 8, 2017)

Abstract—The precise knowledge of the beginning and the end of the growing season is necessary for the calculation of climatic indicators with evident effect on grapevine production. The aim of this study is to develop suitable methods on the basis of thermal conditions that can be used for calculation of the beginning, the end, and the length of the growing season for every single year. The two most accurate methods ('5mid' and 'int') are selected using the root-mean-square error compared to the reference growing season values based on averaging the daily mean temperature for several decades. In case of the '5mid' method, the beginning (or the end) is the middle day of the first (or last) 5-day period with temperature not less than 10 °C. In case of the 'int' method, the beginning (or the end) of the growing season is the day after March 15 (or September 15), when the smoothed series of daily temperature using the monthly average temperatures of March and April (or September and October) exceeds 10 °C (or falls below 10 °C). As a next step, several climatic indicators (e.g., Huglin index and hydrothermal coefficient) are calculated for Hungary for three time periods (1961−1990, 2021−2050, and 2071−2100*) using the '5mid' and 'int' methods. For this purpose, the bias-corrected daily mean, minimum, and maximum temperature and daily precipitation outputs of three different regional climate models (RegCM, ALADIN, and PRECIS) are used. Extreme temperature and precipitation

* In the case of the PRECIS model, due to its shorter simulation time range, we calculated the indicators for the period 2069−2098.

indices are also evaluated as they determine the risk of grapevine production. The spatial distributions of the indicators are presented on maps. We compare the indicators for the past and for the future using one-way completely randomized robust ANOVA (analysis of variance).

Results suggest that changes of temperature conditions in the 21st century will favor the production of red grapevine and late-ripening cultivars. Furthermore, drought seasons will be longer and extreme high summer temperatures will become more frequent, which are clearly considered as high risk factors in grapevine production. Besides the negative effects, the risk of winter frost damage is expected to decrease, which is evidently a favorable change in terms of grapevine production.

Key-words: Vitis vinifera, growing season calculation method, climatic indicator, ANOVA, Bonferroni's correction, RegCM, ALADIN, PRECIS

1. Introduction

Grapevine production in Hungary is enabled by favorable climatic conditions. Certain climatic events, however, can result in risk factors to the current production practices including the selection of specific grapevine cultivars. In this study, we apply indicators related to risk factors, and analyze their temporal and spatial changes.

Wine regions can be characterized with climate indicators that have evident effect on grapevine production based on temperature and precipitation (*Hlaszny*, 2012; *Ramos et al.*, 2008; *Santos et al.*, 2012). The comparison of vine growing regions worldwide can be done by analyzing the climate indicators based on observed meteorological data (*Bois et al.,* 2012; *Jones et al.,* 2009). These indicators can also be calculated using climate model simulation outputs for the 21st century (*Hlaszny*, 2012; *Moriondo et al.*, 2013; *Neumann* and *Matzarakis*, 2011; *Szenteleki et al.*, 2012). These results predict the changes in risk factors (e.g., long dry period and extreme heat), thus they can help farmers make long term decisions about the selection of favorable grapevine cultivars. Usually, a fixed growing season time interval is used in the calculation of the indicators, although the beginning and the end of the growing season depend on the actual meteorological conditions of each year. Since the variability of meteorological parameters (especially temperature) is expected to increase during the 21st century (*IPCC*, 2013), a modified growing season calculation method is reasonable to be used. It is desirable to find methods, which can handle the increasing frequency of extreme meteorological events.

Instead of the commonly used fixed time interval definition (i.e., April 1 – September 30), we calculate the length of the growing season on the basis of actual thermal conditions with the ultimate aim to develop suitable methods for determining the beginning, the end, and the length of the growing season by taking into account the different meteorological conditions throughout every single year.

The methods introduced in this study can handle the extreme temperature events of each year as they follow the temperature conditions on a day-by-day basis.

In our previous study (*Mesterházy et al.*, 2014), we analyzed the changes of climatic indicators having evident effect on grapevine production with a modified growing season calculation method applied to Hungary for the 21st century.

In this paper, we complete the earlier conclusions with new results obtained through model refinement. In this study, a total of ten accurate definitions of the beginning, the end, and the length of the growing season are introduced, compared, and analyzed. We use a method (the so-called 'reference' method), that is based on averaging the daily mean temperatures of a 30-year-long period, which provides roughly accurate overall estimations of the beginning, the end, and the length of the growing seasons for a long time interval. In order to find the most accurate method (or methods), we define nine additional growing season calculation methods and compare their accuracies to the 'reference' method.

After having chosen the two most accurate growing season calculation methods, we use them to create several climatic indicators (e.g., the Huglin index and hydrothermal coefficient) based on temperature and precipitation values. We analyze the spatial and temporal distribution of these climatic indicators and present our results on maps created by ArcGIS. Our study focuses on Hungary and uses bias-corrected outputs (daily minimum, maximum, and mean temperature, as well as daily precipitation) of three different regional climate models (RegCM, ALADIN, PRECIS).

2. Applied methods

2.1. Applied regional climate models and time periods

We use the daily mean, minimum, and maximum temperature, and daily precipitation outputs of the following model simulations carried out in the framework of the European ENSEMBLES project (*van der Linden* and *Mitchell*, 2009): RegCM (*Giorgi et al*., 1993) and ALADIN (*Déqué et al*., 1998) regional climate models and PRECIS regional climate model developed by the UK Met Office Hadley Centre for Climate Prediction and Research (*Wilson et al*., 2007) and applied specifically to the Carpathian Basin (*Pieczka*, 2012). The raw regional climate model (RCM) outputs generally overestimate the temperature in the summer and the precipitation throughout the entire year (*Pongrácz et al.*, 2011; *Pieczka et al.*, 2011). Therefore, they were corrected using a percentile-based bias correction technique (*Formayer* and *Haas*, 2010) by the correction of the simulated daily outputs on the basis of the monthly distributions of observed meteorological data. Observations are available from the gridded E-OBS database (*Haylock et al.*, 2008). The RCM simulations use the A1B emission scenario (*Nakicenovic* and *Swart*, 2000) for the 21st century. All RCMs applied a

horizontal resolution of 25 km in the Carpathian Basin between latitudes 44°−50°N and longitudes 14°–26°E.

We used 228 grid points (g=1, …, 228*)* covering Hungary, and time periods R: 1961−1990 (as the reference period), F_1: 2021−2050, and F_2: 2071−2100*.

2.2. Methods used for calculating the length of the growing season

We aim to define the beginning, the end, and the length of the growing season for year k taken from time periods R, F_1, F_2 or $F_{2,P}$ and for all grid points g of Hungary using nine different methods.

First, we use the moving average method to define the 'reference' method for the calculation of the beginning, the end, and the length of the growing season (*Ambrózy et al.,* 2002). In this method, an array of average daily temperatures is produced – for every day i of the year – by calculating the mean temperatures of the day $(T^g(i,k))$ over a 30-year period:

$$T^g(i) = \underset{k}{Aver}(T^g(i,k)) \ (k \in \mathrm{R} \text{ or } \mathrm{F}_1 \text{ or } \mathrm{F}_2 \text{ or } \mathrm{F}_{2,\mathrm{P}}), \tag{1}$$

and then, the array is smoothed by averaging the array values in 5-day-long time windows.

The beginning and the end of the growing season are defined as the first and last days when the smoothed average temperatures are not less than 10 °C, which is considered as the biological base temperature of grapevines (*Amerine and Winkler,* 1944; *Winkler et al.,* 1974; *Kozma*, 2002). We use this method in calculating datasets for the beginning ($G^g_{B;ref}$), the end ($G^g_{E;ref}$), and the length ($G^g_{L;ref}$) of the growing season for the 30-year time periods R, F_1, F_2, $F_{2,P}$, and for every grid point g in Hungary.

As a next step, we introduce the following methods for calculating the beginning of the growing season:

- **Methods '3' and '5'** choose the first day of the first 3-day ($G^g_{B;3}(k)$) or 5-day ($G^g_{B;5}(k)$) long period that continuously has daily mean temperatures not less than 10 °C;
- **Methods '3mid' and '5mid'** choose the middle day of the first 3-day ($G^g_{B;3mid}(k)$) or 5-day ($G^g_{B;5mid}(k)$ long period that continuously has daily mean temperatures not less than 10 °C;
- **Methods 'MA3' and 'MA5'** choose the first day of the first 3-day ($G^g_{B;MA3}(k)$) or 5-day ($G^g_{B;MA5}(k)$) long period that continuously has daily mean

* In the case of the PRECIS model, due to its shorter simulation time range, we calculated the indicators for the period $F_{2,P}$: 2069−2098.

temperatures not less than 10 °C in the annual temperature dataset smoothed by the 5-day-long moving average (MA) method;

- **Methods 'MA3mid' and 'MA5mid'** choose the middle day of the first 3-day ($G^{g}_{B;MA3mid}(k)$) or 5-day ($G^{g}_{B;MA5mid}(k)$) long period that continuously has daily mean temperatures not less than 10 °C in the annual temperature dataset smoothed by the 5-day-long moving average (MA) method;
- **Method 'int'** uses interpolation method (*Csepregi,* 1997; *Hlaszny,* 2012), where we choose the first day ($G^{g}_{B;int}(k)$) after March 15, when the series of daily temperatures smoothed using the monthly average temperatures of March and April, exceeds 10 °C. The unit temperature change used in this interpolation is given as:

$$d^{g}_{B}(k) = \frac{T^{g}_{April}(k) - T^{g}_{March}(k)}{31}, \tag{2}$$

where $T^{g}_{March}(k)$ and $T^{g}_{April}(k)$ are the monthly mean temperatures in March and April, respectively, for year *k*, and measured in °C units. The first day of the growing season is given as:

$$G^{g}_{B;int}(k) = \left[\text{March } 15^{\text{th}}\right] + n^{g}_{B}(k), \tag{3}$$

where $n^{g}_{B}(k)$ is the lowest natural number above $\frac{10°C - T^{g}_{March}(k)}{d^{g}_{B}(k)}$.

We calculate the end of the growing season ($G^{g}_{E;M}(k)$; where M='3', '5', '3mid', '5mid', 'MA3', 'MA5', 'MA3mid', 'MA5mid') with the same methods, substituting the *first* day with the *last* day of the given periods. For the interpolation method denoted with index 'int', we substitute $d^{g}_{B}(k)$ and $G^{g}_{B;int}(k)$ with $d^{g}_{E}(k)$ and $G^{g}_{E;int}(k)$ defined as:

$$d^{g}_{E}(k) = \frac{T^{g}_{September}(k) - T^{g}_{October}(k)}{30}, \tag{4}$$

$$G^{g}_{E;int}(k) = \left[\text{September } 15^{\text{th}}\right] + \left(n^{g}_{E}(k) - 1\right), \tag{5}$$

where $T^g_{September}(k)$ and $T^g_{October}(k)$ are the monthly mean temperatures in September and October, respectively, for year k, and measured in °C units; and $n^g_E(k)$ is the lowest natural number above $\frac{T^g_{September}(k) - 10°C}{d^g_E(k)}$. This way, $G^g_{E;\mathrm{int}}(k)$ is defined as the first day after September 15 when the daily temperature, smoothed using the monthly average temperatures of September and October, falls below 10 °C.

We calculate the length of the growing season ($G^g_{L,M}(k)$; where M='3', '5', '3mid', '5mid', '7mid', 'MA3', 'MA5', 'MA3mid', 'MA5mid', 'int') with the following formula:

$$G^g_{L,M}(k) = G^g_{E.M}(k) - G^g_{B.M}(k) + 1. \tag{6}$$

For each grid point *g*, we calculate the average length of the growing season for year *k* of the periods R, F_1, F_2, $F_{2,P}$ as:

$$G^g_{L;M} = \underset{k}{Aver}\left(G^g_{L;M}(k)\right). \tag{7}$$

After taking the average values of $G^g_{B;M}$, $G^g_{E;M}$, $G^g_{L;M}$ over all grid points *g*, the results are denoted by $G_{B;M}, G_{E;M}, G_{L;M}$.

We use the average root-mean-square error (RMSE, [day]) taken over all grid points *g* of Hungary to compare the 'reference' growing season values ($G^g_{L;ref}$, $G^g_{B;ref}$ and $G^g_{E;ref}$, respectively), with the other nine growing season datasets (*Table 1*). Percentages of cases are calculated when RMSE values are below a certain value considering the results of all the three regional climate models (RegCM, ALADIN, and PRECIS) and all the three time intervals (1961−1990, 2021−2050, and 2071−2100*) involved in the survey. For the length of the growing season, methods $G^g_{L;5mid}$ and $G^g_{L;\mathrm{int}}$ result in the best estimations, i.e., RMSE values are below 9 days in 89% of the cases.

For the beginning of the growing season, methods $G^g_{B;5mid}$ and $G^g_{B;\mathrm{int}}$, whereas for the end of the growing season, methods $G^g_{E;5}$, $G^g_{E;5mid}$, and $G^g_{E;MA5mid}$ are the best estimators of $G^g_{B;ref}$ and $G^g_{E;ref}$, respectively. These methods give RMSE values below 5 days at least 67% of the cases (see *Table 1*).

For the calculation of the climatic indicators and extreme temperature and precipitation indices (which apply the beginning and/or the end of the growing season), we use the two most accurate methods: '5mid' and 'int'.

* 2069−2098 for the PRECIS model

Table 1. The percentages of the cases when the average RMSE values [day] taken over all grid points of Hungary are below 9 days for the length and are below 5 days for the beginning and the end of the growing season (GS). Percentages are calculated considering the results of all the three regional climate models (RegCM, ALADIN, and PRECIS) and all the three time intervals (1961−1990, 2021−2050, and 2071−2100*) involved in the survey. (For the notations and definitions of growing season calculation methods see Section 2.2.) The best estimations are indicated by bold characters

	Growing season (GS) calculation methods								
	'3'	**'5'**	**'3mid'**	**'5mid'**	**'MA3'**	**'MA5'**	**'MA3mid'**	**MA5mid'**	**'int'**
Length of GS RMSE< 9 days	0%	56%	0%	**89%**	0%	0%	0%	44%	**89%**
Beginning of GS RMSE< 5 days	0%	33%	0%	**67%**	0%	11%	0%	33%	**100%**
End of GS RMSE< 5 days	0%	**78%**	0%	**100%**	0%	22%	11%	**67%**	33%

2.3. The applied indicators and the extreme indices of temperature and precipitation

The following indicators and extreme indices are calculated for a given year *k* for all grid points *g,* and analyzed in this paper:

- $AWI_{GS}^{g}(k)$ (adjusted Winkler index in °C): sum of the residual above 10 °C of daily mean temperatures during the growing season (i.e., the time interval $GS^{g}(k)=\left[G_{B}^{g}(k);G_{E}^{g}(k)\right]$).
- $AHI_{GS}^{g}(k)$ (adjusted Huglin's heliothermal index in °C):

$$AHI_{GS}^{g}(k)=d\sum_{i=G_{B,M}^{g}(k)}^{G_{E,M}^{g}(k)}\frac{\left[\left(T^{g}(k,i)-10\right)+\left(T_{\max}^{g}(k,i)-10\right)\right]}{2}, \tag{8}$$

where *d* is the latitude coefficient (1.05 in Hungary), $T^{g}(k,i)$ is the daily mean temperature (in °C), and $T_{\max}^{g}(k,i)$ is the daily maximum temperature (in °C) on day *i* in year *k*.

- $AHTC_{GS}^{g}(k)$ (adjusted hydrothermal coefficient):

* 2069−2098 for the PRECIS model

$$AHTC^{g}_{GS}(k) = \frac{10 \cdot P^{g}_{GS(k)}}{TempSum^{g}_{GS(k)}(k)}, \tag{9}$$

where $P^{g}_{GS}(k)$ is the sum of precipitation (in mm) during $GS^{g}(k)$, $TempSum^{g}_{GS}(k)$ is the sum of daily mean temperatures (in °C) during $GS^{g}(k)$ when the temperature is not less than 10 °C. The optimal $AHTC^{g}_{GS}(k)$ value for growing grapevines is around 1.0, while the minimum value is 0.3–0.5 and the maximum value is 1.5–2.5. Grapevine growth stops below $AHTC^{g}_{GS}$=0.5, grapevine production in such a case is only possible if the humidity is high or if irrigation is applied.

- $P^{g}_{GS}(k)$ (in mm): the sum of precipitation during $GS^{g}(k)$.
- $LRP^{g}_{A5\_GS}(k)$ (in days): the longest unbroken (rainy) period of precipitation in year *k* with above 5 mm per day during $GS^{g}(k)$.
- $LDP^{g}_{B1\_GS}(k)$ (in days): the longest unbroken (dry) period of precipitation in year *k* with below 1 mm per day during $GS^{g}(k)$.
- $YN^{g}_{A35\_GS}$: the number of years with at least one day when the daily maximum temperature is above 35 °C during GS^{g}.
- $DN^{g}_{B1m\_GSf}(k)$: the number of days when the daily minimum temperature is below −1 °C during the first part of $GS^{g}(k)$ (from $G^{g}_{B}(k)$ to the end of June).
- $DN^{g}_{B17m\_D}(k)$ and $DN^{g}_{B21m\_D}(k)$: the number of days when the daily minimum temperature is below −17 °C or −21 °C during dormancy (i.e., the days between $G^{g}_{E}(k)$ and $G^{g}_{B}(k+1)$).

(For more details about these indicators, see *Seljaninov*, 1928; *Amerine* and *Winkler*, 1944; *Davitaja*, 1959; *Winkler et al.,* 1974; *Huglin,* 1978; *Oláh*, 1979; *Dunkel* and *Kozma,* 1981; *Riou*, 1994; *Kozma*, 2002; *Szenteleki et al.*, 2012.)

For each grid point *g*, the averages of $AWI^{g}_{GS}(k)$, $AHI^{g}_{GS}(k)$, $AHTC^{g}_{GS}(k)$, $P^{g}_{GS}(k)$ $LRP^{g}_{A5\_GS}(k)$, and $LDP^{g}_{B1\_GS}(k)$ are calculated, then the sums of $DN^{g}_{B1m\_GSf}(k)$, $DN^{g}_{B17m\_D}(k)$, and $DN^{g}_{B21m\_D}(k)$ over all *k* are calculated. We denote these averages and sums with AWI^{g}_{GS}, AHI^{g}_{GS}, $AHTC^{g}_{GS}$, P^{g}_{GS}, etc.

2.4. Statistical analysis

In the case of all indicators and extreme indices defined in Section 2.3., we compare the 30-year-long time periods R, F_1, F_2, and $F_{2,P}$ at all grid points, using the one-way completely randomized robust ANOVA (analysis of variance) at all the grid points. When having significant results, we continue the analysis with pairwise comparisons using Bonferroni's Type I error correction (at the $p < 0.05$ level).

The assumption of normality of residuals was accepted, except in a few number of grid points, in all examined time periods and all growing season calculation methods. The homogeneity of variances is violated in a great number of grid points, which can be explained by the increasing variability of temperature data in the 21st century.

3. Results

It is important to note that RCMs assume plain surfaces despite of the built-in topography. This means that our results do not include topography-related variations in heat, sunlight exposure, and microclimatic influences, all having evident effect on grapevine production.

3.1. Beginning, end, and length of growing season ($G^g_{B;M}$, $G^g_{E;M}$, and $G^g_{L;M}$; where M='5mid', 'int')

The average length ($G_{L;5mid}$) of growing seasons $G^g_{L;5mid}$ taken over all grid points *g* and for the reference period (R: 1961–1990) is 192 days (April 10 – October 18). Longer growing seasons (meaning earlier $G^g_{B;5mid}$ and later $G^g_{E;5mid}$) occur typically in plain regions, while shorter growing seasons occur in hilly terrains. Such regional differences are projected for the 21st century (see *Figs. 1* and *2*). According to all three RCMs, the average growing season length ($G_{L;5mid}$) is 214 days (March 30 – October 29) in the time period 2021–2050. RegCM and ALADIN simulation data show 229-day-long growing season (March 21 – November 4) up to the end of the 21st century. The PRECIS model simulation predicts that a 238-day-long growing season (March 20 – November 12) is also possible.

The calculation with the 'int' method shows similar spatial and temporal distributions. The length of the growing season has an average of 182–190 days (April 12 – October 15) in the reference period. RegCM and ALADIN simulations show a 201-day average growing season length (April 4 – October 21), while the PRECIS model estimates it to be 214 days long (March 31 – October 30) in the time period 2021–2050. For the end of the 21st century, RegCM and ALADIN outputs show an average of 210-day-long growing season (March 27 – October 22), and PRECIS simulation results with an up to 226-day-long growing season (March 25 – November 5).

These results suggest that because of the changing thermal conditions, the growing season is expected to be significantly longer in the middle and end of the 21st century, compared to what is calculated for (and observed at) the end of the 20th century. The beginning (the end) of the growing season tends to occur usually earlier (later) in the future, compared to what was experienced in the past.

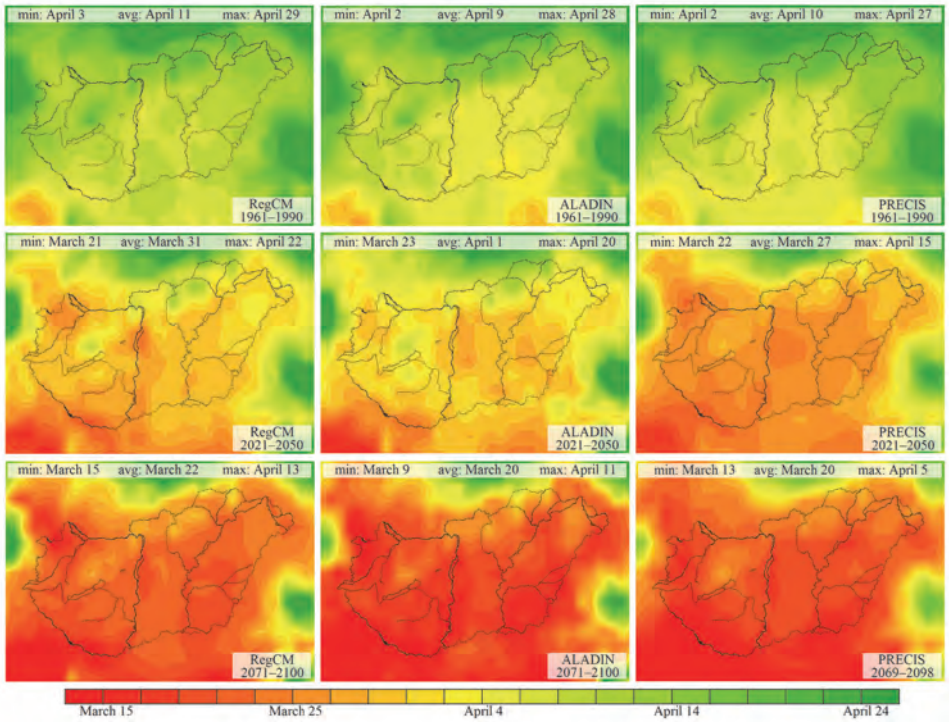

Fig. 1. The beginning of the growing season ($G^{g}_{B;5mid}$) in Hungary calculated with the '5mid' method. Rows represent different time slices, i.e., 1961−1990 (upper row), 2021−2050 (middle row), and 2071−2100* (lower row). Columns correspond to RegCM (left), ALADIN (middle), and PRECIS (right) simulations.

* 2069−2098 for the PRECIS model

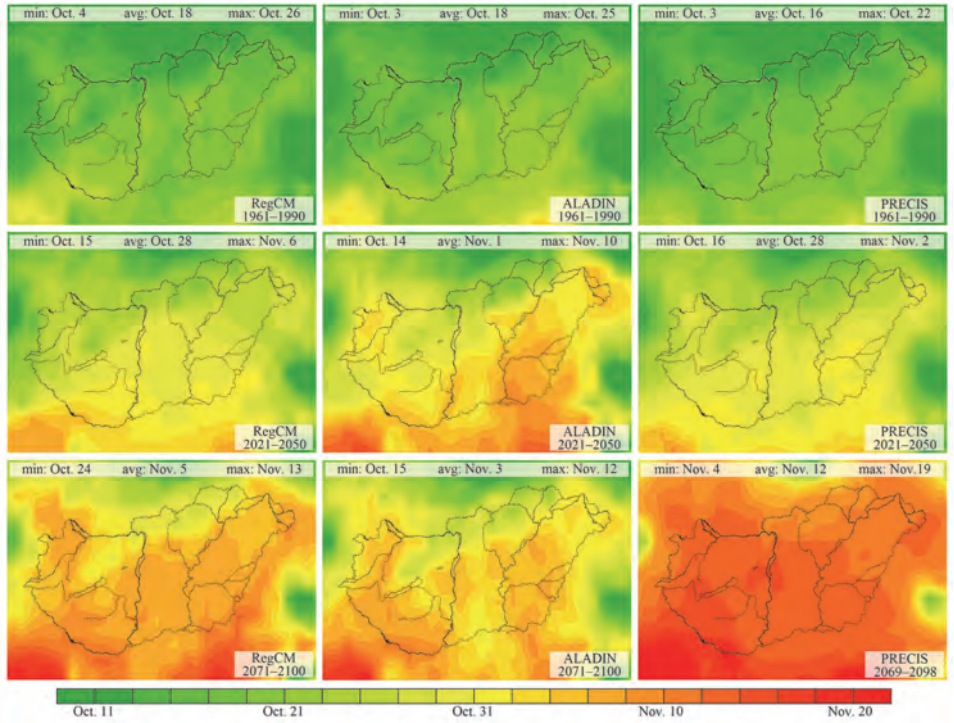

Fig. 2. The end of the growing season ($G^{g}_{E;5mid}$) in Hungary calculated with the '5mid' method. Rows represent different time slices, i.e., 1961−1990 (upper row), 2021−2050 (middle row), and 2071−2100* (lower row). Columns correspond to RegCM (left), ALADIN (middle), and PRECIS (right) simulations.

3.2. Adjusted Winkler index and adjusted Huglin's heliothermal index ($^{AWI^{g}_{GS}}$ and $^{AHI^{g}_{GS}}$)

The average length of the growing season calculated with the '5mid' method is usually longer than the one calculated with the 'int' method, therefore, the heat sum indicator values (AWI^{g}_{GS} and AHI^{g}_{GS}) are evidently higher, with an average of 0–150 °C.

According to the RCMs, values of AWI^{g}_{GS} calculated for the reference period with the '5mid' and 'int' methods are in the range of 833–1540 °C and 813–1501 °C, respectively. Higher values are usually in the plain regions, and lower values can be found in hilly terrains. Values of AWI^{g}_{GS} estimated for the middle of the 21st century can be as high as 1700–2000 °C in the southern part of the Great Hungarian Plain. The

* 2069−2098 for the PRECIS model

highest AWI_{GS}^{g} values at the end of the 21st century ('5mid': 1806–2657 °C; 'int': 1782–2607 °C) are projected by the PRECIS outputs, while the lowest values ('5mid': 1369–2248 °C; 'int': 1338–2161 °C) are predicted by the RegCM simulation.

Values of AHI_{GS}^{g} calculated for the reference period are 1363–2204 °C, and 1305–2161 °C calculated with the '5mid' and 'int' (see *Fig. 3*) methods, respectively. Similarly to AWI_{GS}^{g}, higher values appear in the southern part of the Great Hungarian Plain. At the end of the 21st century, AHI_{GS}^{g} values are projected to exceed even 3000 °C in this region. RegCM simulation shows the smallest increase (600–800 °C increase) and PRECIS outputs show the largest increase (1000–1300 °C increase) by the end of the 21st century.

Values of $AWI_{GS}^{g}(k)$ and $AHI_{GS}^{g}(k)$ calculated with both methods ('5mid' and 'int') project significant ($p < 0.05$) increases from all examined time periods to later time period(s).

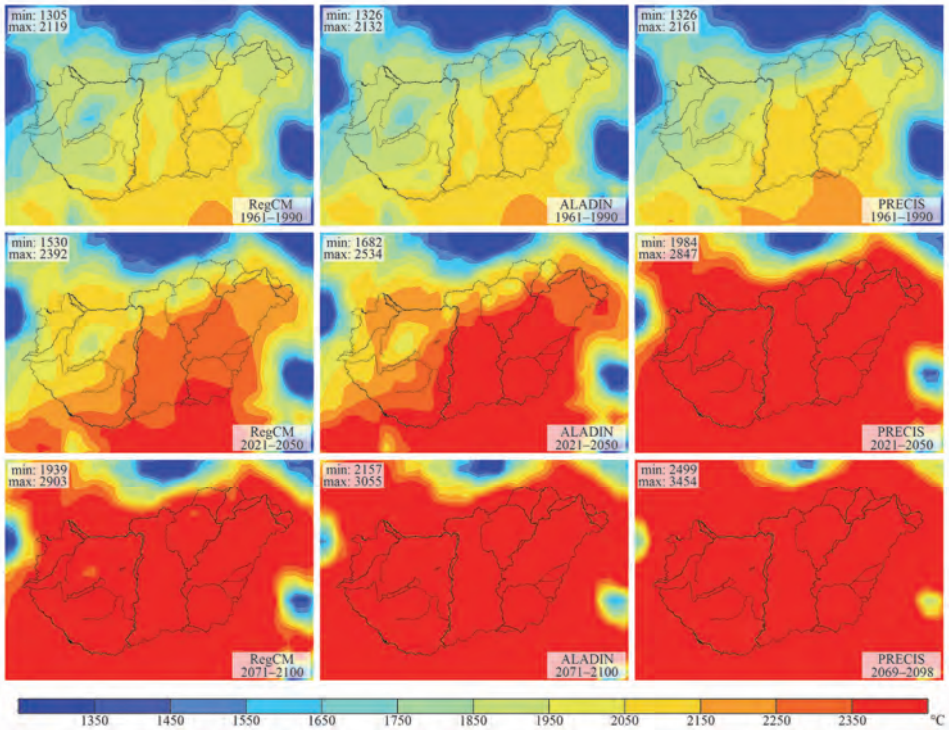

Fig. 3. Values of adjusted Huglin's heliothermal index (AHI_{GS}^{g}, °C) in Hungary calculated with the 'int' method. Rows represent different time slices, i.e., 1961−1990 (upper row), 2021−2050 (middle row), and 2071−2100* (lower row). Columns correspond to RegCM (left), ALADIN (middle), and PRECIS (right) simulations.

* 2069−2098 for the PRECIS model

3.3. *Adjusted hydrothermal coefficient ($AHTC_{GS}^{g}$)*

Values of $AHTC_{GS}^{g}$ are in the range of 0.82–1.69 in Hungary in the reference period (see *Fig. 4*). High temperature with low precipitation ($AHTC_{GS}^{g}$ values below 1.0) is usual in the plain regions, while $AHTC_{GS}^{g}$ values above 1.0 appear in the hilly terrains. The RCM simulations predict decreasing $AHTC_{GS}^{g}$ values ($AHTC_{GS}^{g}$: 0.54−1.44) during the 21st century. This prediction corresponds to a decrease of the dominance of temperature over precipitation, however, $AHTC_{GS}^{g}$ values are not expected to fall into the critical interval (i.e., below 0.5).

$AHTC_{GS}^{g}(k)$ values predicted by PRECIS outputs for the end of the 21st century differ significantly ($p < 0.05$) from the estimated values of the reference period (see *Fig. 5*).

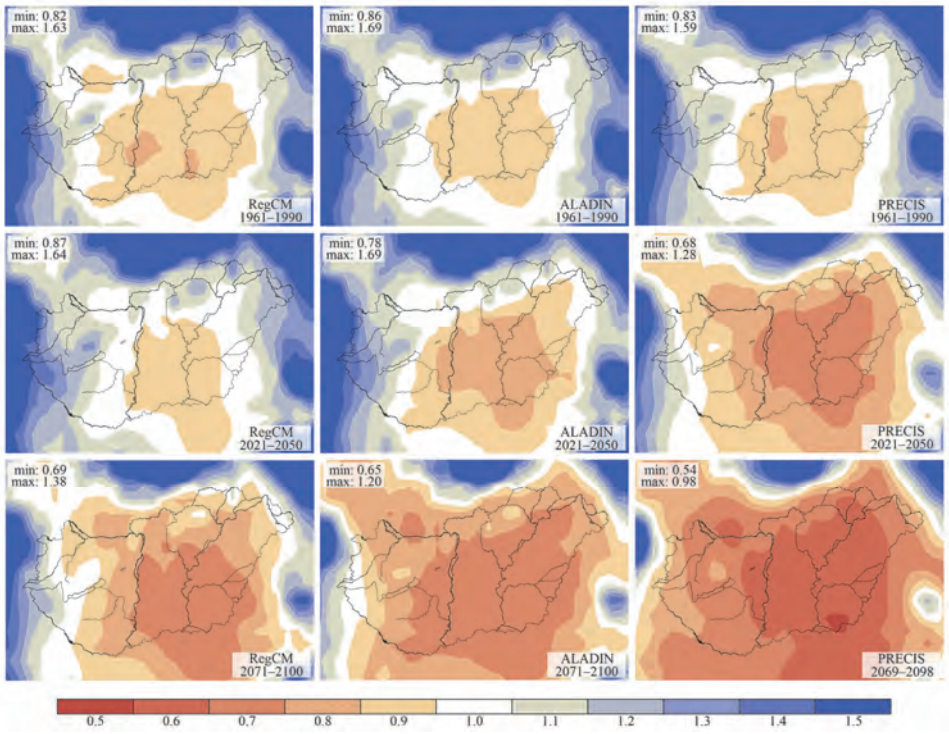

Fig. 4. Values of the adjusted hydrothermal coefficient ($AHTC_{GS}^{g}$) in Hungary calculated with the 'int' method. Rows represent different time slices, i.e., 1961−1990 (upper row), 2021−2050 (middle row), and 2071−2100* (lower row). Columns correspond to RegCM (left), ALADIN (middle), and PRECIS (right) simulations.

* 2069−2098 for the PRECIS model

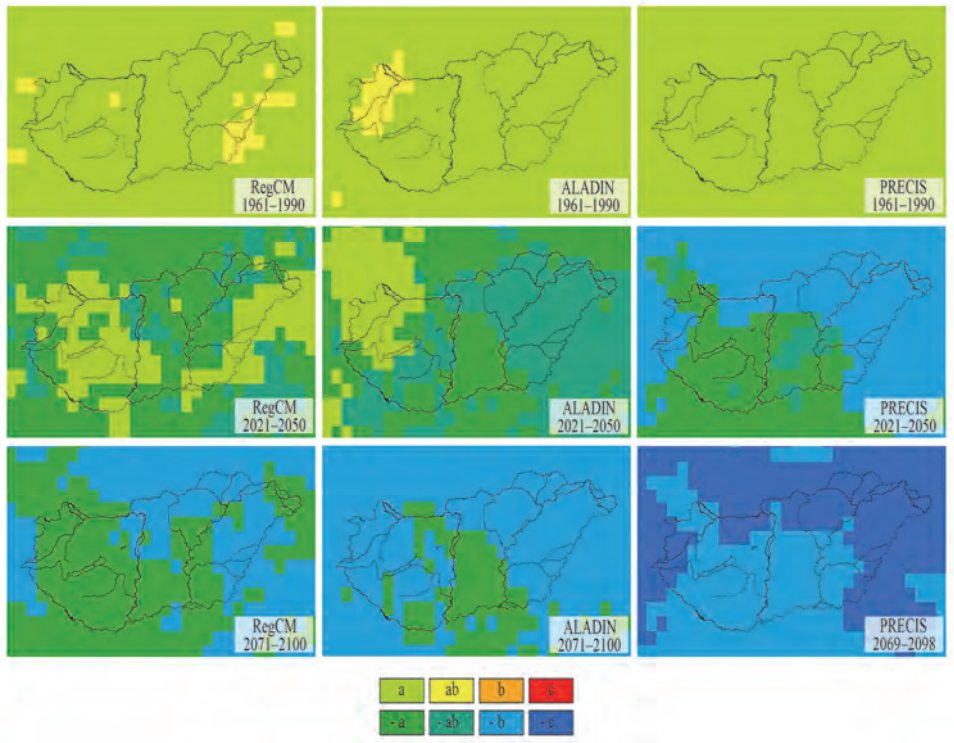

Fig. 5. Comparison of the adjusted hydrothermal coefficient ($AHTC_{GS}^{g}$) for Hungary calculated with the 'int' method. Rows represent different time slices, i.e., 1961−1990 (upper row), 2021−2050 (middle row), and 2071−2100* (lower row). Columns correspond to RegCM (left), ALADIN (middle), and PRECIS (right) simulations. The different letters (or colors) show significantly different values with Bonferroni's correction at the $p < 0.05$ level.

3.4. Sum of precipitation (P_{GS}^{g})

According to all three RCMs, values are in the range of 270−445 mm in Hungary in the time period 1961−1990. This amount is sufficient for the vital activities of grapevine (*Kozma*, 2002). $P_{GS}^{g}(k)$ values do not show significant ($p > 0.05$) change for the 21st century. Results calculated from the RegCM outputs with the '5mid' method show significant ($p < 0.05$) increase of $P_{GS}^{g}(k)$ in the Transdanubian region and in northeastern Hungary during the 21st century.

* 2069−2098 for the PRECIS model

3.5. *The length of the annual longest rainy and dry unbroken periods of precipitation (*$LRP^{g}_{A5\_GS}$ *and* $LDP^{g}_{B1\_GS}$*)*

The distribution of precipitation during the year is also important for grapevine production. The projected changes of $LRP^{g}_{A5\_GS}(k)$ values are not significant ($p > 0.05$) in the investigated time period. The average values of $LRP^{g}_{A5\_GS}$ are 3–4 days. Statistically significant ($p < 0.05$) increase in the $LDP^{g}_{B1\_GS}(k)$ values is projected by ALADIN (using both the '5mid' and 'int' methods) and PRECIS (using the '5mid' method). $LDP^{g}_{B1\_GS}(k)$ values are estimated to increase from means of 12–29 days during the reference period to averages of 15–39 days by the end of the 21st century (see *Fig. 6*). Higher values are expected primarily in the region of the Great Hungarian Plain.

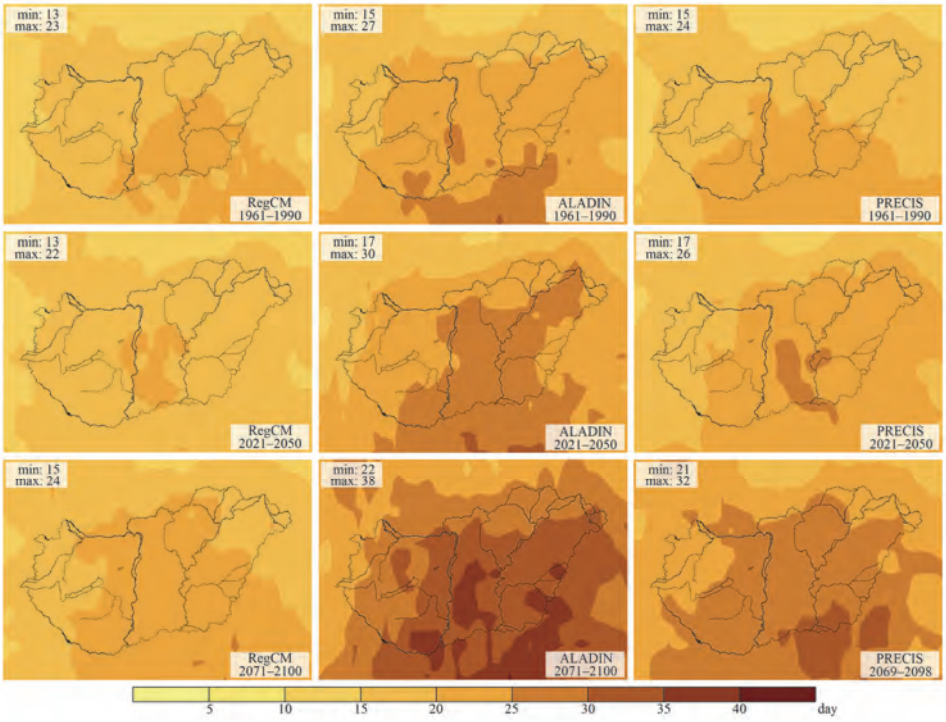

Fig. 6. Average length of the annual longest unbroken (dry) period of precipitation with below 1 mm per day during growing season ($LDP^{g}_{B1\_GS}$, day) in Hungary calculated with the 'int' method. Rows represent different time slices, i.e., 1961−1990 (upper row), 2021−2050 (middle row), and 2071−2100* (lower row). Columns correspond to RegCM (left), ALADIN (middle), and PRECIS (right) simulations.

* 2069−2098 for the PRECIS model

3.6. The number of years with extreme high temperature ($YN^{g}_{A35\_GS}$)

Extreme temperature indices as risk factors in grapevine production are also examined. According to RCM simulations, at least one day occurs every second or third year that has a maximum temperature above 35 °C in the reference period. Such extreme events are most frequent in the southeastern and northwestern parts of Hungary. Day(s) with a maximum temperature above 35 °C are projected to occur in almost every year at the end of the 21st century.

3.7. The number of days with extreme low temperature ($DN^{g}_{B1m\_GSf}$, $DN^{g}_{B17m\_D}$ and $DN^{g}_{B21m\_D}$)

The different RCM simulations and growing season calculation methods provide quite diverse results. The maximum value of $DN^{g}_{B1m\_GSf}$ are 20 and 99 when using the 'int' method in case of the ALADIN and RegCM simulations, respectively. Spatial distributions of $DN^{g}_{B1m\_GSf}$ derived with different growing season calculation methods are also diverse. Using the 'int' method, we get lower values of $DN^{g}_{B1m\_GSf}$ in plain regions are lower than in hilly terrains. Contrary to this, based on the '5mid' method, values of $DN^{g}_{B1m\_GSf}$ are usually higher in the plain regions.

On one hand, the PRECIS simulation predicts no day at all with a daily minimum temperature below −17 °C (−21 °C). On the other hand, $DN^{g}_{B17m\_D}$ values are estimated in the range of 6−113 days (RegCM simulation) and 6−100 days (ALADIN simulation) for the reference period by the other two RCM simulations. The highest values appear in the Northern Hungarian Mountains. According to both the RegCM and ALADIN simulations, the number of days with a daily minimum temperature below −17 °C may become zero during the 21st century. The likely range for $DN^{g}_{B17m\_D}$ values by the end of the 21st century is 0−8 days.

$DN^{g}_{B21m\_D}$ values are in the range of 0−20 days and 0−13 days (according to RegCM and ALADIN simulations, respectively) in the time period 1961−1990. During the 21st century, these extreme temperature events are likely to disappear almost completely.

4. Discussion and conclusions

The aim of the presented study is to refine the growing season calculation methods based on fixed calendar days and find the most accurate ones ('5mid' and 'int') using the root-mean-square error compared to the reference growing season values based on averaging the daily mean temperature for several decades. The selected methods are able to handle the extreme temperature events. First we use

the ‘5mid’ and ‘int’ methods for the calculation of the beginning, the end, and the length of the growing season. We apply these methods to prepare some climatic indicators which are usually used in viticulture studies. In the calculations, a fixed biological base temperature (10 °C) is used for the grapevine (*Amerine* and *Winkler,* 1944; *Winkler et al.,* 1974; *Kozma,* 2002). Our further aim is to sensitize the growing season calculation methods for different grapevine cultivars by modeling their special temperature demands (*Hlaszny,* 2012; *Fraga et al.,* 2016).

Our results suggest that the growing season is to become significantly longer during the 21st century, which should be taken into account when calculating the growing season, and thus, should be adjusted to the thermal conditions. The increasing length of the growing season appears in a form of an earlier beginning and a later end.

Hungary is considered as a one of the countries close to the northern border of quality wine production (*Schultz* and *Jones,* 2010). Therefore, grapevine cultivar assortment is limited by climatic conditions. According to *Van Leeuwen et al.* (2008), grapevine cultivars have different heat requirements for their phenological stages, including the ripening time. The sum of heat claim has a large range across the varieties, from 1204 °C to 1940 °C for Chasselas and Mourvèdre, respectively. However, the necessary sum of heat for a given variety is not consistent for cool and warm climates.

The increase of heat sum indicator values (e.g., Huglin index) for the 21st century, is projected by regional climate models based on A1B scenario (*Nakicenovic* and *Swart*, 2000) in several studies for European wine regions (e.g., *Malheiro et al.,* 2010; *Neumann* and *Matzarakis,* 2011). Based on the projection for the future, complex analyses of climatic indicators are necessary (*Fraga et al.,* 2014).

Also, according to our results, values of heat sum indicators are expected to increase. Therefore, wide settlement and economical production of late-ripening and red grapevine cultivars with higher heat demand can become more likely in Hungary. Moreover, the length of periods with low precipitation and the occurrence frequency of days with extreme high temperature are expected to increase significantly, which are potential risk factors in grapevine production (*Kozma*, 2002). Nevertheless, a highly probable propitious effect is the projected significant decrease of winter frost damage events.

Acknowledgments: Simulation of the PRECIS regional climate model was supported by grant OTKA K-78125. The authors are grateful for Ildikó Pieczka (Eötvös Lorand University, Dpt. of Meteorology) for providing bias-corrected model outputs. The RegCM and ALADIN simulations were developed within the ENSEMBLES project (505539) which was funded by the EU FP6 integrated program. The E-OBS database was provided by the ENSEMBLES and ECA&D projects. This work has been supported by OTKA grants K109109 and K109361, and also by the Agrárklíma2 project (VKSZ_12-1-2013-0034). The research was supported by the European Union and the European Social Fund (TÁMOP-4.2.1/B-09/1/KMR-2010-0003, FuturICT.hu grant no.: TÁMOP-4.2.2.C-11/1/KONV-2012-0013), and by the Széchenyi 2020 programme, the European Regional Development Fund and the Hungarian Government (GINOP-2.3.2-15-2016-00028). We would also like to thank Peter Raffai for his valuable help with the English revision.

References

Ambrózy P., Bartholy J., Bozó L., Hunkár M.K., Bihari Z., Mika J., Németh P.R., Paál A., Szalai S., Kövér Zs., Tóth Z., Wantuch F., and *Zoboki J.,* 2002: *Magyarország éghajlati atlasza*. Hungarian Meteorological Service, Budapest. (in Hungarian)

Amerine, M. A. and *Winkler, A. J.*, 1944: Composition and quality of musts and wines of Californian grapes. *Hilgardia 15*, 493–675. https://doi.org/10.3733/hilg.v15n06p493

Bois, B., Blais, A., Moriondo, M., and *Jones, G.V.,* 2012: High resolution climate spatial analysis of European winegrowing regions. IXe International Terroirs Congress 2012, 17–20.

Csepregi P., 1997: Szőlőtermesztési ismeretek. Mezőgazda Kiadó, Budapest. (in Hungarian)

Davitaja, F., F. (Давитая, Ф., Ф.), 1959: Климатические показатели сырьевой базы виноградо-винодельческой промышленности. *Труды ВНИИВиВ „Магарач", 6(1),* 12–32. (in Russian)

Déqué, *M.*, *Marquet*, *P.*, and *Jones*, *R.G.*, 1998: Simulation of climate change over Europe using a global variable resolution general circulation model. *Clim. Dynam. 14*, 173–189. https://doi.org/10.1007/s003820050216

Dunkel, Z. and *Kozma, F.,* 1981: A szőlő téli kritikus hőmérsékleti értékeinek területi eloszlása és gyakorisága Magyarországon. *Légkör 26(2)*, 13–15. (in Hungarian)

Formayer, H., and *Haas, P.,* 2010: Correction of RegCM3 model output data using a rank matching approach applied on various meteorological parameters. Deliverable D3.2 RCM output localization methods (BOKU-contribution of the FP 6 CECILIA project).

Fraga, H., Malheiro, A.C., Moutinho-Pereira, J., Jones, G.V., Alves, F., Pinto, J.G., and *Santos, J.A.,* 2014: Very high resolution bioclimatic zoning of Portuguese wine regions: present and future scenarios. *Reg. Environ. Change 14,* 295–306. https://doi.org/10.1007/s10113-013-0490-y

Fraga, H., Santos, J.A., Moutinho-Pereira, J., Carlos, C., Silvestre, J., Eiras-Dias, J., Mota, T., and *Malheiro, A.C.,* 2016: Statistical modelling of grapevine phenology in Portuguese wine regions: observed trends and climate change projections. *J. Agric. Sci. 154*, 795–811. https://doi.org/10.1017/S0021859615000933

Giorgi, F., *Marinucci*, M.R., *Bates*, G.T., and *DeCanio*, G., 1993: Development of a second generation regional climate model (RegCM2). Part II: Convective processes and assimilation of lateral boundary conditions. *Mon. Weather Rev. 121*, 2814–2832. https://doi.org/10.1175/1520-0493(1993)121<2814:DOASGR>2.0.CO;2

Haylock, M.R., Hofstra, N., Klein Tank, A.M.G., Klok, E.J., Jones, P.D., and New, M., 2008: A European daily highresolution gridded data set of surface temperature and precipitation for 1950-2006. *Journal of Geophysical Research, Vol. 113*, 1–12. https://doi.org/10.1029/2008JD010201

Hlaszny E., 2012: A szőlő *(Vitis Vinifera L.)* korai fenológiai válaszadásának modellezése a kunsági borvidéken növényfelvételezések, időjárási megfigyelések és regionális klímamodell alapján. Ph.D. thesis, Corvinus University of Budapest, Budapest. (in Hungarian)

Huglin, P., 1978: Nouveau mode d'évaluation des possibilités héliothermiques d'un milieo viticole. Symposium International sur l'ecologie de la Vigne. Ministére de l'Agriculture et de l'Industrie Alimentaire, Contanca, 89–98. (in French)

IPCC, 2013: Climate Change 2013: The Physical Science Basis. Contribution of Working Group I to the Fifth Assessment Report of the Intergovernmental Panel on Climate Change (Eds. *Stocker T.F., Qin D., Plattner G.-K., Tignor M., Allen S.K., Boschung J., Nauels A., Xia Y., Bex V., Midgley P.M.*,). Cambridge University Press, Cambridge, United Kingdom and New York, NY, USA.

Jones, G.V., Moriondo, M., Bois, B., Hall, A., and *Duff, A.,* 2009: Analysis of the spatial climate structure in viticulture regions worldwide. *Le Bulletin de l'OIV82(944,945,946),* 507–518.

Kozma, P., 2002: A szőlő és termesztése I. Akadémiai Kiadó, Budapest. (in Hungarian)

van der Linden, P. and *Mitchell, J.F.B.,* (Eds.)*,* 2009: ENSEMBLES: Climate Change and Its Impacts: Summary of research and results from the ENSEMBLES project. UK Met Office Hadley Centre, Exeter, UK.

Malheiro, A.C., Santos, J.A., Fraga, H., and *Pinto, J.G.,* 2010: Climate change scenarios applied to viticultural zoning in Europe. *Climate Res. 43*, 163−177. https://doi.org/10.3354/cr00918

Mesterházy, I., Mészáros, R., and *Pongrácz, R.,* 2014: The Effects of Climate Change on Grape production in Hungary. *Időjárás 118*, 193−206.

Moriondo, M., Jones, G.V., Bois, B., and *Dibari, C.,* 2013: Projected shifts of wine regions in response to climate change. *Climate Change 119,* 825−839. https://doi.org/10.1007/s10584-013-0739-y

Nakicenovic, N. and *Swart, R.J.,* 2000: Emissions Scenarios 2000 – Special Report of the Intergovernmental Panel on Climate Change. Cambridge University Press, Cambridge.

Neumann, P.A. and *Matzarakis, A.,* 2011: Viticulture in southwest Germany under climate change conditions. *Climate Res. 47,* 161–169. https://doi.org/10.3354/cr01000

Oláh, L., 1979: *S*zőlészek zsebkönyve. Mezőgazdasági Kiadó, Budapest. (in Hungarian)

Pieczka, I., Pongrácz, R., Bartholy, J., Kis, A., and *Miklós, E.,* 2011: A szélsőségek várható alakulása a Kárpát-medence térségében az ENSEMBLES projekt eredményei alapján. In (Ed.: *Lakatos M.*) 36. Meteorológiai Tudományos Napok - Változó éghajlat és következményei a Kárpát-medencében. Országos Meteorológiai Szolgálat, Budapest*.* 77–87. (in Hungarian)

Pieczka, I., 2012: A Kárpát-medence térségére vonatkozó éghajlati szcenáriók elemzése a PRECIS finom felbontású regionális klímamodell felhasználásával. Ph.D. thesis. Eötvös Loránd University, Department of Meteorology, Budapest. (in Hungarian)

Pongrácz, R., Bartholy, J., and *Miklós, E.,* 2011: Analysis of projected climate change for Hungary using ENSEMBLES simulations. *Appl. Ecol. Environ. Res. 9,* 387–398. https://doi.org/10.15666/aeer/0904_387398

Ramos, MC., Jones, G.V., and *Martinez-Casasnovas, J.A.,* 2008: Structure and trends in climate parameters affecting winegrape production in northeast Spain. *Climate Res. 38*, 1–15. https://doi.org/10.3354/cr00759

Riou, C., 1994: The Effect of Climate on Grape Ripening: Application to the Zoning of Sugar Content in the European Community. European Commission, Brussels, Luxembourg.

Santos, J.A., Malheiro, A.C., Pinto, J.G, and *Jones, G.V.,* 2012: Macroclimate and viticultural zoning in Europe: observed trends and atmospheric forcing. *Climate Res. 51,* 89–103. https://doi.org/10.3354/cr01056

Schultz, H.R. and *Jones, G.V.,* 2010: Climate Induces Historic and Future Changes in Viticulture*. J. Wine Res. 21,* 137−145. https://doi.org/10.1080/09571264.2010.530098

Seljaninov, G.T., 1928: О сельскохозяйственной оценке климата. *Сельскохозяйственной метеорологии, 20,* 165–177. (in Russian)

Szenteleki, K., Ladányi, M., Gaál, M., Zanathy, G., and *Bisztray, Gy.D.,* 2012: Climatic risk factors of Central Hungarian grape growing regions. *Appl. Ecol. Environ. Res. 10*, 87–105. https://doi.org/10.15666/aeer/1001_087105

Van Leeuwen, C., Garnier, C., Agut, C., Baculat, B., Barbeau, G., Besnard, E., Bois, B., Boursiquot J.-M., Chuine, I., Dessup, T., Dufourcq, T., Garcia-Cortazar, I., Marguerit, E., Monamy, C., Koundouras, S., Payan, J.-C., Parker, A., Renouf, V., Rodriguez-Lovelle, B., Roby, J.-P., Tonietto, J., and *Trambouze, W.,* 2008: Heat requirements for grapevine varieties is essential information to adapt plant material in a changing climate. 7th International Terroir Congress, Agroscope Changins-Wädenswil, Switzerland, 222–227.

Wilson, S., Hassell, D., Hein, D., Jones, R., and *Taylor, R.,* 2007: Installing and using the Hadley Centre regional climate modelling system, PRECIS. Version 1.5.1. UK Met Office Hadley Centre, Exeter.

Winkler, A.J., Cook, J.A., Kliewer, W.M., and *Lider, L.A.,* 1974: General Viticulture. University of California Press, California.

DOI:10.28974/idojaras.2018.3.2

IDŐJÁRÁS

Quarterly Journal of the Hungarian Meteorological Service
Vol. 122, No. 3, July – September, 2018, pp. 237–257

An assessment of daily extreme temperature forecasts – stations average view

Hristo Hristov* and **Andrey Bogatchev**

National Institute of Meteorology and Hydrology,
Bulgarian Academy of Sciences,
66 Tsarigradsko shose Blvd., 1784 Sofia, Bulgaria

** Corresponding author Email: hristo.hristov@meteo.bg*

(Manuscript received in final form September 6, 2017)

Abstract—The present article is the first one of a couple of articles, related to the assessment of the human forecasts (forecast made by weather forecasters). In this article, we have performed an integral assessment of the human-derived extreme temperature forecasts during 2009–2014. It will give us a more general picture of the forecasts, their accuracy over the years of the period in consideration, and their change through the different months of the year. We will show how the accuracy of the forecasts increases in the assessing period, and also how human forecasts underestimate extreme temperatures. The integral assessment gives us a more clear view on the movement of the various errors in time, but it has a significant shortcoming – the spatial distribution of the information is lost. The spatial distribution would give us a valuable feedback, that could be used to correct the forecasts. It will be discussed in the second article, where an assessment by stations will be made.

Key-words: verification, assessment, evaluation, extreme temperature, mean error, mean absolute error

1. Introduction

The purpose of the assessment of the extreme daily temperatures is to look deeper in and to give a more detailed picture of the short-range forecast (forecast for the next day) of the National Institute of Meteorology and Hydrology, Bulgarian Academy of Science (NIMH-BAS), Bulgaria. The results of the forecast analysis (the assessment) will provide a feedback to the forecaster, that should lead to an improvement of the forecast's quality.

In Bulgaria, meteorological observations has been effectuated for more than 100 years, and civil meteorological forecasts have been drawn up for more than 60 years. Regardless this long period, such extensive and in-depth study of the human weather forecasts issued by the National Weather Service has never been done up to now.

For this aim, different kinds of errors, as well as the percent of correct forecasts are calculated, using the guidance of the World Meteorological Organization (http://www.wmo.int/pages/prog/amp/pwsp/pdf/TD-1023.pdf). It uses ±2 °C or ±3 °C as a limit when calculating the percent correct. This assessment is very suitable to be used for the general public or other users. This study uses a margin of admissible error up to 2 °C, i.e., ±2 °C for calculating the percent correct. In order to be trusted by the public, to trust a weather forecast needs to be both: accurate and consistent. Accuracy is important, as public will not trust the forecast that has proven to be inaccurate over a time period, especially if this period is short (just a few days). A consistent forecast, covering usually seven days, is a forecast sequence that does not have large swings (flip-flops) from one forecast to the next (for the same date). Consistency is just as important as accuracy, because the public will not trust to forecasts that flip-flops and changes on a day to day basis (*Lashley et al.*, 2008). These flip flops of the forecast (for one and the same day) are measured with the Ruth-Glahn Forecast Convergence Score (FCS), developed by *David Ruth* and *Harry Glahn* (*Ruth et al.,* 2009).

Brier and *Allen* (1951) point some economical, administrative, and scientific reasons for evaluation. *A.H. Murphy* (1993) says that goodness of a forecast has different faces and determines three types:

- consistency (correspondence between the forecasters' judgment and the forecast),
- quality (correspondence between the forecasts and the matching observations), and
- value (incremental economic and/or other benefits realized by decision makers through the use of the forecasts).

In this work, only the second type (quality) will be discussed.

Globally, there are number of researches that approach the present work. There, the quality of the forecasts for minimum and maximum temperatures and precipitations is calculated. In *Riply* and *Archibold* (2002), several points in Canada (with different climate), in the year 2000, were assessed by calculating the quality of the short-range and medium-range (up to 5 days) forecasts. Determined parameters were: mean error, mean absolute error, Skill score (climate norm was used) for temperatures and Brier score (*Brier*, 1950) for the precipitation probability. It was shown how forecast errors gradually increase from day 1 to day 5.

In *Fajman* (2011), for the area of Omaha Valley during the period 2008–2009, basic errors were calculated, such as: mean error, mean absolute error, Brier score, and forecast convergence score, for maximum and minimum temperatures and precipitation probability for a 3-day and a 7-days period. These statistics were calculated for the forecasts issued from the Meteorological Office (human forecasts) and for the forecasts produced by the GFS model. It was emphasized that the comparison between these two forecasts showed that human forecasts were better. Although, it has to be mentioned, that human forecasts were based mainly on the numerical model predictions.

In 1998 a verification program, named SOLVER, started at the Meteorological Office Corpus Christi in Texas (*Wilk*, 2005). The software package (SOLVER) was developed by Jamie Frederic, a chief forecaster at the meteorological office in Tulsa, Oklahoma at that time. Over the following few years, this software underwent some changes, and since 2003, an overall assessment and personal assessments (sent via e-mail to the weather forecasters) have been made for minimum temperatures, maximum temperatures, and precipitation every month and every six months (for the cold and warm halves of the year). The computer program calculated mean error, mean absolute error as well as percent correct with deviation up to 3 °F for minimum and maximum temperatures. For the precipitation, the Brier score was calculated. These errors were calculated for 6 points using 5 lead-time periods (each having 12 hours) and incorporated human forecasts and the three numerical models in use: GFS (Global Forecast System), NAM (North American Mesoscale Model), NGM (Nested Grid Model). A comparison of errors and results has been made in form of graphics, and placed in the forecasters' restroom. Furthermore, the personal assessments gave possibility for competition between the forecasters, and those with the best results (every six months) received diplomas. The purpose of this verification program was to provide the best forecasts for the area of responsibility of Corpus Christi. In the paper of *Wilk* (2007), the methodology described in *Wilk* (2005) was used. Moreover it was found that the human forecast was about 10% better than the numerical forecast and, furthermore, the Meteorological Office of Corpus Christi had the best results, compared to all other meteorological offices in the USA.

In Bulgaria, in the work of *Spiridonov* (1987), various errors were calculated for minimum and maximum temperatures in Sofia during the period 1983–1984. Beside the human forecast's error, the persistence forecast error was calculated as well. However, the mean error was not determined, which would have given the systematic error of the forecast.

In *Bogatchev* (1988), a scheme was developed for a medium-range forecast of the daily mean temperature and the daily amounts of precipitation for five days (day by day), based on the field AT500 of the ECMWF model. The forecast was made for 8 stations on the territory of Bulgaria. An assessment of the results was made, and it showed that they were satisfactory.

In *Bogatchev* (1994), the work of *Bogatchev* (1988) was described and a predictive scheme (statistical) for forecasting extreme temperatures up to six days for 17 stations in Bulgaria was created. The scheme was developed on the basis of the fields: AT500, surface pressure, and T850, derived from the ECMWF model. Various types of evaluation of the output data have been made; also a comparison with the mean absolute error of the human forecast for the period of November 1991 – October 1992.

In the present work, the method of the continuous variables is used for evaluation; a useful tool is the website of the Joint Working Group on Forecast Verification Research (http://cawcr.gov.au/projects/verification/). It gives a good presentation of the modern assessment methods, some of which are used in this study.

2. Methodology

The short-range weather forecast of NIMH is up to 36-48 hours ahead, and it is prepared till 11 a.m. every day. It consists of a forecast for today and a forecast for the next day (that will be assessed). Besides of the text forecast, a numerical forecast is issued as well; it includes minimum and maximum temperatures and a symbol for the phenomena expected (sun, clouds, rain, snow, thunders, fog, etc.). The numerical forecast is elaborated for 68 points in Bulgaria, 37 of which coincide with synoptic stations. For these 37 points (shown in *Fig. 1*) the assessment will be carried out. Four of these 37 points are mountainous. The period for assessing is the years 2009–2014.

In the followings we give the definitions of the error estimations used in this study.

Mean error or bias. It can be interpreted as systematic error. The mean error indicates the difference between the forecast and the observations for the day. For a definite period of time, the sign and the magnitude of the systematic error can be seen.

$$ME = \frac{1}{n}\sum_{i=1}^{n}(F_i - O_i), \tag{1}$$

where F_i and O_i are the values of the forecast and observations for day i, respectively.

Mean Absolute error. It determines the accuracy of the forecast. It does not take into account the direction of the error, only its magnitude.

$$MAE = A_h = \frac{1}{n}\sum_{i=1}^{n}|F_i - O_i|, \tag{2}$$

where h is human.

Fig. 1. Map of the points, where the assessment carried out, names of the stations, and their WMO code. First 2 digits (15) are omitted.

Many of the meteorological elements, including the temperature, do not vary very sharply, and they are often close to their previous values. So, if the climatic value or persistence forecast (recent observations) is issued as a forecast, the result would be fairly good (with small errors). It must be acknowledged that a forecaster, using a persistence forecast, would get even better results. To assess the contribution of the persistence forecast to the human forecast of the temperature, it has to be determined. So, to calculate the persistence forecast's error, O_i is used instead of F_i, and O_i is replaced by $O_{(i-1)}$.

$$MAE_p = A_P = \frac{1}{n}\sum_{i=1}^{n} |O_i - O_{(i-1)}|, \quad (3)$$

where p is persistence.

The persistence error is suitable to be used for the forecast of the minimum temperatures, as they are available (at 8 or 9 a. m. in local time, depending on the season) before the forecast is issued (11 a. m.). However, for the maximum temperatures, the last data available are those from the previous day. Thus, there are 2 days difference between observations and forecast. Thus, to get the real error of the persistence forecast, as will be in practice, it should be calculated as follows:

$$MAE_{P_{T_{max}}} = A_p = \frac{1}{n}\sum_{i=1}^{n} |O_i - O_{(i-2)}| \quad (4)$$

In 2012, in the operational forecasting office of NIMH BAS, a program was released in operational mode, that evaluates the predicted temperatures (minimum and maximum) for 37 points (shown on the map above). Every day it calculates the mean error, mean absolute error, maximum error, mean square error, and the percent correct for these 37 stations. Thus, in near-real-time, the forecaster can see these types of errors of his/her own forecast. He can look in more details in the meteorological conditions and analyze the consequences and the reasons for the deviations in his/her forecast.

Percent correct is determined as followed:

$$PC = \frac{1}{n}\sum_{i=1}^{n} \begin{cases} correct, if\ (F_i - O_i) \leq 2°C \\ not\ correct, if\ (F_i - O_i) > 2°C \end{cases} \times 100\ \% \quad (5)$$

Using Eqs. (2), (3), and (4), the Skill scores of the forecaster can be calculated for the minimum and maximum temperatures using the formula:

$$Skill\ scores = \left(\frac{A_p - A_h}{A_p}\right) 100\% \quad (6)$$

where A_h is *MAE* of human forecast (Eq. (2)), and A_p is *MAE* of persistence forecast (Eqs. (3) and (4) – the minimum and maximum temperature respectively). *Skill scores* change from 0% persistence forecast to 100% perfect forecast.

3. Results

To make a stations-averaged (integral) assessment, first the assessment is made in space and then in time, i.e., first, all points for a given day are evaluated (as it is made by the internal verification program), and then they are evaluated for a certain past period. Here, we look at the data by years and by months. The information that will be presented is: mean error (*ME*), mean absolute error (*MAE*), percent correct (*PC*), *Skill scores* and *ME, MAE* and *PC* of the persistent forecast.

3.1. Mean absolute error (MAE)

We will discuss the mean absolute error, first by years (*Fig. 2*).

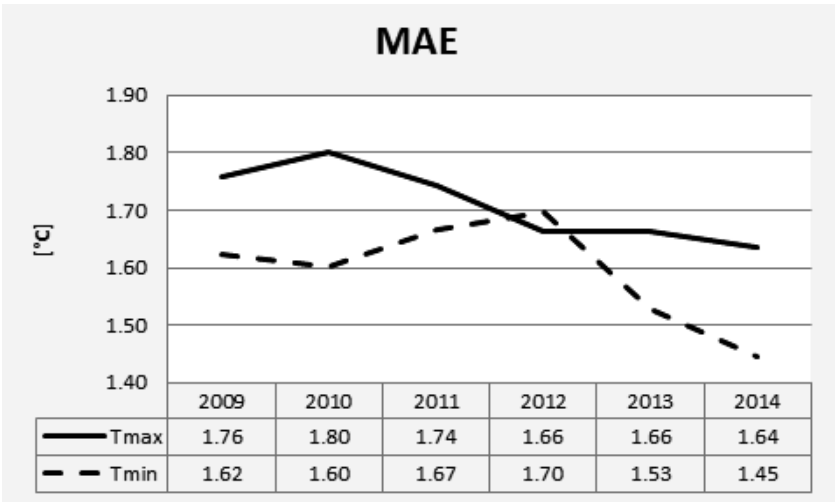

Fig. 2. Mean absolute error of the human forecast for the minimum and maximum temperatures.

It is seen that:

- The minimum temperature *MAE* is less than the maximum temperature *MAE*, i.e., the minimum temperature forecast is more accurate than the maximum temperature forecast.
- In general, the course of *MAE* decreases with the years, due to various factors, such as: improvement of the numerical models, accumulation of more experience from the forecasters, partially probably the release in an operational mode of evaluation system, and others.

At the minimum temperatures, there is a slight increase of the error in 2011 and 2012 with less than 0.1 °C. The maximum temperatures have an increase of the error in 2010 and a delayed decrease of the error in 2013. These fluctuations are normal and can be due to different factors.

In *Fig. 3*, the *MAE* of the persistence forecast is added to the *MAE* of the human forecast. *Tmax_In1* is also presented just to make the comparison between *MAE* of the persistence forecast for the minimum and maximum temperatures. Later on, the *Tmax_In1* will not be used, and *Tmax_In2* will be discussed instead (this would be the real conditions error).

To compare, considering *Tmax_In1* and *Tmin_In1*, it is seen (*Fig. 3*) that the error in the minimum temperatures is smaller, that leads to the conclusion that the fluctuations (day to day) in the minimum temperatures are smaller.

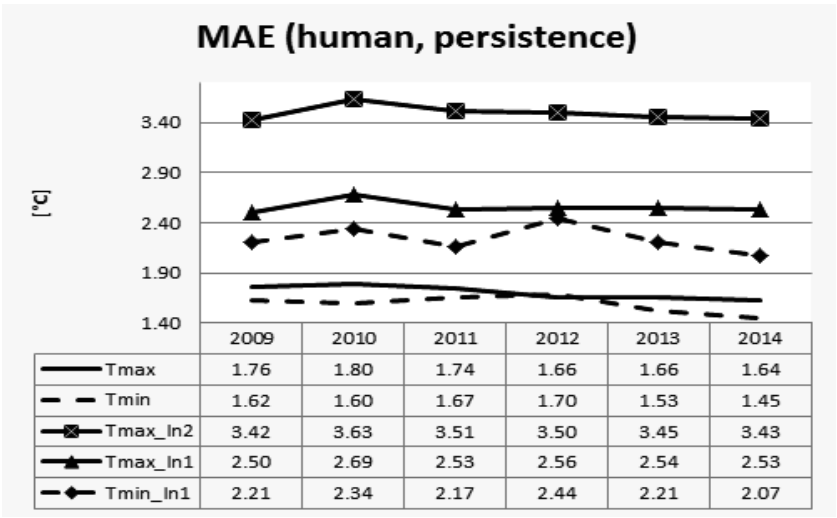

	2009	2010	2011	2012	2013	2014
Tmax	1.76	1.80	1.74	1.66	1.66	1.64
Tmin	1.62	1.60	1.67	1.70	1.53	1.45
Tmax_In2	3.42	3.63	3.51	3.50	3.45	3.43
Tmax_In1	2.50	2.69	2.53	2.56	2.54	2.53
Tmin_In1	2.21	2.34	2.17	2.44	2.21	2.07

Fig. 3. *MAE* for the human and persistence forecasts. *Tmax_In2* is *MAE* of the persistence forecast for the maximum temperatures calculated in Eq.(4), i.e. the forecast and the observations difference by two days. *Tmax_In1* and *Tmin_In1 MAE* of the persistence forecast for the maximum and the minimum temperatures calculated by Eq.(3), or one day difference between the prediction and the observation.

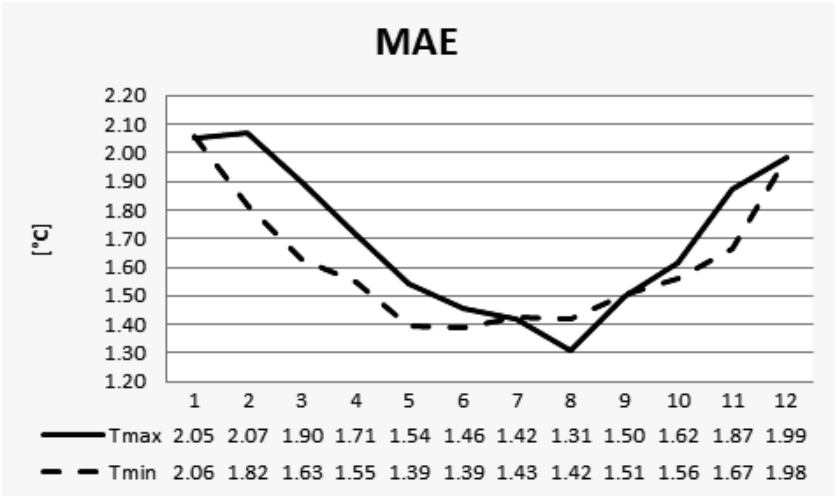

Fig. 4. *MAE* for the minimum and maximum temperatures of the human forecast.

Looking now at *Tmax_In2* and *Tmin_In1* (*Fig. 3*), it is seen that the persistence forecast error is significantly greater than the forecast error of the meteorological office. It is especially true for the maximum temperature, where the difference is almost 2 °C, and this is a double, in some years even, greater

error. For the minimum temperature, the difference is about 0.5 °C. Besides, the correlation between *Tmin_In1* and *Tmin* is high, and this leads to the conclusion that the influence of the persistence forecast on the minimum temperatures is quite big and moreover, it is bigger than the maximum temperatures.

Let us now consider the mean absolute error changes in months. The monthly averaged absolute error for the minimum and maximum temperatures is presented in *Fig. 4*.

One can see in *Fig. 4* that, during the warm months, *MAE* decreases and during the cold months, it grows. The course of the maximum temperatures shows a minimum in August and a maximum in February. The difference between August and February is nearly 0.8 °C, and this is a significant difference in the absolute error. The results are almost identical to those shown by *Wilk* (2005). At the minimum temperatures, there is a minimum in May and June (*Fig. 4*) and a maximum in January; the difference between them is nearly 0.7 °C, i.e., the fluctuations in the minimum temperatures' absolute error are slightly smaller than those in maximum temperatures.

Let us add now the persistence forecast error (*Fig. 5*).

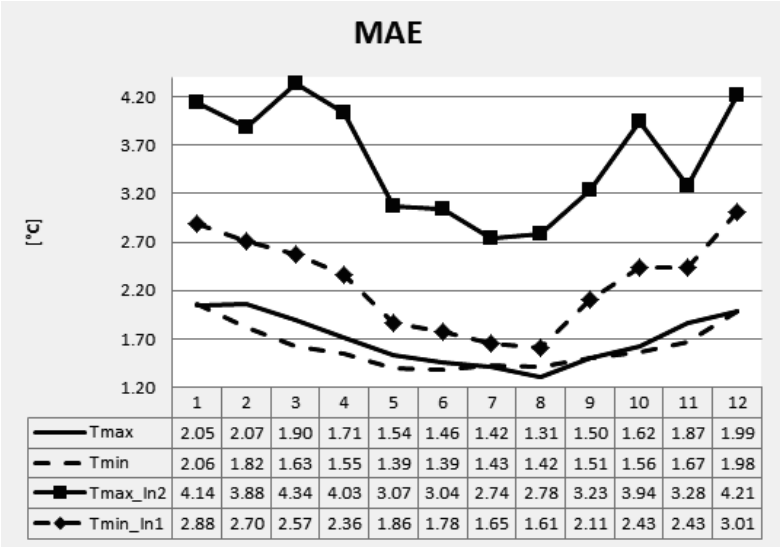

	1	2	3	4	5	6	7	8	9	10	11	12
Tmax	2.05	2.07	1.90	1.71	1.54	1.46	1.42	1.31	1.50	1.62	1.87	1.99
Tmin	2.06	1.82	1.63	1.55	1.39	1.39	1.43	1.42	1.51	1.56	1.67	1.98
Tmax_In2	4.14	3.88	4.34	4.03	3.07	3.04	2.74	2.78	3.23	3.94	3.28	4.21
Tmin_In1	2.88	2.70	2.57	2.36	1.86	1.78	1.65	1.61	2.11	2.43	2.43	3.01

Fig. 5. *MAE* of the human and persistence forecasts. *Tmax_In2* is *MAE* of the persistence forecast for the maximum temperatures calculated by Eq. (4). *Tmin_In1* is *MAE* of the persistence forecast for minimum temperatures calculated by Eq. (3).

Fig. 5 shows that *MAE* of the persistence forecast also decreases during the warm months, and this is logical, since during the warm months the atmosphere is more stable. In addition, the correlation between the *MAE* of the human and

persistence forecasts is good enough (especially for the minimum temperatures), so that a conclusion can be drawn that the contribution of the persistence forecast in the human forecast is big, and it is bigger at the minimum temperatures. Moreover, the figure shows that the *MAE* of the persistence forecast for minimum temperatures (*Tmin_In1*) during the warm months is less than the human forecast error during the cold months, i.e., the persistence forecast in summer is more accurate than human forecast in winter.

At the maximum temperatures (*Tmax_In2*), the situation is a little different. The error is much greater than the human error. But it is normal to expect, since when calculating *Tmax_In2*, a two-day difference is used, moreover, the fluctuations (from day to day) of the maximum temperatures are higher.

3.2. Percent correct (PC)

As mentioned before, a forecast with an error up to 2 °C is considered to be correct. *Fig. 6* presents the *PC* for maximum and minimum temperatures, by years.

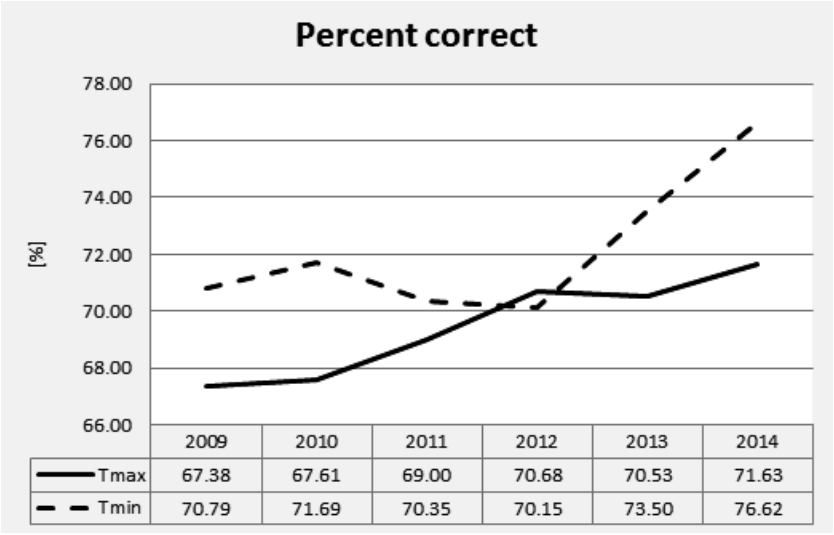

	2009	2010	2011	2012	2013	2014
Tmax	67.38	67.61	69.00	70.68	70.53	71.63
Tmin	70.79	71.69	70.35	70.15	73.50	76.62

Fig. 6. Percent correct for the human forecast

Fig. 6 indicates that the *PC* for minimum temperatures is greater than for the maximum temperatures. Furthermore, the *PC* increases over the years (contrary to *MAE*); for the maximum temperatures this rise is a little more than 4%, and for the minimum temperatures nearly 6%. At the minimum

temperatures, there is a slight decrease of the *PC* in 2011 and 2012, which fully corresponds with the increase of the *MAE* in these two years.

At the maximum temperatures, there is a drop in 2013 for the *PC*, but the *MAE* does not have a rise (2012 and 2013 have the same error). In addition, the *MAE* has an increase in 2010, but it does not correspond to the *PC* (also increasing). It is completely normal to get, if *MAE* is more evenly distributed and more stations fall in this interval of 2 °C. So, it is seen that the *MAE* and the *PC* are not necessarily always opposite.

Now, let's add the *PC* of the persistence forecast (*Fig. 7*).

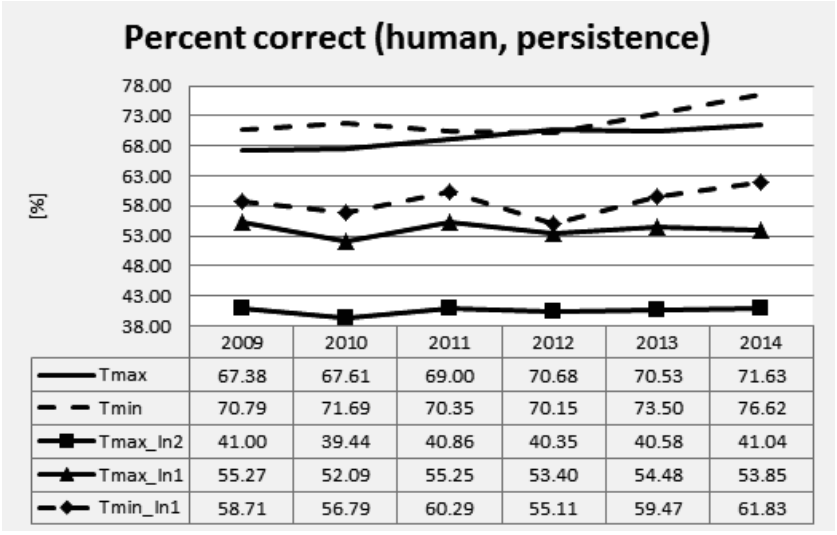

	2009	2010	2011	2012	2013	2014
Tmax	67.38	67.61	69.00	70.68	70.53	71.63
Tmin	70.79	71.69	70.35	70.15	73.50	76.62
Tmax_ln2	41.00	39.44	40.86	40.35	40.58	41.04
Tmax_ln1	55.27	52.09	55.25	53.40	54.48	53.85
Tmin_ln1	58.71	56.79	60.29	55.11	59.47	61.83

Fig. 7. Percent correct for the human and persistence forecast. *Tmin_In1* and *Tmax_In1* are the *PC* for the minimum and maximum temperatures with one day difference between forecast and observation. *Tmax_In2* is the *PC* for the maximum temperature with two days difference.

Here *Tmax_In2*, *Tmax_In1,* and *Tmin_In1* are described below *Fig. 3,* and *Tmax_In1* is used only for an initial comparison, from which it is seen that the maximum temperature has a smaller *PC* (53–55%) compared to the minimum temperature (55–61%). Moreover, *Tmin_In1* decrease in 2012 coincides with the fall in *Tmin*, proving once again the big influence of the persistence forecast on the human forecasts.

We made the difference between the *PC* of the human forecasts and the *PC* of the persistence forecast: *Tmin-Tmin_In1* and *Tmax–Tmax_In2*, with the aim to check approximately what percentage from the *PC* is not due to the persistence forecast. These are presented in *Fig. 8*.

Fig. 8 indicates that at the minimum temperatures, from 10% to 15% of the errors are NOT due to the persistence forecast. In fact, some of these 10–15% are due to the persistence forecast with correction, so the forecaster's experience is of great importance.

Can we state that at minimum temperatures between 85 and 90% of the human forecasts are due to persistence forecast? The answer is NO.

The reason is that the *PC* of the human forecast, which is about 70–76% for the minimum temperatures (*Fig. 7*), is a superposition of three elements: persistence forecast, numerical models, and the forecasters' decisions (strongly depending on his/her experience). Till now, we studied just one of these three elements, so in this "equation" still two unknown remain. In a next work, we shall investigate the numerical models and find one more of factors. Then, only one unknown element, the forecaster's decision will remain; and we would be, to a great extent, able to say what parts of the human forecast is due to the numerical models and to the persistence forecast.

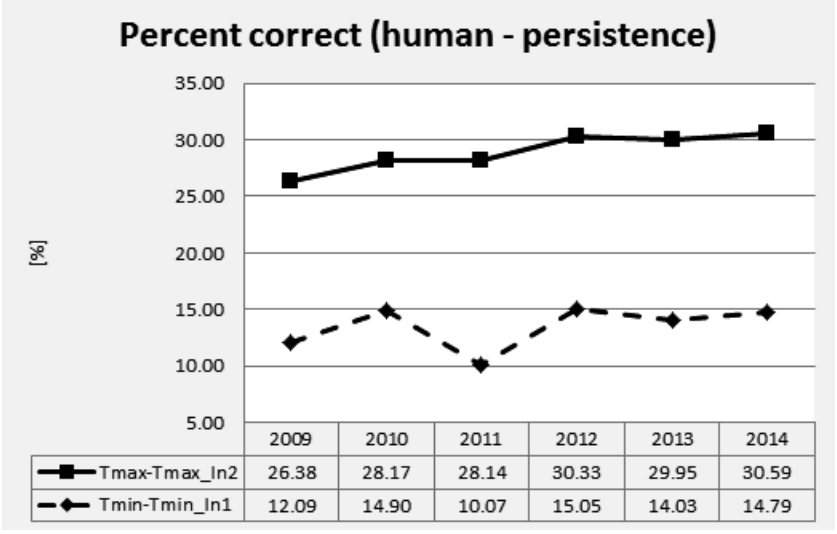

	2009	2010	2011	2012	2013	2014
Tmax-Tmax_In2	26.38	28.17	28.14	30.33	29.95	30.59
Tmin-Tmin_In1	12.09	14.90	10.07	15.05	14.03	14.79

Fig. 8. Percent correct of the human forecast minus persistence forecast.

So far, we could only state (based on 15 years experiences as forecaster), that the impact of the persistence forecast on the human is really big. The reason is that every morning after the arriving of the synoptic data at 6 UTC, minimum temperatures are available, and the forecaster uses them to prepare the forecast for the minimum temperatures for the next day, making adjustments. This technique is very useful for a static atmosphere, but not applicable in case of

active dynamics (a cold front passage, for example). However, cases with more intensive dynamics occur relatively rarely compared to cases with more static atmosphere, that is why the *PC* of the persistence forecast (*Fig. 7 – Tmin_In1*) is about 60%, i.e., the big impact of the persistence forecast on the human is obvious.

At the maximum temperatures, this percentage (of NON-persistence forecast) is significantly higher, between 26 and 30%. Also, an increase of about 4% is noticed over the years. *Fig. 7* shows that the *PC* of the maximum temperatures (*Tmax_In2*) is almost constant over the years. It follows that these 4% of increase are due to other factors, as numerical models and forecaster's experience. In addition, the *PC* is not influenced by the type of the year. For example, 2014 is one of the most humid years (more dynamics), but nevertheless, no drop in the difference is noticed (*Fig. 8*) in the drier years (when the influence of the persistence forecast should be greater). This is a proof that, in case of more dynamics (little influence of the persistence forecast), numerical models and forecaster's experience compensate the smaller impact of the persistence forecast.

The difference between the *PC* in the maximum and minimum temperatures in *Fig. 8* is 15–20%. This difference results, on one hand, from the fact that for the maximum temperatures a persistence forecast from two days ago is used, and on the other hand, from the fact that at minimum temperatures fluctuations (day to day changes) are smaller.

Looking at the skill scores in *Fig. 9*, calculated using Eq. (6), a big difference is seen between minimum and maximum temperatures.

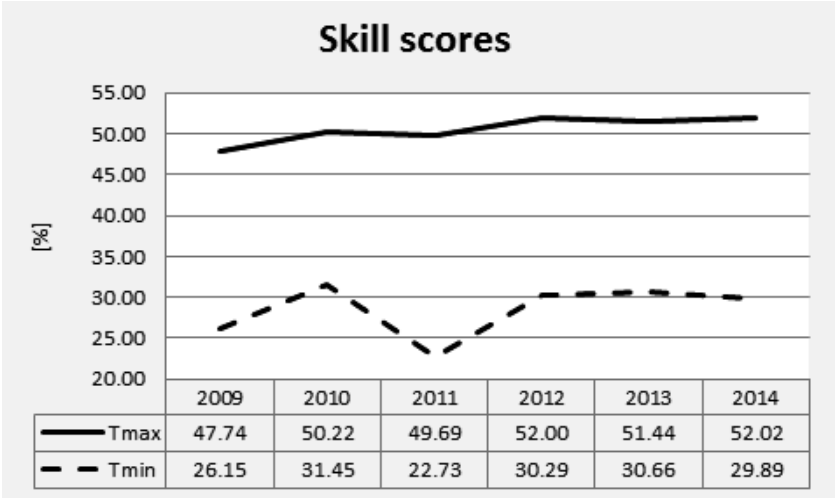

Fig. 9. Skill scores of the human forecast for the minimum and maximum temperatures.

Skill scores at minimum temperatures is 25–30% and at the maximum temperatures about 50%, i.e., the difference in between is 20–25%. This corresponds to the above statements, namely that at the maximum temperatures about 30% of the errors are due to the non-persistence forecast, i.e., to the numerical models and the **forecaster's skill**; at the minimum temperatures they are 10–15%. These numbers are just obtained in a different way, not with the formula for the skill scores; that's why they are different, but the end results and the conclusions are similar.

Now, let's go back to the results of the skill scores. The reason for this big difference in the skills at minimum and maximum temperatures is that in calculating the skill scores of the maximum temperatures, a *MAE* of the persistence forecast from two days ago is used, and these results in nearly 2 °C difference between the human and the persistence forecasts (*Fig. 3*). At minimum temperatures, the *MAE* of persistence forecast is from just one day before, and thus, the difference between the human and persistence forecasts is only about 0.5 °C. Even if we use the *MAE* of the persistence forecast at the maximum temperature from one day before (*Fig. 3*), we would have a difference of 0.7–0.9 °C between the human and persistence forecasts, i.e., skills at maximum temperatures would be greater again.

Therefore, we think that the main reason for the smaller skill for the minimum temperatures is the smaller fluctuation (day to day changes) in the minimum temperatures, which leads to a smaller error in the persistence forecast, and on its side, this leads to less skills at minimum temperatures.

Let's now have a look at the *PC* by months. We start with the averaged *PC* at the human forecasts (*Fig. 10*).

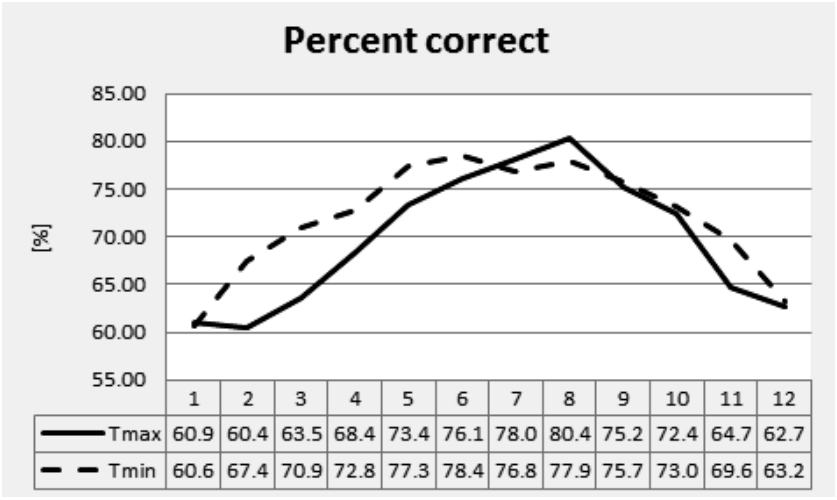

	1	2	3	4	5	6	7	8	9	10	11	12
Tmax	60.9	60.4	63.5	68.4	73.4	76.1	78.0	80.4	75.2	72.4	64.7	62.7
Tmin	60.6	67.4	70.9	72.8	77.3	78.4	76.8	77.9	75.7	73.0	69.6	63.2

Fig. 10. Monthly averages of *PC* of the human forecast for the minimum and the maximum temperatures.

Looking at *Fig. 10*, it is noticed that the percent correct gradually grows from winter to summer; for the maximum temperatures it is the highest in August and the lowest in February. This totally corresponds (inversely proportional) with the *MAE* (*Fig. 4*), unlike the distribution by years. In addition, in most months, the *PC* of the human forecasts at the minimum temperatures is greater than at the maximum temperatures. At the minimum temperatures, there is a minimum in January, and the maximum is in June; this almost totally corresponds to the *MAE*. There is a difference only in May (the *MAE* in May and June is the same, while the *PC* in May is smaller than in June). This confirms the statement above, that the *MAE* and the *PC* are not necessarily always opposite (in inverse correlation).

In *Fig. 11*, the averaged *PC* of the persistence forecast (*Tmin_In1* and *Tmax_In2*) by months are added to the averaged *PC* of the human forecast (*Tmin* and *Tmax*). The Fig. shows that there is a good correlation between human and the persistence forecast.

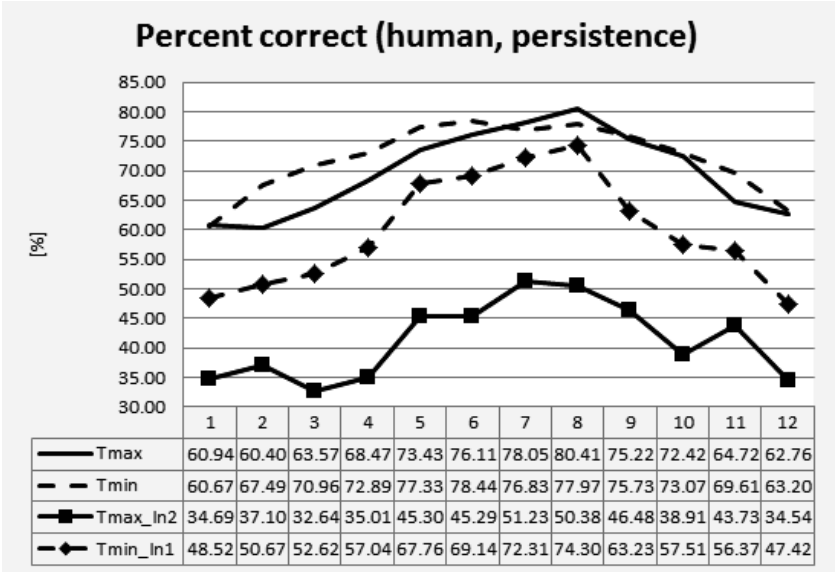

	1	2	3	4	5	6	7	8	9	10	11	12
Tmax	60.94	60.40	63.57	68.47	73.43	76.11	78.05	80.41	75.22	72.42	64.72	62.76
Tmin	60.67	67.49	70.96	72.89	77.33	78.44	76.83	77.97	75.73	73.07	69.61	63.20
Tmax_In2	34.69	37.10	32.64	35.01	45.30	45.29	51.23	50.38	46.48	38.91	43.73	34.54
Tmin_In1	48.52	50.67	52.62	57.04	67.76	69.14	72.31	74.30	63.23	57.51	56.37	47.42

Fig. 11. Monthly averages of *PC* for the minimum and maximum temperatures of the human and persistence forecasts.

In the next figure (*Fig. 12*), we will show what percentage is due to the non-persistence forecast, i.e., we will make the difference: *Tmin-Tmin_In1* and *Tmax-Tmax_In2*.

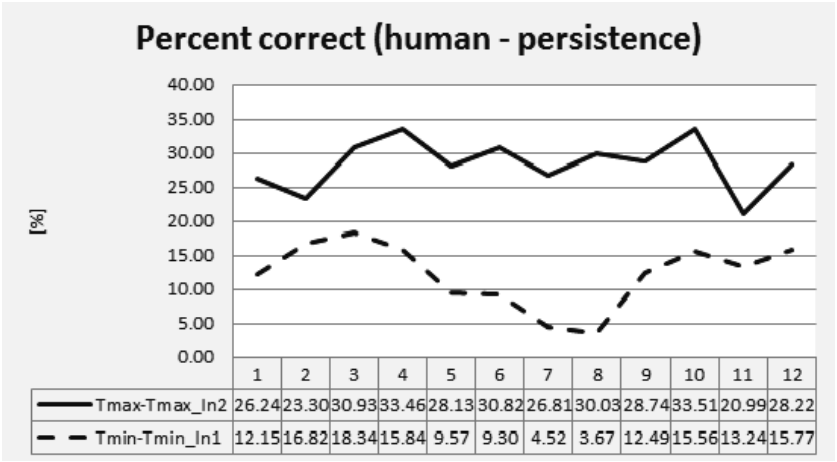

	1	2	3	4	5	6	7	8	9	10	11	12
Tmax-Tmax_ln2	26.24	23.30	30.93	33.46	28.13	30.82	26.81	30.03	28.74	33.51	20.99	28.22
Tmin-Tmin_ln1	12.15	16.82	18.34	15.84	9.57	9.30	4.52	3.67	12.49	15.56	13.24	15.77

Fig. 12. Monthly averages of the *PC* of the human forecast minus the persistence forecast.

Fig. 12 indicates that at the minimum temperatures, the non-persistence forecast changes between 4% and 18%, the minimum of 4% is in July and August, and this is the proof for the big impact of the persistence forecast on the human forecast in summer, when dynamics in the atmosphere are weak. Looking at the situation over the years (*Fig. 13*), it is seen that in August 2010 and 2013, there are even negative values, which means that the persistence forecast is better than the human.

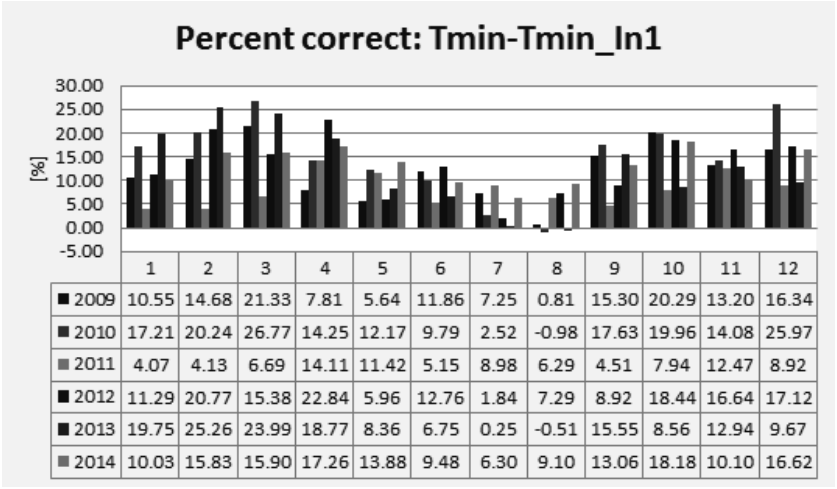

	1	2	3	4	5	6	7	8	9	10	11	12
2009	10.55	14.68	21.33	7.81	5.64	11.86	7.25	0.81	15.30	20.29	13.20	16.34
2010	17.21	20.24	26.77	14.25	12.17	9.79	2.52	-0.98	17.63	19.96	14.08	25.97
2011	4.07	4.13	6.69	14.11	11.42	5.15	8.98	6.29	4.51	7.94	12.47	8.92
2012	11.29	20.77	15.38	22.84	5.96	12.76	1.84	7.29	8.92	18.44	16.64	17.12
2013	19.75	25.26	23.99	18.77	8.36	6.75	0.25	-0.51	15.55	8.56	12.94	9.67
2014	10.03	15.83	15.90	17.26	13.88	9.48	6.30	9.10	13.06	18.18	10.10	16.62

Fig. 13. Monthly and yearly distribution of *PC* for the minimum temperatures of the human forecast minus the persistence forecast.

For the maximum temperatures (*Fig. 12*), the difference between the human and persistence forecasts (with some variations) is also constant, i.e., about 30% of the human are due to the non-persistence forecast (as it was when looking by years). There are two big minima in February and in November – the persistence forecast had higher values (*Fig. 11*). In fact, there is a minimum at the minimum temperatures as well, but it is less pronounced.

3.3. Mean error (ME)

Finally for this study, we will discuss a very important error - the mean error. First, we shall examine it by years (*Fig. 14*), however, here we shall not consider the change over the years, but the concrete values only.

The mean error of the persistence forecast is also included in *Fig. 14*. Looking at the errors (human forecast) of the minimum and maximum temperatures, it is seen that during all of the six years, they have negative values, i.e., there is a systematic underestimate in the minimum and maximum temperatures forecast.

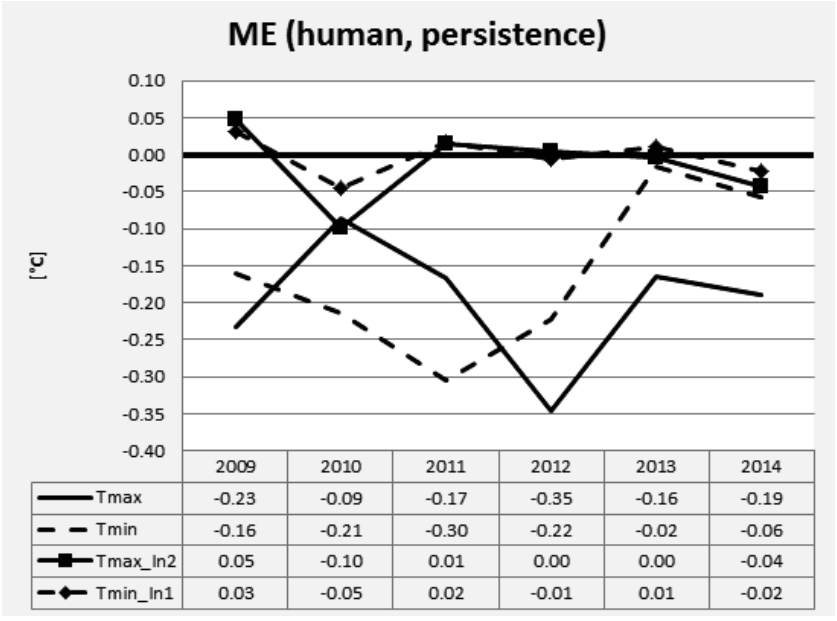

	2009	2010	2011	2012	2013	2014
Tmax	-0.23	-0.09	-0.17	-0.35	-0.16	-0.19
Tmin	-0.16	-0.21	-0.30	-0.22	-0.02	-0.06
Tmax_In2	0.05	-0.10	0.01	0.00	0.00	-0.04
Tmin_In1	0.03	-0.05	0.02	-0.01	0.01	-0.02

Fig. 14. Mean error of the minimum and the maximum temperatures of the human and persistence forecasts through the different years. *Tmin_In1* is the persistence forecast of the minimum temperatures from one day ago, and *Tmax_In2* is the persistence forecast for the maximum temperature from two days ago.

It is also seen that at the minimum temperatures, the biggest systematic error is in 2011, while that at the maximum temperatures is in 2012. It has to be mentioned as well, that over the past two years, the systematic error at the minimum temperatures is very small. Looking at the mean error of the persistence forecast, it is seen that it is very small, almost there is no systematic error. As mentioned above, when elaborating the forecast, the forecaster uses the persistence forecast, the numerical models, and his own experience. Based on personal experience, the numerical models underestimate the maximum temperatures, i.e., they have a negative systematic error (we shall discuss this error in a further work). From everything said till now, a conclusion can be drawn that the systematic error is mainly due to the numerical forecasts and the weather forecasters.

Let us now discuss the situation by months (*Fig. 15*). What impresses is that there is an underestimate (systematic error) from September till April, while during the warm months (from May to August) the deviation is minimal and positive. In other words, during the cold months, the temperatures are underestimated, and during the warm months they are overestimated.

One can say that if the systematic error could be reduced, then the forecast accuracy would be improved. This is, namely, the purpose of this study. To a great extent, this purpose can be achieved through the results in the second panel part, where assessment by stations will be made.

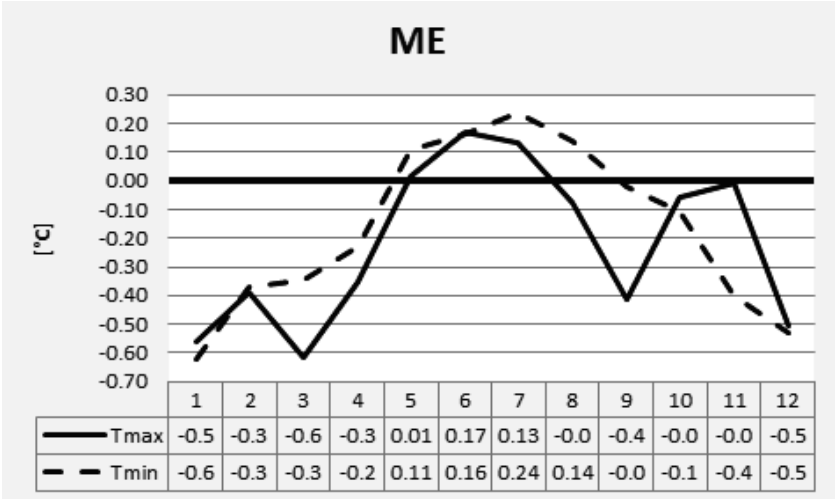

	1	2	3	4	5	6	7	8	9	10	11	12
Tmax	-0.5	-0.3	-0.6	-0.3	0.01	0.17	0.13	-0.0	-0.4	-0.0	-0.0	-0.5
Tmin	-0.6	-0.3	-0.3	-0.2	0.11	0.16	0.24	0.14	-0.0	-0.1	-0.4	-0.5

Fig. 15. Mean error for the minimum and maximum temperatures of the human forecast through the different months.

Next figure (*Fig. 16*) comprises the mean error of the persistence forecast. *Fig. 16* indicates the conclusion, that during the transition months (spring and autumn), there is a bigger systematic error of the persistence forecast, especially at the maximum temperatures.

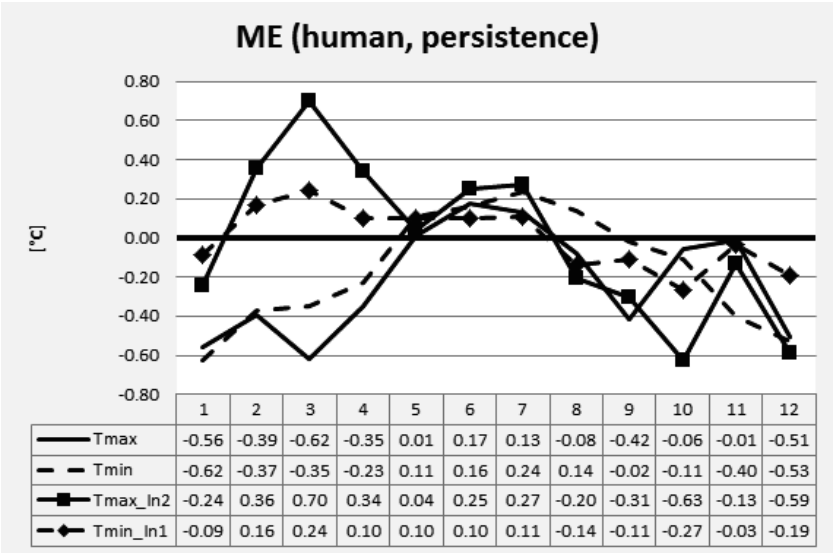

	1	2	3	4	5	6	7	8	9	10	11	12
Tmax	-0.56	-0.39	-0.62	-0.35	0.01	0.17	0.13	-0.08	-0.42	-0.06	-0.01	-0.51
Tmin	-0.62	-0.37	-0.35	-0.23	0.11	0.16	0.24	0.14	-0.02	-0.11	-0.40	-0.53
Tmax_ln2	-0.24	0.36	0.70	0.34	0.04	0.25	0.27	-0.20	-0.31	-0.63	-0.13	-0.59
Tmin_ln1	-0.09	0.16	0.24	0.10	0.10	0.10	0.11	-0.14	-0.11	-0.27	-0.03	-0.19

Fig. 16. Mean error for the minimum and maximum temperatures of the human and persistence forecasts through the different months.

Despite the bigger positive bias of the persistence forecast in spring (February, March, and April), which is more than 0.3 °C, it does not compensate the significant negative mean error in the human forecast. There is an overlap only in September and December, when there is a negative bias of more than 0.3 °C in the maximum temperatures. Thus, it can be stated that the persistence forecast, even by months, does not import a big systematic error in the human forecast. Or, we can say, that by months and by years, the persistence forecast does not bring a serious defect (systematic error) in the human forecast. Therefore, the systematic error in the human forecast is primarily due to the numerical models and the weather forecasters.

4. Conclusion

1. Over the years (2009–2014), the accuracy of the forecasts increases and the *PC* rises in the minimum temperatures with nearly 6%, while in the maximum temperatures with a little more than 4%.
2. The accuracy of the forecast is higher during the warm months (when dynamics of the atmosphere are lower); expressed in the *PC* this difference is nearly 20% (*Fig. 10*).
3. The accuracy of the minimum temperature forecast is greater, which is caused by smaller fluctuations (day to day), compared to the maximum temperatures (*Fig. 3*).
4. The influence of the persistence forecast on the human is great, and it is greater at the minimum temperatures.
5. Human forecast during the cold months underestimates the temperatures, while in the warm months slightly overestimates them.
6. Summarized by years, there is a negative systematic error: an underestimation of the temperatures (*Fig. 14*).
7. The systematic error in the human forecast is mainly due to the numerical models and to the forecasters.

References

Bogatchev, A., 1988: A five-day forecast method of mean daily temperatures and daily precipitation totals. *Probl. Meteorol. Hydrol. 4*, 17–22.

Bogatchev, A., 1994: Statistical schemes for medium-range weather forecast. Abstract of a PHD thesis.

Brier, G.W., 1950: Verification of forecasts expressed in terms of probability. *Month. Weather Rev. 78*, 1–3.

Brier, G.W. and *Allen, R.A*., 1951*:* Verification of weather forecasts. Compendium of meteorology, 841–848.

Fajman, P., 2011: Improved verification and analysis of national weather service point forecast matrices. For the Degree of Master of Science in the Graduate College at the University of Nebraska.

Lashley, S.L., Fisher, L., Simpson, B., Taylor, J., Weisser, S., Logsdon, J., and *Lammers, A.,* 2008: Observing verification trends and applying a methodology to probabilistic precipitation forecasts at a national weather service forecast office. 19th Conf. on Probability and Statistics, New Orleans, LA, Amer. Meteor. Soc., 9.4. http://ams.confex.com/ams/pdfpapers/134204.pdf

Murphy, A.H., 1993: What is a good forecast? An essay on the nature of goodness in weather forecasting. *Weather Forecast. 8,* 281–293.

Ripley, E. and *Archibold, O*., 2002: Accuracy of Canadian short-and medium-range weather forecasts, *Weather 57*, 448–457. https://doi.org/10.1256/wea.245.01

Ruth, D.P., Glahn, B., Dagostaro, V., and *Gilbert, K.,* 2009: The performance of MOS in the digital age. *Weather Forecast. 24,* 504–519. https://doi.org/10.1175/2008WAF2222158.1

Spiridonov, *V.,* 1987: Skill measures of daily extreme temperature forecast. *Probl. Meteorol. Hydrol* 2, 19–26.

Wilk, G.E., 2005: The Temperature and Precipitation Verification Program at WFO Corpus Christi Texas, United States Department of Commerce, National Oceanic and Atmospheric Administration, National Weather Service.

Wilk, G.E., 2007: Temperature and Precipitation Verification Results and Interpretation at WFO Corpus Christi and Other WFOS January 2004 Through June 2006, United States Department of Commerce, National Oceanic and Atmospheric Administration, National Weather Service.

Joint Working Group on Forecast Verification Research: http://cawcr.gov.au/projects/verification/

DOI:10.28974/idojaras.2018.3.3

IDŐJÁRÁS

Quarterly Journal of the Hungarian Meteorological Service
Vol. 122, No. 3, July – September, 2018, pp. 259–283

Spatial analysis of air temperature and its impact on the sustainable development of mountain tourism in Central and Western Serbia

Danijela Vukoičić[1*], **Saša Milosavljević**[1], **Ivana Penjišević**[1], **Nikola Bačević**[1], **Milena Nikolić**[2], **Radomir Ivanović**[1], and **Bojana Jandžiković**[1]

[1] *Department of Geography, Natural Sciences and Mathematics, University of Pristina, 38220 Kosovska Mitrovica, Serbia*

[2] *Belgrade Business School, Higher Education Institution for Applied Studies, 11000 Belgrade, Serbia*

**Corresponding author E-mail: danijela.vukoicic@pr.ac.rs*

(Manuscript received in final form May 29, 2017)

Abstract—Empirical studies of the late twentieth and early twenty-first century indicate the existence of a growth trend in air temperature. This trend is particularly pronounced in the region of Southern Europe, including the Republic of Serbia. Many problems occur in the socio-economic areas due to global warming, which directly influences the development of tourism. In this study, we will deal with the influence of climate change on the sustainable development of mountain tourism in the area of the western and central Serbia tourist zones, which includes Starovlaška and Kopaonik mountain chain. The data on changes in the temperature of air will be gathered at six different altitude meteorological stations, for the period from 1990 to 2014. All weather stations in the studied area were classified into three groups: lowland, middle and high mountain. In order to obtain trends, three sets of data were used: the average monthly temperature, the maximum monthly temperature, and the monthly minimum temperature, recorded in each station. The seasonal classification has been conducted based on four seasons: spring, summer, autumn, and winter. Three statistical approaches were used to analyze the temperature trends in 15 time series, for each group of stations individually. First, the trend equation was calculated for each time series, then, completely separate from the first approach, all trends were assessed using the Mann-Kendall test, and in the end, in all cases, the trend magnitude was calculated based on the trend equation. The results show that there is a significant positive trend of temperature rise on an annual basis, while the trend is significantly positive during the fall and spring seasons. In winter, the trend is slightly positive or absent, while in the summer trend is moderately positive in all three groups of stations.

Key-words: analysis of temperature, sustainable development, mountain tourism, turist zone, Serbia

1. Introduction

The analysis of the mean value of air temperature changes in the last couple of decades is an important theme of climate research. The studies include different regions in the world, and the scales show that there is an air temperature growth trend during the twentieth century (*Jones* and *Moberg*, 2003; *Luterbacher et al.,* 2004; *Rebetez* and *Reinhard,* 2008; *Manabe et al.,* 2011; *Tabari* and *Talaee*, 2011; *Christy*, 2013; *Wang et al.,* 2014; *Kuang et al.,* 2014; *Omondi et al.,* 2014; *Croitoru et al.,* 2014). According to the Intergovernmental Panel on Climate Change report (*IPCC*, 2007), Europe is isolated as one of the regions especially sensitive to climate change. It is pointed out that climatic changes can increase regional differences concerning natural resources and their values. Mean annual temperatures in Europe in the last fifty years have increased faster than the global average. One of the regions where especially significant warming has been recorded is the southeast part of Europe. High temperatures can lead to a gradual decrease of summer tourism in the Mediterranean, but also to an increase in spring and autumn tourism. Ski resorts in Europe can be affected by a significant reduction in snow cover at the beginning and end of the winter season, which can significantly affect the overall economic development (*Unger et al.,* 2016).

The Intergovernmental Panel on Climate Change report (*IPCC*, 2014) made a conclusion that the human impact on the climate is indisputable and that the effects can be seen in several regions of the world. High mountainous regions are the most exposed to big climate changes (*Diaz* and *Bradley*, 1997; *Croitoru et al.,* 2014, 2016). The consequences of this are reflected in the different socio-economic and ecological areas: tourism industry, health of human population, ecosystems, mountain glaciers, water resources (Mountain Agenda, 1998; *Beniston*, 2003, 2005; *Walther et al.,* 2005; *Boisvenue* and *Running*, 2006; EEA, 2008; *Micu*, 2009, 2012; *Toreti et al.,* 2010; *Croitoru et al.,* 2014, 2016). There are a number of studies dealing with the analysis of climate change in Serbia. Observed mean annual temperature in the last 50 years show a positive trend almost everywhere in Serbia. It is expected that the increase in temperature has a different trend during different seasons, up to 0.04 °C per year. The greatest increase in temperature is recorded during the fall period. The analysis of climate change through temperature trends was done on annual and seasonal levels for the whole territory of Serbia (*Popović et al.,* 2005, 2009).

The individual linear trends were not measured for the stations in the mountainous areas of Serbia, neither were the impacts of climate change on tourism development in the region. The Republic of Serbia has a lot of potential for the development of mountain tourism, but only 30% are utilized (*Milijić et al.,* 2013). These are high mountain areas above 1500 m above sea level (Kopaonik), and partly the medium height mountains, from 1000 to 1500 m high (Zlatibor, Tara, Zlatar). Given that previously performed studies of the highest

areas of Serbia (western and central tourist zones of Serbia) are modest and insufficient, the aim of this paper is to analyze temperature trends and highlight their impact on the sustainable development of mountain tourism.

2. Materials and methods

2.1. Area

The research area is a mountainous area in Serbia that includes mountains of Starovlaška and Kopaonik, as well as part of a western zone under younger fold mountains. In structural terms, the western zone of younger fold mountains belong to the Dinaric Alps in the broad sense (*Rodic* and *Pavlovic*, 1994). It is part of the southern Alpine orogenic belt. It was formed during the late Alpine orogeny in a spacious geosyncline of Tethys. According to the geological structure, impervious Paleozoic rocks occupy the largest space, although Starovlaška mountains contain Mesozoic limestone as well. According to the spatial plan of the Republic of Serbia in 1996, the area of research belongs to the Western and Central Serbia tourist zone (*Jovičić*, 2009). In the regional organization of Serbian tourist area, Zlatibor tourist region (Tara-Zlatibor-Zlatar) belongs to the Western tourist zone, while Kopaonik and Golija belong to the Central tourist zone *(Fig. 1)*.

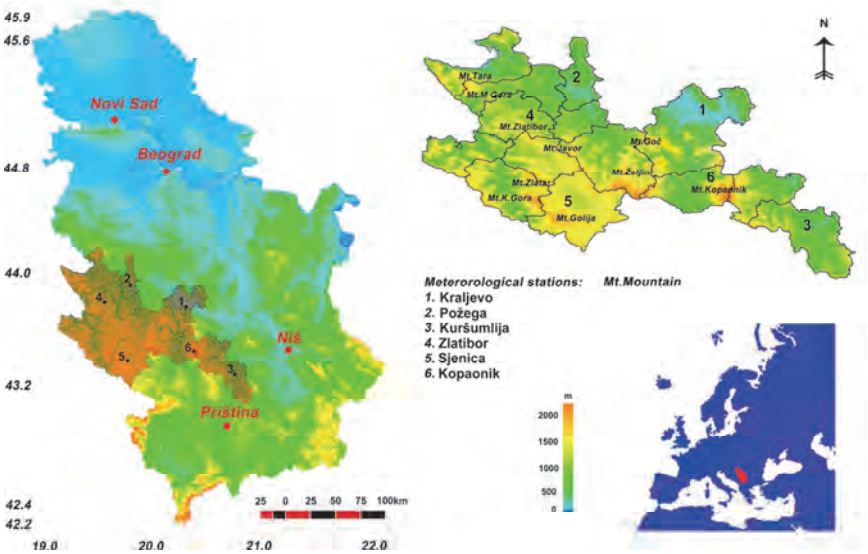

Fig. 1. Western and Central Serbia tourist zone and spatial distribution of the analyzed meteorological stations on the Serbian map.

2.2. Data

This work contains an analysis of surface air temperature trends obtained for six meteorological stations. The locations of the stations are presented in *Fig. 1*, and their main parameters are given in *Table 1* in accordance with the Hydrometeorological Service of Serbia (http://www.hidmet.gov.rs/). Weather stations are divided into three groups depending on the altitude of the area for the period (*P*) from 1990 to 2014. The western tourist zone has an altitude of 1500 m, the central tourist zone reaches 2017 m, and the valley areas of these zones range from 200 m to 500 m (*Marović*, 2001). Based on that, the cells are grouped into three groups: lowland (*L*), medium-sized mountains (*M1*), and high mountains (*M2*).

Table 1. List of meteorological stations and their geographical coordinates and elevations

Number	Meteorological station	Latitude (°N)	Longitude (°E)	Elevation (m)
1.	Kraljevo	43°43'	20°42'	215
2.	Požega	43°50'	20°02'	310
3.	Kuršumlija	43°08'	21°16'	383
4.	Zlatibor	43°44'	19°43'	1027
5.	Sjenica	43°17'	20°00'	1038
6.	Kopaonik	43°17'	20°48'	1711

In order to obtain trends, three sets of data were used: the average monthly temperature, the maximum monthly temperature, and the minimum monthly temperature for each station. Using the average monthly temperature, the minimum average annual temperature and the maximum average annual temperature have been calculated, as well as the average annual temperature and the average seasonal temperature for each season. Finally, based on these three types of average air temperature, new data sets for each month referred to as *T*, *Tx*, *Tn* are derived, for calculating trends for three lowland stations (*L*): Kraljevo, Požega, and Kuršumlija; two stations in the medium-sized mountains (*M1*): Zlatibor and Sjenica, while Kopaonik was treated as a separate data set, because it is a high mountain station (*M2*).

Seasons definitions are used: winter (*W*), spring (*Sp*), summer (*Su*), and autumn (*A*), which are arranged in divided into sets of three months: January, February, and March; April, May, and June; July, August, and September; and October, November, and December (*Hrnjak et al.,* 2014), respectively (*Gavrilov et al.,* 2015).

During this research, the database was formed according to the year (*Y*), season (*W*, *Sp*, *Su*, *A*), and three types of temperatures (*T*, *Tx*, and *Tn*). There are 15 stations in each group, 45 time series in total (*15x3*), which are used to determine the trend. Each of these 15 stations is marked with the acronym consisting of the abbreviation for the year/season and type of temperature *(Table 2).*

Table 2. List of 15 time series to calculate surface air temperature trends

	Year (Y)	**Winter (W)**	**Spring (Sp)**	**Summer (Su)**	**Autumn (A)**
T	*YT*	*WT*	*SpT*	*SuT*	*AT*
Tx	*YTx*	*WTx*	*SpTx*	*SuTx*	*ATx*
Tn	*YTn*	*WTn*	*SpTn*	*SuTn*	*ATn*

Before the previous calculation, the homogeneity of the temperature data was examined according to the *Alexandersson* (1986) test. The test showed that the time series are not non-homogeneous for a significance level of 5% (*Gavrilov et al*., 2017).

2.3. Methodology

We adopted three statistical approaches in order to analyze the temperature trends in 15 time series, for each group of stations individually. First, we calculated the trend equation for each time series using linear interpolation of the mean annual and seasonal temperatures (*Feidas et al.,* 2004). When the coefficient direction of the trend equation is greater than zero, the trend is positive, when it is less than zero, the trend is negative, and when it is equal to zero, there is no trend (no change). Completely independent of the first approach, in the second one we used the Mann-Kendall test (hereinafter MK test) in order to assess the significance of temperature trends (*Kendall*, 1938, 1975; *Mann*, 1945; *Gilbert*, 1987). This test is widely applicable in the climatological time series. Ultimately, the trend magnitude in all cases was calculated using the trend equation (*Gavrilov et al.,* 2015, 2016, 2017).

According to the MK test, two hypotheses were tested: the null hypothesis, H_0, when the trend is absent in the time series; and the alternative hypothesis, H_a, when there is a significant trend in the series, for a given level of significance. The probability, *p*, was calculated to determine the level of confidence in the hypothesis.

In the following study, the brief mathematical procedure for the hypothesis, test, and assessment of the significance of the temperature trends will be

described. A key step in the application of MK test is the calculation of the MK statistics (*Karmeshu*, 2012):

$$S = \sum_{i=1}^{n-1} \sum_{j=i+1}^{n} \operatorname{sgn}\left(T_j - T_i\right), \tag{1}$$

where:

$$\operatorname{sgn}\left(T_j - T_i\right) = \begin{cases} 1 & if \quad T_j - T_i > 0 \\ 0 & if \quad T_j - T_i = 0 \\ -1 & if \quad T_j - T_i < 0 \end{cases}. \tag{2}$$

Here, T_j and T_i are the time series of the annual and/or seasonal values of the temperatures in years $j = i + 1$, $i + 2$, $i + 3$,...,n and $i = 1, 2, 3,..., n\text{-}1$, where $j > i$, and n is the last year in the time series.

As seen in Eqs. (1) and (2), if the temperature from the later year is higher than the temperature from the earlier year, S is incremented by 1. On the other hand, if the temperature from the later year is lower than the temperature of the earlier year, S is decremented by 1. The net result of all such increments and decrements yields the final value S. Statistics S can serve for evaluation of the temperature trend, because a very high positive value of S is an indicator of an increasing trend, and a very low negative value of S indicates a decreasing trend. However, to statistically quantify the significance of the trend, it is necessary to compute the probability associated with S and the number of years, n.

Now, we will describe the procedure to compute this probability. For this purpose, the normalized/standard test statistic Z is calculated as:

$$Z = \begin{cases} \dfrac{S-1}{\sigma} & for \quad S > 0 \\ 0 & for \quad S = 0 \\ \dfrac{S+1}{\sigma} & for \quad S < 0 \end{cases}, \tag{3}$$

where σ^2 is the variance for the approximately normally distributed statistics S for $n \geq 10$. Finally, for measuring the significance of the temperature trend, the probability p is computed as:

$$p = \left[1 - f\left(Z\right)\right] \cdot 100 . \tag{4}$$

Here, $f(Z)$, as the probability density function for a normal distribution with a mean of 0 and a standard deviation of 1, is given by the following equation:

$$f(z)=\frac{1}{\sqrt{2\pi}}\exp\left(-\frac{Z^2}{2}\right). \quad (5)$$

As seen in Eq. (4), the probability p takes values between 0 and 100 in %. In fact, p is used to test the level of confidence in the hypothesis (*Gavrilov et al.,* 2010, 2011, 2013, 2015). If the computed value p is lower than the chosen significance level, α *(e. g.,* α=5%*),* the H_0 (*there is no trend*) should be rejected, and the H_a (*there is a significant trend*) should be accepted; and if p is greater than the significance level, the H_0 cannot be rejected. We used XLSTAT software (http://www.xlstat.com/) for calculating the probability, p, and hypothesis testing.

It is considered that accepting the H_a indicates that a trend is statistically significant. On the other hand, acceptance of the H_0 implies that there is no trend (no change), while often in practice, the trend equation indicates the opposite*,* i. e., there is a trend. Therefore, to reduce the contradiction in analyzing the temperature trends between two independent statistical approaches, trend equation, and applying the previous or classical interpretation of the MK test, the modified interpretation of the MK test will be used (*Gavrilov et al.,* 2015).

It is quite clear that with decreasing the probability p, the statistical confidence in the H_0 is decreasing and the confidence in the H_a is increasing, and vice versa. For the purposes of this study, a modified MK test with four levels of confidence was declared. Based on the computed probability p, these four levels of confidence are: less or equal than 5%: *there is a significant positive/negative trend*; greater than 5% and less or equal than 30%: *there is a moderately positive/negative trend*; greater than 30% and less or equal than 50%: *there is a slightly positive/negative trend*, and greater than 50%: *there is no trend.*

As it can be seen, in cases (a) and (d) both interpretations of the MK tests have the same meaning. Differences occur in cases (b) and (c), where the classical MK test claims there is no trend, and the modified MK test allows trend with reduced levels of confidence. It is clear that modified interpretation is more subtle, and it enables obtaining diverse assessments (*Gavrilov et al.,* 2015).

Namely, the modified Mann–Kendall test is used for smoother quantization of confidence levels than the regular Mann-Kendall test. The Modified Mann–Kendall test just verifies the results obtained by the direct method (for positive trend, the modified Mann-Kendall test shows positive moderate trend in cases when by observing Mann-Kendall tests no trend is detected because of more robust quantization of confidence level).

In the third statistical approach, *the trend magnitude* was calculated as:

$$\Delta y = y(1990) - y(2014), \quad (6)$$

where Δy is the trend magnitude in °C, y (1990) and y (2014) are temperatures from the trend equation in the beginning, 1990, and at the end, 2014, of the period, both in °C. When Δy is greater than zero, less than zero, or equal to zero, the sign of the trend is *negative* (decrease), *positive* (increase), or *no trend* (no change), respectively. Moreover, when Δy is less than or equal to the standard error of the temperature measurement, certainly *there is no trend* (*Gavrilov et al.,* 2015).

3. Results and discussion

Each of *Figs. 4–12* shows annual and seasonal temperatures during the period 1990–2014, the trend equation, where y is the mean annual and seasonal value of the temperature in °C, x is the time in years; and the trend line. The probability confidence, p, and the trend magnitude, Δy, for each time series over the territory of the western and central tourist zones of Serbia are shown in *Tables 4–6*, respectively. In all cases, the significance level was the same, α=5% (*Karmeshu*, 2012; *Gavrilov et al.,* 2017).

Table 3. Probability confidences and trends magnitudes for all time series for the group of stations *L*

	T		***Tx***		***Tn***	
	***p* [%]**	***Δy* [°C]**	***p* [%]**	***Δy* [°C]**	***p* [%]**	***Δy* [°C]**
Y	0.19	–1.35	2.23	–1.225	0.05	–1.4
W	42.72	–1.025	90.26	0.075	20.92	–1.55
Sp	3.43	–1.4	11.96	–1.475	1.72	–1.1
Su	4.97	–1.55	27.50	–1.475	4.40	–1.475
A	4.19	–1.1	6.27	–1.4	4.19	–1

Table 4. Probability confidences and trends magnitudes for all time series for the group of stations *M1*

	T		***Tx***		***Tn***	
	***p* [%]**	***Δy* [°C]**	***p* [%]**	***Δy* [°C]**	***p* [%]**	***Δy* [°C]**
Y	0.63	–1.325	0.23	–1.675	0.15	–1.425
W	78.77	0.6	24.76	–0.9	33.81	–1.6
Sp	2.31	–2.075	4.40	–2.9	0.51	–1.525
Su	20.56	–1.65	17.52	–2.425	3.01	–1.425
A	7.87	–1.3	5.29	–1.875	7.87	–1.025

Table 5. Probability confidences and trends magnitudes for all time series for the group of stations *M2*

	T		*Tx*		*Tn*	
	p **[%]**	***Δy*** **[°C]**	***p*** **[%]**	***Δy*** **[°C]**	***p*** **[%]**	***Δy*** **[°C]**
Y	0.36	–1.3	0.62	–1.35	0.24	–1.2
W	71.33	–0.175	78.77	0.675	39.89	–0.675
Sp	1.50	–1.875	6.27	–2.2	1.13	–1.55
Su	24.34	–1.625	19.70	–1.875	14.97	–1.225
A	5.60	–1.45	4.18	–1.8	7.80	–1.25

Average maximum temperatures (*Tx*) in the area of the western and central tourist zones of Serbia for the period 1990–2014 are summarized in *Fig. 2*, which clearly indicates the observed temperature difference. In lowland areas (Kraljevo, Kuršumlija, and Požega), *Tx* ranges from 16.7 to 17.5 °C, in the middle-sized venues (Sjenica and Zlatibor) it is 13 °C, and in the higest mountainous areas (Kopaonik) *Tx* is 8 °C.

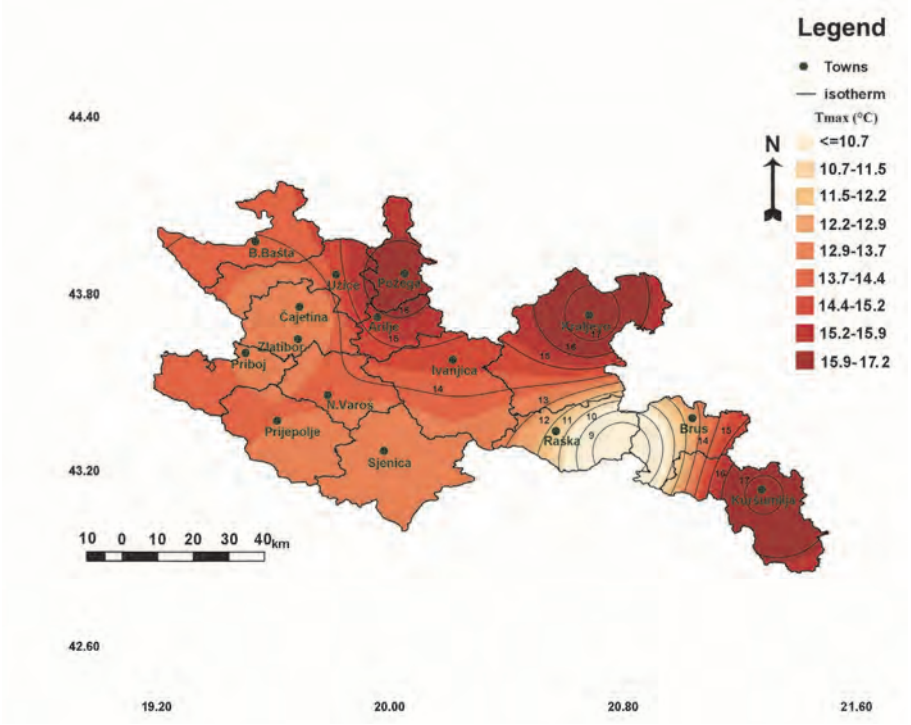

Fig. 2. Mean maximum air temperature (Tx) on an annual basis in the western and central tourist zones of Serbia for the period from 1990 to 2014.

Fig. 3 shows the distribution average of minimum temperature (*Tn*). In the lowland areas of the western and central tourist zones, *Tn* ranges from 4.8 to 6.6 °C (Požega, Kraljevo, and Kuršumlija), and this difference is more pronounced in some areas of the middle-size mountain ranging from 1.5 °C (Sjenica) to 4.1 °C (Zlatibor). The highest mountain areas (Kopaonik) have an average minimum temperature (*Tn*) of 0.5 °C.

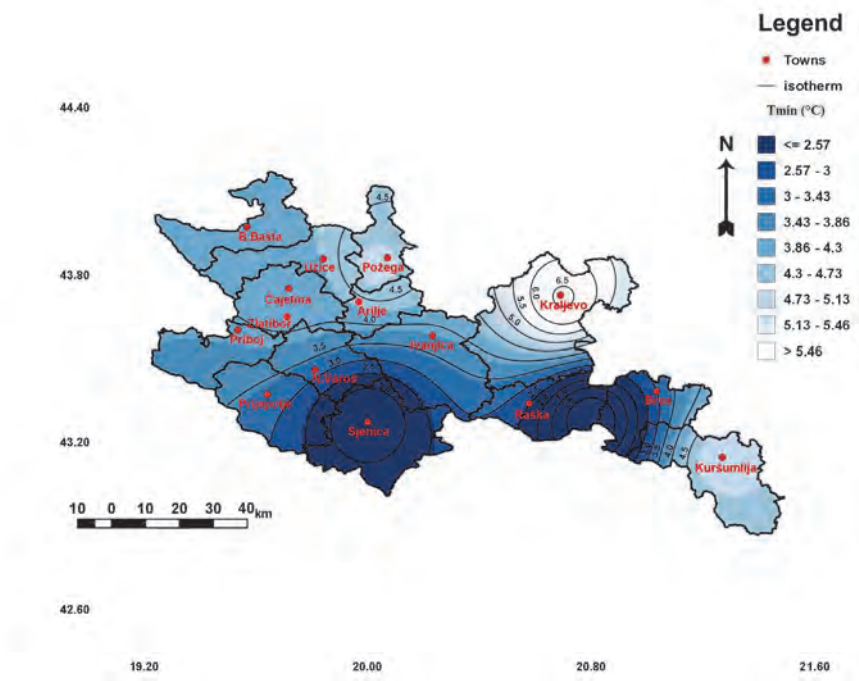

Fig. 3. Mean minimum air temperature (*Tn*) on an annual basis in the western and central tourist zones of Serbia for the period from 1990 to 2014.

In strictly formal terms, some trends can be observed in all cases. However, all trends do not have the same positive or negative sign, probability, and magnitude. In order to obtain a final evaluation of the temperature trends in the western and central tourist zones, all numerical parameters, the visual representation of trends and, most importantly, the results of both MK tests were used.

Figs. 4–6 and trend equations show that for the time series *YT*, *WT*, *SpT*, *SuT*, *AT*, *YTx*, *SpTx*, *SuTx*, *ATx*, *YTn*, *WTn*, *SpTn*, *SuTn*, and *ATn*, trends are positive; and in the cases of *WTx*, the trends are negative. MK testing will prove whether these statements are true.

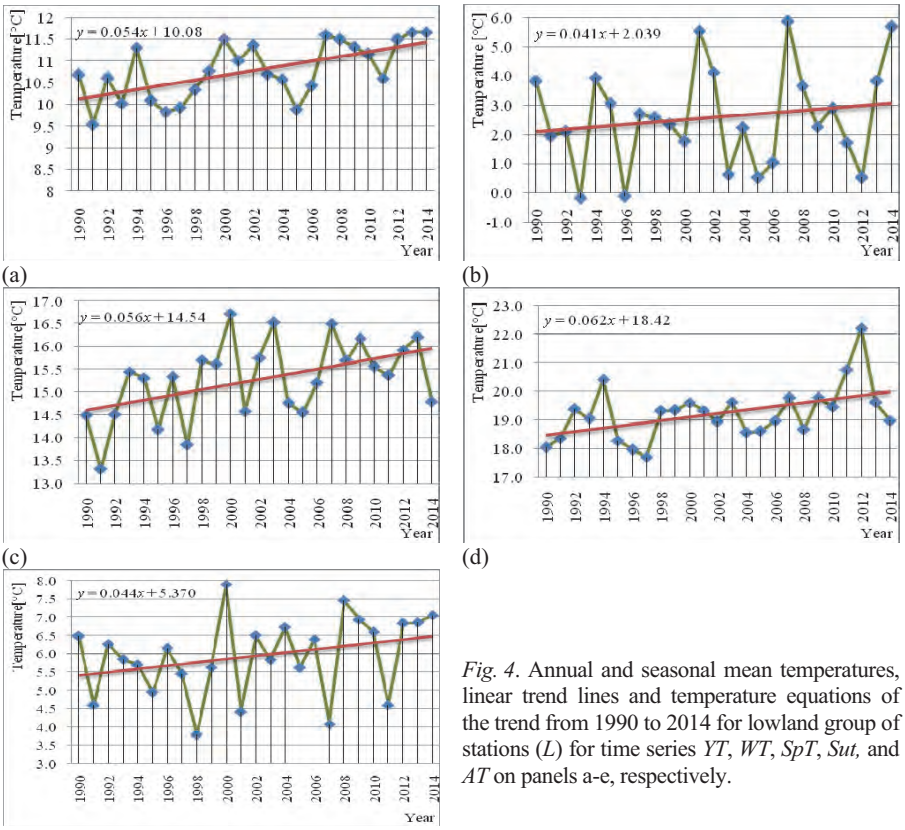

Fig. 4. Annual and seasonal mean temperatures, linear trend lines and temperature equations of the trend from 1990 to 2014 for lowland group of stations (*L*) for time series *YT*, *WT*, *SpT*, *Sut,* and *AT* on panels a-e, respectively.

Results shown in *Fig. 4* and *Table 3* where futher analyzed to estimate the final trends. As the computed values of probability *p* fot the time series *YT, SpT, SuT* and *AT* is lower than the level of significance of α=5%, the null hypothesis H_0 should not reject, and alternative hypothesis H_a is accepted. The risks to reject the null hypothesis are smaller than 4.97% for all time series. The calculated *p*-value of the time series *WT* is greater than the level of significance of α=5%, so we can reject the null hypothesis H_0. The risk to reject the null hypothesis H_0 while it is true is 42.72%. In accordance with the classical MK tests, the first, third, fourth, and fifth cases have a *positive trend*, while the second case is *without trend*. The modified MK test declared that the first, third, fourth, and fifth cases have *positive significant trend,* while the second have *slightly positive trend.*

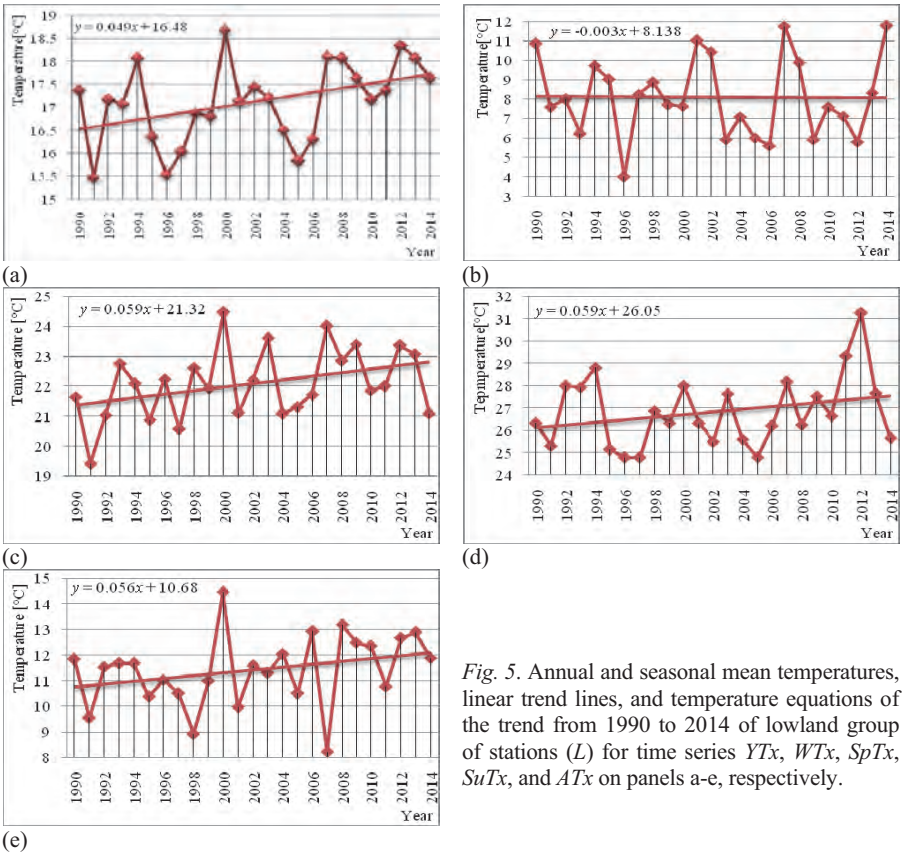

Fig. 5. Annual and seasonal mean temperatures, linear trend lines, and temperature equations of the trend from 1990 to 2014 of lowland group of stations (*L*) for time series *YTx*, *WTx*, *SpTx*, *SuTx*, and *ATx* on panels a-e, respectively.

Based on the observed results presented in *Fig. 5* and *Table 3*, the hypothesis was futher analyzed. Since the calculated value of *p* of the time series *YTx* is lower than the level of significance α=5%, the null hypothesis H_0 should be reject, and the alternative hypothesis H_a is accepted. The risk to reject the null hypothesis is less than 2.23%. The calculated *p* value of the time series *WTx, SpTx, SuTx* and *ATx* are higher than the level of significance of α=5%, so it can not reject the null hypothesis H0. The risk to reject the null hypothesis H0 while it is true is 90.26, 11.96, 27.50, and 6.27 (all in %) for all time series, respectively. In accordance with the classical MK tests, the second, third, fourth, and fifth cases are without trend, while the first case has a trend. The modified MK test declared that the third, fourth and fifth cases have *moderately positive trend*, the first has *positive significant trend,* while the second case is *without trend*.

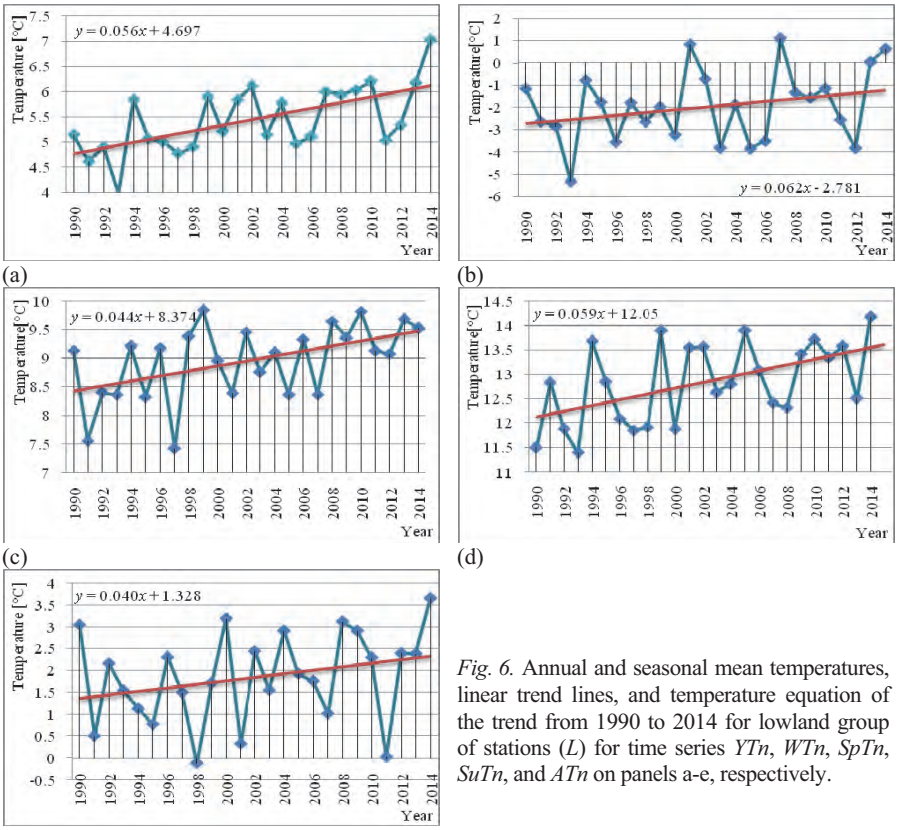

Fig. 6. Annual and seasonal mean temperatures, linear trend lines, and temperature equation of the trend from 1990 to 2014 for lowland group of stations (*L*) for time series *YTn*, *WTn*, *SpTn*, *SuTn*, and *ATn* on panels a-e, respectively.

Fig. 6 and *Table 3* give the values of the analyzed hypothesis. Since the calculated *p* value of the time series *YTn, SpTn, SuTn,* and *ATn* is lower than the significance level α=5%, we should reject the null hypothesis H_0 and accept the alternative hypothesis H_a. Risks to reject the null hypothesis are less than 4.40% for all time series. The calculated *p* value of the time series *WTn* is greater than the level of significance of α=5%, so we can reject the null hypothesis H_0. The risk to reject the null hypothesis H_0 while it is true is 20.92%. In accordance with the classical MK tests, the first, third, fourth, and fifth cases have a trend, while the second case is without trend. The modified MK test declared that the first, third, fourth, and fifth cases have *positive significant trend,* while the second case has *moderately positive trend.*

Figs. 7–9 and trend equations show that for the time series *YT*, *SpT*, *SuT*, *AT*, *YTx*, *WTx*, *SpTx*, *SuTx, ATx*, *YTn*, *WTn*, *SpTn*, *SuTn*, and *ATn* trends are positive; and in the *WT* cases the trends are negative. MK testing will prove whether these statements are true.

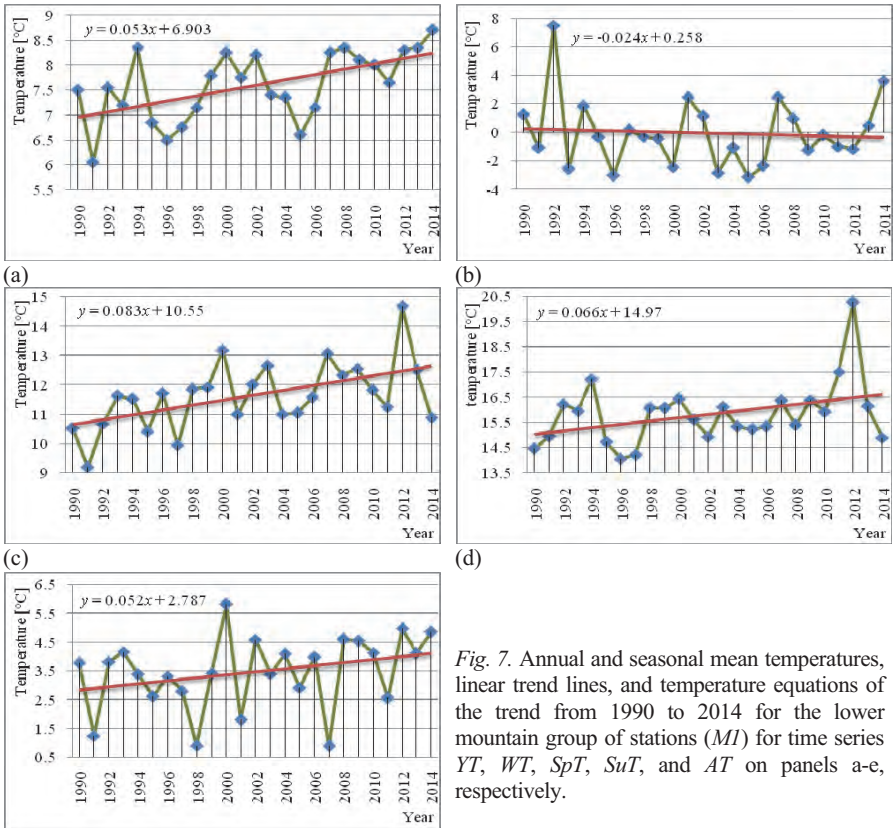

Fig. 7. Annual and seasonal mean temperatures, linear trend lines, and temperature equations of the trend from 1990 to 2014 for the lower mountain group of stations (*M1*) for time series *YT*, *WT*, *SpT*, *SuT*, and *AT* on panels a-e, respectively.

Results of the mean annual and seasonal temperature for the lower mountain group of station (*M1*) are shown in *Fig. 7* and *Table 4.* The calculated *p* value of the time series *YT* and *SpT* is lower than the level of significance of α=5%, so we can reject the null hypothesis H_0 and to accept the alternative hypothesis H_a. The risk to reject the null hypothesis is lower than 2.31% in both series. The calculated *p* value of the time series *WT, SuT* and *AT* is greater than the level significance of α=5%, so we can reject the null hypothesis H_0. The risks to reject the null hypothesis while it is true are 78.77, 20.56, and 7.87 (all in %) for all time series, respectively. In accordance with the classical MK tests, the first and third cases have a trend, the second, fourth, and fifth cases are without trend. The modified MK test declared that the first and third case have *positive significant trend,* the fourth and fifth cases have *moderately positive trend,* while the second case is *without trend.*

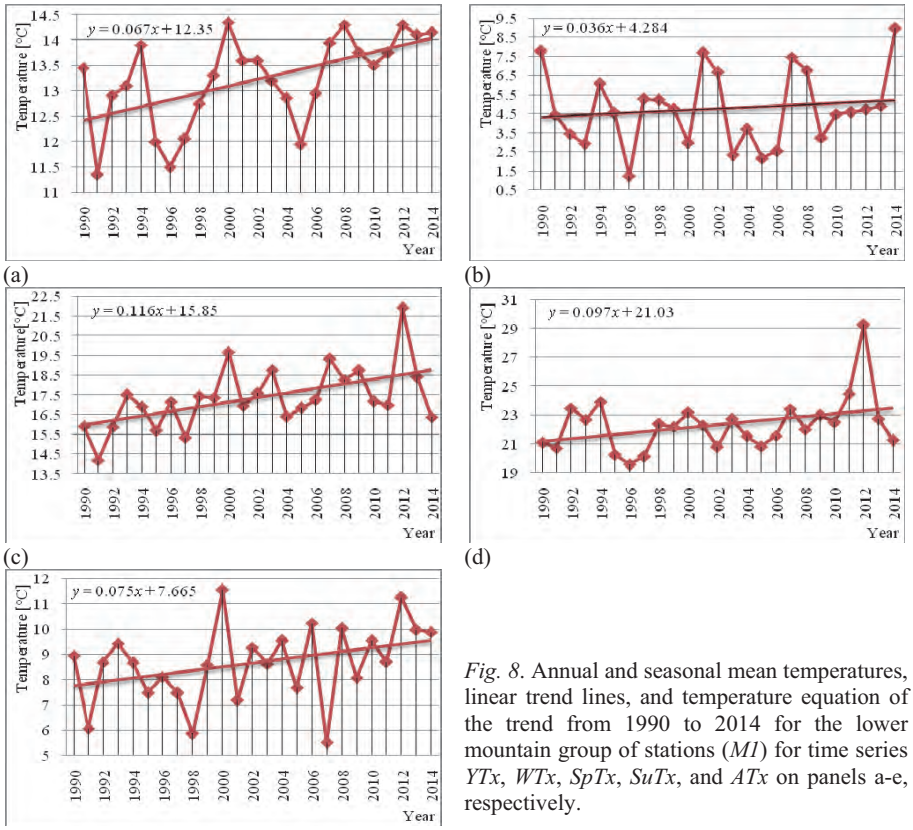

Fig. 8. Annual and seasonal mean temperatures, linear trend lines, and temperature equation of the trend from 1990 to 2014 for the lower mountain group of stations (*MI*) for time series *YTx*, *WTx*, *SpTx*, *SuTx*, and *ATx* on panels a-e, respectively.

Fig. 8 and *Table 4* give the results of the analyzed hypotheses. As the computed values of probability *p* for the time series *WTx, SuTx* and *ATx* are greater than the significance level α=5%, the H_0 cannot be rejected in all cases. The risks to reject the null hypothesis while it is true are 24.76, 17.52, and 5.29 (all in %) for all time series, respectively. In accordance with the classical MK tests, the second, fourth, and fifth cases are without trend. The modified MK test declared that all cases have *moderately positive trend.*

As the computed probability value *p* for the time series *YTx* and *SpTx* are lower than the significance level α=5%, the H0 should be rejected, and the Ha should be accepted for both time series. The risks to reject the null hypothesis are lower than 4.40%. The statement that there is a significant trend is correct with probabilities greater than 95.60% in both MK tests.

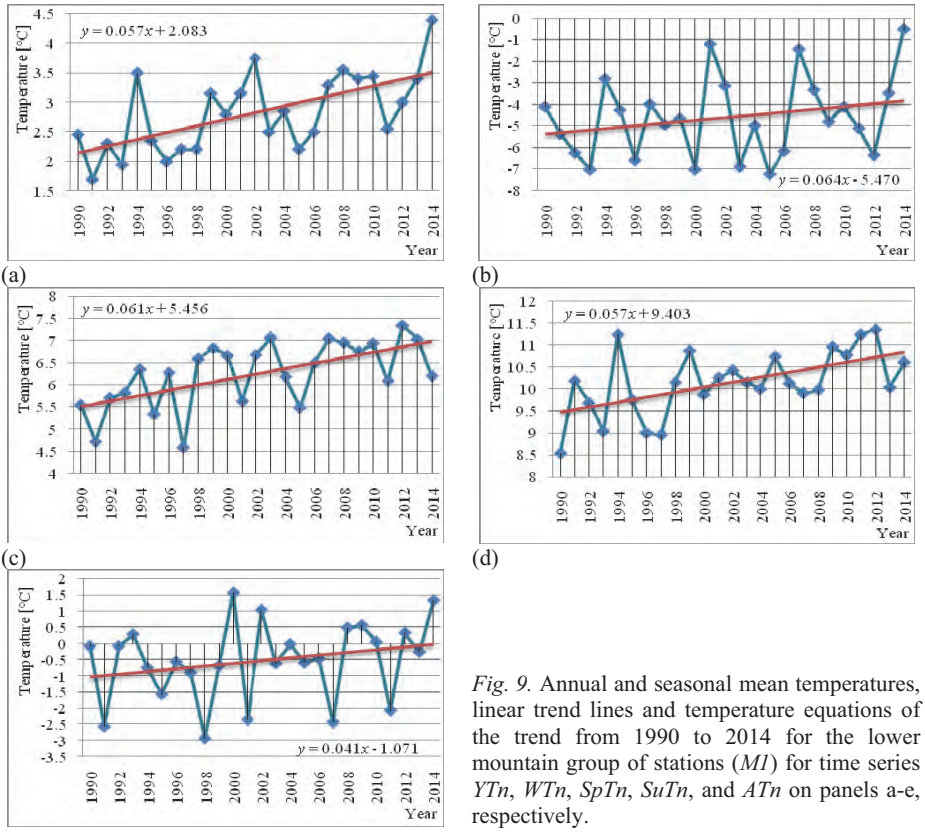

Fig. 9. Annual and seasonal mean temperatures, linear trend lines and temperature equations of the trend from 1990 to 2014 for the lower mountain group of stations (*M1*) for time series *YTn*, *WTn*, *SpTn*, *SuTn*, and *ATn* on panels a-e, respectively.

Fig. 9 and *Table 4* show the results which were further analyzed. As the computed values of probability *p* for the time series *WTn* and *ATn* are greater than the significance level *a*=5%, the H0 cannot be rejected in all cases. The risks to reject the null hypothesis while it is true are 33.81 and 7.87%. In accordance with the classical MK tests, the second and fifth cases are without trend, while the modified MK test declared that second case has slightly positive trend, and the fifth case has *moderately positive trend.*

As the computed probability *p* value for the time series *YTn*, *SpTn,* and *SuTn* are lower than the significance level *a*=5%, the H_0 should be rejected and the H_a should be accepted for both time series. The risks to reject the null hypothesis are lower than 3.01%. The statement that there is a significant trend is correct with probabilities greater than 96.99% in both MK tests.

Figs. 10–12 and trend equations show that for the time series *YT, WT, SpT*, *SuT, AT, YTx, SpTx, SuTx, ATx, YTn, WTn, SpTn, SuTn* and *ATn* trends are positive; and in the case *WTx*, the trend is negative. MK testing will prove whether these statements are true.

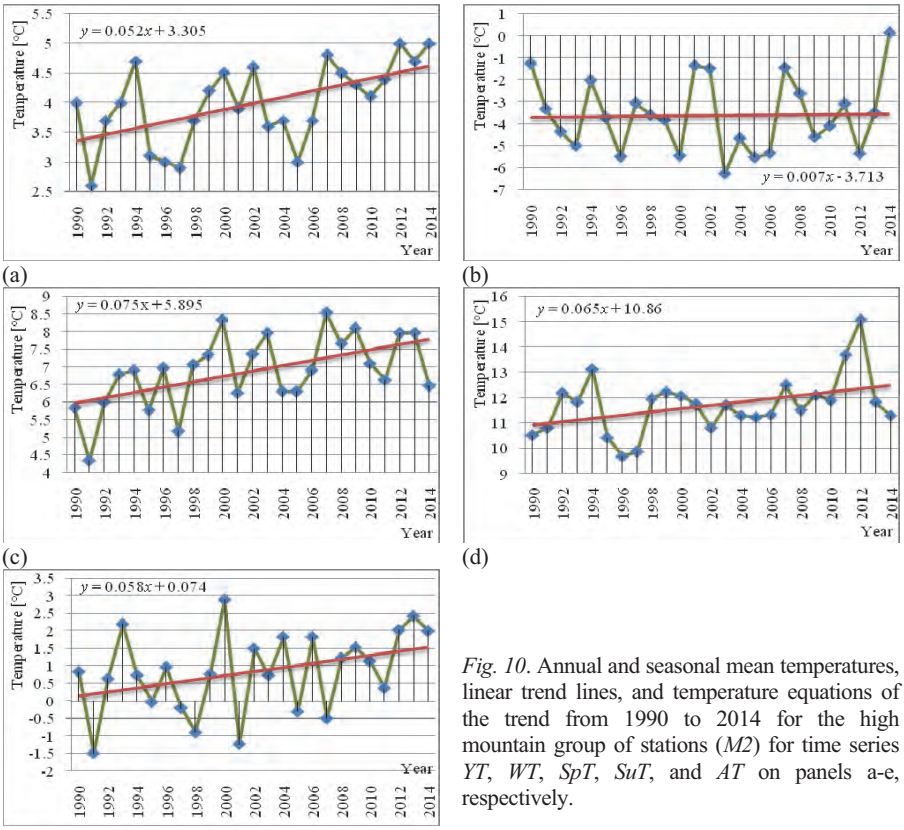

Fig. 10. Annual and seasonal mean temperatures, linear trend lines, and temperature equations of the trend from 1990 to 2014 for the high mountain group of stations (*M2*) for time series *YT*, *WT*, *SpT*, *SuT*, and *AT* on panels a-e, respectively.

Results of the mean annual and seasonal air temperature for the high mountainous group of stations (*M2*) are shown in *Fig. 10* and *Table 5.* As the computed values of probability *p* for the time series *WT, SuT*, and *AT* are greater than the significance level α=5%, the H_0 cannot be rejected in all cases. The risks to reject the null hypothesis when it is true are 71.33, 24.34, and 5.60 (all in %) for all time series, respectively. In accordance with the classical MK tests, it can be declared that there was no trend in all cases, while the modified MK test declared that the second case has *no trend,* and the fourth and fifth cases have *moderately positive trend.*

As the computed probability value *p* for the time series *YT* and *SpT* are lower than the significance level *a*, the H_0 should be rejected and the H_a should be accepted for both time series. The risks to reject the null hypothesis are lower than 1.50%. The statement that there is a significant trend is correct with probabilities greater than 98.50% in both MK tests.

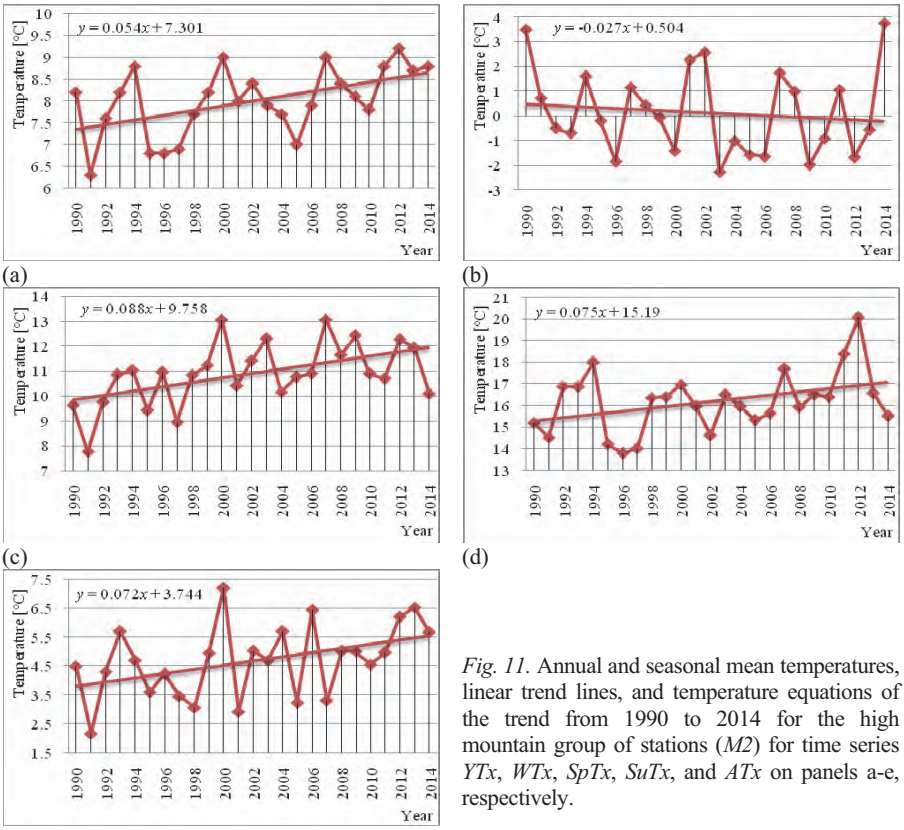

Fig. 11. Annual and seasonal mean temperatures, linear trend lines, and temperature equations of the trend from 1990 to 2014 for the high mountain group of stations (*M2*) for time series *YTx*, *WTx*, *SpTx*, *SuTx*, and *ATx* on panels a-e, respectively.

Fig. 11 and *Table 5* show the results of the hypotheses, which were futher analyzed for the final assessment of trends in air temperature. As the computed values of probability *p* for the time series *WTx, SpTx,* and *SuTx* are greater than the significance level *a*=5%, the H_0 cannot be rejected in all cases. The risks to reject the null hypothesis while it is true are 78.77, 6.27, and 19.70 (all in %) for all time series, respectively. In accordance with the classical MK tests, the second, third and fourth case are *without trend*, while the modified MK test declared that third and fourth case have *moderately positive trend,* and second case have *no trend.*

As the computed probability value *p* for the time series *YTx* and *ATx* are lower than the significance level *a*, the H_0 should be rejected, and the H_a should be accepted for both time series. The risks to reject the null hypothesis are lower than 4.18%. The statement that there is a significant trend is correct with probabilities greater than 95.82% in both MK tests.

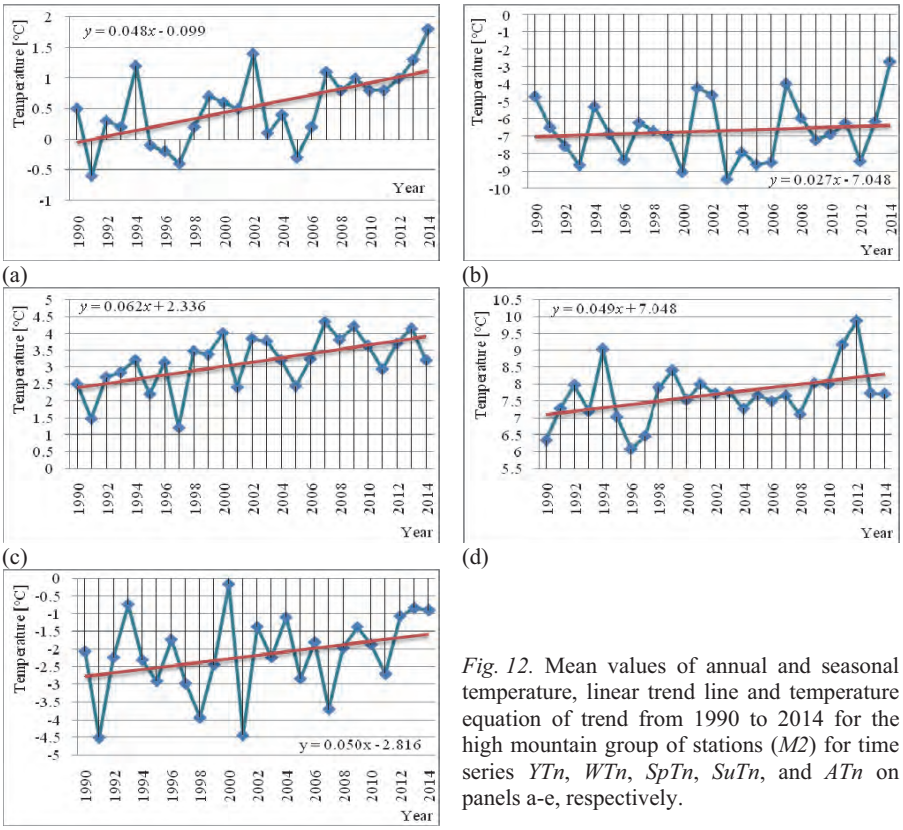

Fig. 12. Mean values of annual and seasonal temperature, linear trend line and temperature equation of trend from 1990 to 2014 for the high mountain group of stations (*M2*) for time series *YTn*, *WTn*, *SpTn*, *SuTn*, and *ATn* on panels a-e, respectively.

Results of the analyzed hypothesis (*Fig. 12* and *Table 5*) were futher analyzed in order to obtain the final temperature trend estimates. As the computed values of probability *p* for the time series *WTn*, *SuTn* and *ATn* are greater than the significance level α=5%, the H_0 cannot be rejected in all cases. The risks to reject the null hypothesis when it is true are 39.89, 14.97, and 7.80 (all in %) for all time series, respectively. In accordance with the classical MK tests, the second, fourth, and fifth cases are without trend, while the modified MK test declared that the fourth and fifth cases have *moderately positive trend* and the second case has *slightly positive trend.*

As the computed probability value *p* for the time series *YTn* and *SpTn* are lower than the significance level *a*, the H_0 should be rejected, and the H_a should be accepted for both time series. The risks to reject the null hypothesis are lower than 1.13%. The statement that there is a significant trend is correct with probabilities greater than 98.87% in both MK tests.

The main results of our analysis of temperature trends in the western and central tourist zones in Serbia are given in *Tables 6–8* depending on the altitude of the hydrometeorological stations. It seems that the positive temperature trends are dominant.

Table 6. The main results of the analysis of temperature trends for the lowland group of stations (*L*)

Time series	Trend equation	Classical MK test	Modified MK test
YT	*positive trend*	*positive significant trend*	*positive significant trend*
WT	*positive trend*	*no trend*	*slightly positive trend*
SpT	*positive trend*	*positive significant trend*	*positive significant trend*
SuT	*positive trend*	*positive significant trend*	*positive significant trend*
AT	*positive trend*	*positive significant trend*	*positive significant trend*
YTx	*positive trend*	*positive significant trend*	*positive significant trend*
WTx	*negative trend*	*no trend*	*no trend*
SpTx	*positive trend*	*no trend*	*positive moderate trend*
SuTx	*positive trend*	*no trend*	*positive moderate trend*
ATx	*positive trend*	*no trend*	*positive moderate trend*
YTn	*positive trend*	*positive significant trend*	*positive significant trend*
WTn	*positive trend*	*no trend*	*positive moderate trend*
SpTn	*positive trend*	*positive significant trend*	*positive significant trend*
SuTn	*positive trend*	*positive significant trend*	*positive significant trend*
ATn	*positive trend*	*positive significant trend*	*positive significant trend*

In accordance with the trend equations in the lowland group of stations (*L*), positive trends were found in 14 time series and negative trends were found only in one of them. After applying the classical MK test, only nine positive trends were statistically significant, and in the remaining cases there were no trends. Also, after applying the modified MK test, (I) significant positive trends were confirmed in nine time series; and in the remaining cases the trends were declared as: (II) moderately and slightly positive in four series; (III) moderately and slightly negative in one case; and (IV) there was no trend in one case.

For all temperatures, *T*, *Tx,* and *Tn*, the annual trends were declared as significantly positive. All winter trends were declared as significantly positive, moderately positive and without a trend. The spring, summer, and autumn trends were declared as significantly positive, moderately positive, and significantly positive, respectively.

In accordance with the trend equations for the lower mountain group of stations (*M1*), positive trends were found in 14 time series, and negative trends were found only in one of them. After applying the classical MK test, only seven positive trends were statistically significant, and in the remaining cases there were no trends. Also, after applying the modified MK test, (I) significant positive trends were confirmed in seven time series; and in the remaining cases the trends were declared as: (II) moderately and slightly positive in six series; (III) moderately and slightly negative in one case; and (IV) there was no trend in one case.

Table 7. The main results of the analysis of temperature trends for the lower mountain group of stations (*M1*)

Time series	Trend equation	Classical MK test	Modified MK test
YT	*positive trend*	*positive significant trend*	*positive significant trend*
WT	*negative trend*	*no trend*	*no trend*
SpT	*positive trend*	*positive significant trend*	*positive significant trend*
SuT	*positive trend*	*no trend*	*positive moderate trend*
AT	*positive trend*	*no trend*	*positive moderate trend*
YTx	*positive trend*	*positive significant trend*	*positive significant trend*
WTx	*positive trend*	*no trend*	*positive moderate trend*
SpTx	*positive trend*	*positive significant trend*	*positive significant trend*
SuTx	*positive trend*	*no trend*	*positive moderate trend*
ATx	*positive trend*	*no trend*	*positive moderate trend*
YTn	*positive trend*	*positive significant trend*	*positive significant trend*
WTn	*positive trend*	*no trend*	*slightly positive trend*
SpTn	*positive trend*	*positive significant trend*	*positive significant trend*
SuTn	*positive trend*	*positive significant trend*	*positive significant trend*
ATn	*positive trend*	*no trend*	*positive moderate trend*

For all temperatures, *T*, *Tx*, and *Tn*, the annual trends were declared as significantly positive. All winter trends were declared nonexistent, moderately positive, and slightly positive. All spring trends were declared significantly positive. Summer trends are declared as moderately positive and significantly positive, while the autumn trends were moderately positive.

Table 8. The main results of the analysis of temperature trends for the high mountain group of stations (*M2*)

Time series	Trend equation	Classical MK test	Modified MK test
YT	*positive trend*	*positive significant trend*	*positive significant trend*
WT	*positive trend*	*no trend*	*no trend*
SpT	*positive trend*	*positive significant trend*	*positive significant trend*
SuT	*positive trend*	*no trend*	*positive moderate trend*
AT	*positive trend*	*no trend*	*positive moderate trend*
YTx	*positive trend*	*positive significant trend*	*positive significant trend*
WTx	*negative trend*	*no trend*	*no trend*
SpTx	*positive trend*	*no trend*	*positive moderate trend*
SuTx	*positive trend*	*no trend*	*positive moderate trend*
ATx	*positive trend*	*positive significant trend*	*positive significant trend*
YTn	*positive trend*	*positive significant trend*	*positive significant trend*
WTn	*positive trend*	*no trend*	*slightly positive trend*
SpTn	*positive trend*	*positive significant trend*	*positive significant trend*
SuTn	*positive trend*	*no trend*	*positive moderate trend*
ATn	*positive trend*	*no trend*	*positive moderate trend*

In accordance with the trend equations for the high mountain group of stations (*M2*), positive trends were found in 14 time series and negative trends were found in one time series. After applying the classical MK test, only 6 positive trends were statistically significant, and in the remaining cases there were no trends. Also, after applying the modified MK test, (I) significant positive trends were confirmed in 6 time series; and in the remaining cases the trends were declared as: (II) moderately and slightly positive in six series; (III) moderately and slightly negative in one case; and (IV) in two cases trend was nonexistent.

For all temperatures, *T*, *Tx*, and *Tn*, the annual trends were declared as significantly positive. With winter trends, in two cases there was no trend, and in the third case the trend was slightly positive. For the spring, trends were found significantly positive, moderately positive, and significantly positive. As for summer, trends are declared as moderately positive, while the autumn trends were moderately positive and significantly positive.

The results show that there is a significant positive trend of temperature rise on an annual basis, while the trend is significantly positive during the autumn and spring seasons. In winter, the trend is slightly positive or absent, while in summer the trend is moderately positive in all three groups of stations.

4. Conclusions

In the researched area, the mountain tourism takes place in the areas over 1000 m above sea level, so that climate changes directly affect areas of the western tourist zone and the lower parts of the central zone (from 1000 to 1500 m above sea level).

Thus, this area, as a future development factor, represents a new subject of planning for the protection and sustainable development. The new strategies have to be based on the experiences of the countries with a higher level of development of mountain areas, on the examples of tourism development. Research has proven that there is no trend int he average temperatures on an annual basis in the winter for middle-sized mountain areas, up to 1500 m above sea level, and that the trend int he mean maximum temperature on an annual basis is moderately positive, while the average minimum temperature recorded a slight growth.

In other seasons, there is a significantly positive and moderately positive temperature trend, which gives priority to the development of summer tourism. The traditional way of doing agriculture and the arrangement of traditional settlements in this area are complementary to other activities. Protection and presentation of nature and natural values of these areas in the future give priority to the development of health and recreational tourism (Zlatibor, Zlatar, Tara, Brzeće).

Medium high and high mountain areas (Kopaonik), which were explored here, were equally affected by the current climate changes, while the consequences for mountain tourism were significant in lower areas. This impact will vary with the increasing altitude, and a small increase in winter temperatures can eliminate ski-centers at lower altitudes. Thus, the importance of high-mountain tourist centers and the need for sustainable development is increased.

References

Alexandersson, H., 1986: A homogeneity test applied to precipitation data. *J. Climatol.* 6, 661–675. https://doi.org/10.1002/joc.3370060607

Beniston, M., 2005: Mountain climates and climatic change: An overview of processes focusing on the European Alps. *Pure Appl. Geophys. 162*, 8–9. https://doi.org/10.1007/s00024-005-2684-9

Beniston, M., 2003: Climatic change in mountain regions: a review of possible impacts. *Climatic Change 59*, 5–31. https://doi.org/10.1023/A:1024458411589

Boisvenue, C. and *Running, S.W.,* 2006: Impacts of climate change on natural forest productivity — evidence since the middle of the 20th century. *Glob. Change Biol. 12*, 862–882. https://doi.org/10.1111/j.1365-2486.2006.01134.x

Christy, J.R., 2013: Monthly temperature observations for Uganda. *J. Appl. Meteorol. Climatol. 52,* 2363–2372. https://doi.org/10.1175/JAMC-D-13-012.1

Croitoru, A.E., Drignei, D., Dragotă, C.S., Imecs, Z., and *Burada, D.C.,* 2014: Sharper detection of winter temperature changes in the Romanian higher-elevations. *Glob. Planet. Change 122*, 122–129. https://doi.org/10.1016/j.gloplacha.2014.08.011

Croitoru, A.E., Drignei, D., Burada, D.C., Dragota, C.S., and *Imecs, Z.,* 2016: Altitudinal changes of summer air temperature trends in the Romanian Carpathians based on serially correlated models. *Quaternary Int. 415*, 336–343. https://doi.org/10.1016/j.quaint.2015.05.075

Diaz, H.F. and *Bradley, R.S.,* 1997: Temperature variations during the last century at high elevation sites. *Climatic Change 36*, 253–279. https://doi.org/10.1023/A:1005335731187

EEA, 2008: Impacts of Europe's Changing Climate – 2008 Indicator Based Assessment, EEA Report 4.

Feidas, H., Makrogiannis, T., and *Bora-Senta, E.,* 2004: Trend Analysis of Air Temperature Time Series in Greece and their Relationship with Circulation Using Surface and Satellite Data: 1955-2001, *Theor. Appl. Climatol. 79*, 185-208. https://doi.org/10.1007/s00704-004-0064-5

Gavrilov, M.B., Lazić, L., Pešić, A., Milutinović, M., Marković, D., Stanković, A. and *Gavrilov, M.,* 2010: Influence of hail suppression on the hail trend in Serbia. Physical geography 31(5): 441–454. https://doi.org/10.2747/0272-3646.31.5.441

Gavrilov, M.B., Lazić, L., Milutinović, M., and *Gavrilov, M.M.,* 2011: Influence of hail suppression on the hail trend in Vojvodina, Serbia. *Geographica Pannonica 15*, 36–41. https://doi.org/10.5937/GeoPan1102036G

Gavrilov, M.B., Marković, S.B., Zorn, M., Komac, B., Lukić, T., Milošević, M., and *Janićević, S.,* 2013: Is hail suppression useful in Serbia? – General review and new results. *Acta Geographica Slovenica 53,* 165–179. https://doi.org/10.3986/AGS53302

Gavrilov, M.B., Marković, S.B., Jarad, A., and *Korać, V.M.,* 2015: The analysis of temperature trends in Vojvodina (Serbia) from 1949 to 2006. *Thermal Sci. 19,* 339–350. https://doi.org/10.2298/TSCI150207062G

Gavrilov, M.B., Tošić, I., and *Marković, S.B.,* 2016: The analysis of annual and seasonal temperature trends using the Mann-Kendall test in Vojvodina, Serbia. *Időjárás 120,* 183–198.

Gavrilov, M.B., Marković, S.B., Janc, N., Nikolić, M., Valjarević, A.Đ., Komac, B., Zorn, M., Punišić, M., and *Bačević, N.,* 2017: Assessing average annual air temperature trends using the Mann-Kendall test in Kosovo. *Acta Geographica Slovenica 58*, 7–26. https://doi.org/10.3986/AGS.1309

Gilbert, R.O., 1987: Statistical Methods for Environmental Pollution Monitoring. Wiley, New York, USA

Hrnjak, I., Lukić, T., Gavrilov, M.B., Marković, S., Unkašević, M., and *Tošić I.,* 2014: Aridity in Vojvodina, Serbia. *Theor. Appl. Climatol. 115*, 323–332. https://doi.org/10.1007/s00704-013-0893-1

IPCC, 2007: Climate Change 2007: Synthesis Report. Contribution of Working Groups I, II and III to the Fourth Assessment Report of the Intergovernmental Panel on Climate Change [Core Writing Team, *Pachauri, R.K* and *Reisinger, A*. (eds.)]. IPCC, Geneva, Switzerland.

IPCC, 2014: Climate Change 2014: Synthesis Report. Contribution of Working Groups I, II and III to the Fifth Assessment Report of the Intergovernmental Panel on Climate Change [Core Writing Team, *R.K. Pachauri* and *L.A. Meyer* (eds.)]. IPCC, Geneva, Switzerland.

Jones, P.D. and *Moberg, A.,* 2003; Hemispheric and Large-Scale Surface Air Temperature Variations: An Extensive Revision and Update to 2001. Journal of Climate, 16, 206-223.

Jovičić, D., 2009: Turistička geografija Srbije. Univerzitet u Beogradu, Geografski fakultet, Beograd.

Karmeshu, N., 2012: Trend Detection in Annual Temperature & Precipitation using the Mann Kendall Test – A Case Study to Assess Climate Change on Select States in the Northeastern United States. M. Sc. thesis, University of Pennsylvania. USA.

Kendal, M., 1938: A new measure of rank correlation. *Biometrica 30*, 81–89. https://doi.org/10.1093/biomet/30.1-2.81

Kendall, M.G., 1975; Rank correlation methods, 4th end. Charles Griffin, London.

Kuang, X.Y., Zhang, Y.C., Huang, Y., and *Huang, D.Q.,* 2014: Changes in the frequencies of record-breaking temperature events in China and its association with East Asian Winter Monsoon variability. *J. Geophys. Res. Atmos. 119,* 1234–1248. https://doi.org/10.1002/2013JD020965

Luterbacher, J., Dietrich, D., Xoplaki, E., Grosjean, M., and *Wanner, H.,* 2004: European seasonal and annual temperature variability, trends and extremes since 1500. Science 303 (5663): 1499- 503.

Mann, H.B., 1945: Non-parametric tests against trend. *Econometrica 13*, 245–259. https://doi.org/10.2307/1907187

Manabe, S., Ploshay, J., and *Lau, N.C.,* 2011: Seasonal variation of surface temperature change during the last several decades. *J. Climatol. 24*, 3817–3821. https://doi.org/10.1007/s00703-009-0035-6

Marović, M., 2001: Geologija Jugoslavije. Rudarsko–geološki fakultet Univerzitet u Beogradu, Beograd. (in Serbian)

Micu, D., 2009: Snow pack in the Romanian Carpathians under changing climatic conditions. *Meteorol. Atmosp. Phys*.*105*, 1–16. https://doi.org/10.1007/s00703-009-0035-6

Micu, D., 2012: Cold waves in the Romanian Carpathians, an indicator of negative temperature extremes. Proceedings of the Conference Air and Water - Components of the Environment, IV. Cluj University. 97–104.

Milijić, S., and *Nenković-Riznić, M.* 2013: Sustainable development of mountain areas – planning and protection in the context of climate change. Climate change and the built environment policies and practice in Scotland and Serbia. *Monography, Special edition 70*, 137–164.

Mountain Agend, 1998: Mountains of the World: Waters Towers for the 21st Century, Prepared for the United Nations Commission on Sustainable Development Institute of Geography, University of Berne (Centre for Development and Environment and Group for Hydrology) and Swiss Agency for Development and Cooperation Paul Haupt, Bern, Switzerland.

Omondi, P.A., Awange, J.L., Forootan, E., Ogallo, L.A., Barakiza, R., Girmaw,G.B., Fesseha, I., Kululetera, V., Kilembe, C., Mbati, M.M., Kilavi, M., King'uyu, S.M., Omeny, P.A., Njogu, A., Badr, E.M., Musa, T.A., Muchiri, P., Bamanya, D., and *Komutunga, E.,* 2014. Changes in temperature and precipitation extremes over the Greater Horn of Africa region from 1961 to 2010. *Int. J. Climatol. 34*, 1262–1277. https://doi.org/10.1002/joc.3763

Popovic, T., Radulovic, E., and *Jovanovic, M.,* 2005: Koliko nam se menja klima, kakva ce biti nasa buduca klima? In: EnE05—Zivotna sredina ka Evropi, Beograd. 210–218. (In Serbian)

Popovic, T., Djurdjevic, V., Zivkovic, M., Jović, B., and *Jovanović, M.,* 2009: Promena klime u Srbiji i očekivani uticaji. Ministarstvo zastite zivotne sredine, Agencija za zastitu zivotne sredine Republike Srbije, Peta regionalna konferencija "EnE09—Zivotna sredina ka Evropi". (In Serbian) www.sepa.gov.rs (In Serbian)

Republic Hydromet. Service of Serbia, http://www.hidmet.gov.rs/ciril/meteorologija/klimatologija_godisnjaci.php

Rebetez, M., and *Reinhard, M.,* 2008: Monthly air temperature trends in Switzerland 1901-2000 and 1975-2004.Theor. Appl. Climatol. 91, 27-34. DOI 10.1007 / s00704-007-0296-2

Rodić, D. and *Pavlović, M.,* 1994; Zapadna zona mlađih venačnih planina i kotlina. U: Geografija Jugoslavije. Savremena administracija, Beograd. 62–73. (In Serbian)

Tabari, H. and *Talaee, P.H.,* 2011: Analysis of trends in temperature data in arid and semi-arid regions of Iran. *Glob. Planet. Change 79,* 1–10. https://doi.org/10.1016/j.gloplacha.2011.07.008

Toreti, A., Desiato, F., Fioravanti, G., and *Perconti, W.,* 2010: Seasonal temperatures over Italy and their relationship with low-frequency atmospheric circulation patterns. *Climatic Change 99*, 211–227. https://doi.org/10.1007/s10584-009-9640-0

Unger, R., Abegg, B., Mailer, M., and *Stampfl, P.,* 2016: Energy Consumption and Greenhouse Gas Emissions Resulting From Tourism Travel in an Alpine Setting. *Mount. Res. Develop. 36*, 475–483. https://doi.org/10.1659/MRD-JOURNAL-D-16-00058.1

Walther, G.R., Beissner, S., and *Burga, C.A.,* 2005: Trends in upward shift of alpine plants. Journal of Vegetation Science 16: 541–548. www.meteoromania.ro (accessed 04. 28.15.)

Wang, S.J., Zhang, M.J., Pepin, N.C., Li, Z., Sun, M., Huang, X. and *Wang, Q.,* 2014: Recent changes in freezing level heights in High Asia and their impact on glacier changes. *J. Geophys. Res. Atmos. 119*, 1753–1765. https://doi.org/10.1002/2013JD020490

XLSTAT, http://www.xlstat.com/en/ (accessed 5.12.2016)

DOI:10.28974/idojaras.2018.3.4

IDŐJÁRÁS

Quarterly Journal of the Hungarian Meteorological Service
Vol. 122, No. 3, July – September, 2018, pp. 285–304

Statistical structure of day by day alteration of daily average wind speeds

Károly Tar [1*] and **István Lázár** [2]

[1]*Institute of Tourism and Geography, University of Nyíregyháza*
Berek u.4, H-4029, Debrecen, Hungary

[2]*Department of Meteorology, University of Debrecen*
P.O.B. 13, H-4010, Debrecen, Hungary

**Corresponding author E-mail: tarko47@gmail.com*

(Manuscript received in final form August 7, 2017)

Abstract— One of the most complex problems of wind power plant operators is to compose a so-called "timetable" that is based on estimating the amount of power produced on the next day divided into small time units. Creation of this timetable could be based on the mathematical statistical method presented in this paper. Our statistical method is based on the construction of a model based on the statistical structure of the change of measured daily average wind speed, that enables the estimation of the probability of decreasing or increasing daily average wind speed by the next day in certain time periods or at various weather conditions. The statistical structure of daily average wind speed changing day by day provides further important information on the wind climate of Hungary and may help protection against wind erosion, building planning, and estimating bioclimatic factors. The basics of the method and the estimation of the sign of changes for the next day are presented in the following. The database is composed of daily average wind speed data measured at nine Hungarian meteorological stations between 1991 and 2000. Studies were performed for the whole period and for anticyclone and cyclone conditions based on Péczely's macrosynoptic situations and their transitional situations as well. The relative amount characterizing the change of daily average wind speed day by day was defined, and then the most important basic statics were analyzed. The distribution by sign of this amount and the relationship with the actual daily average wind speed were studied. Based on the results, the sign of wind speed change by the next day is estimated. As a conclusion, it can be stated that the presented model yields best results if the present day belongs to cyclone conditions.

Key-words: daily average wind speed, day by day changes of average wind speed, statistical estimations, error of estimations

1. Introduction

The total capacity of established wind power plants in Hungary is 329.325 MW with 172 wind power plants operating at 39 sites. The process of wind energy utilization in Hungary and the evaluation of this process are discussed in detail by *Tóth* and *Bíróné Kircsi* (2013, 2014, 2015).

With the integration of wind energy into electricity grids, it is becoming increasingly important to obtain accurate wind speed/power forecasts. Accurate wind speed forecasts are necessary to schedule dispatchable generation and tariffs in the day-ahead electricity market (*Bremnes et al.,* 2002; *Kavasseri* and *Seetharaman*, 2009; *Shukur* and *Lee*, 2015).

One of the most complex problems of wind power plant operators is to compose a so-called "timetable" that is based on estimating the amount of power produced on the next day divided into small time units. The complexity of the task is given by, for example, the difficulty of predicting wind speed for every hour.

Composition of this timetable could be improved using the statistical method presented in this paper. The basis for the model was established and published in previous works (*Tar* and *Puskás*, 2010ab; *Tar,* 2011, 2014ab, 2015; *Puskás et al.,* 2014; *Tar* et al., 2015, 2016; *Lázár*, 2015; *Tar* and *Lázár,* 2016). The model presented here is suitable for predicting the probability of the decrease or increase of daily average wind speed, and thus, average wind energy by the next day for certain time periods (e.g., season, year) and in different weather conditions (macrosynoptic conditions), or in the cases of transition between them. Studying the statistical structure of daily average wind speed changes in detail enable us to estimate the average wind speed of the "next day", on the basis of one of the basic statistics yielding a tool for wind power plant operators for composing the compulsory timetable. Moreover, it will give important information on the wind climate of Hungary and may help to estimate bioclimatic factors, as well.

The basis of the method and the estimation of the sign of changes by the next day that could be utilised from climatological points of view as well are presented in the following.

2. Methods, database

Database of the study is composed of the hourly wind speed data of nine meteorological stations (Szombathely, Győr, Pécs, Budapest, Kékestető, Szeged, Békéscsaba, Miskolc, and Debrecen) for the time period between 1991 and 2000 supplied by the National Meteorological Survey. Location of the stations is given in *Fig. 1*.

Fig. 1. Geographical location of the observatories comprising the analyzed database.

The data series cannot be regarded homogeneous at all stations, since certain devices or even the stations were moved in the studied period. Although the parameter describing the change of the daily average wind speed is independent of the height of the anemometer with good approximation, wind speed values were transformed for 10 m applying the WMO formula (see e.g., *Mezősi* and *Simon*, 1981; *Tar* and *Puskás*, 2010a) to make results comparable.

Analyses were made for the whole time period and for anticyclone and cyclone situation groups based on the Péczely's macrosynoptic conditions and for their various transitions. Macrosynoptic codes of the given days were taken from the works of *Károssy* (1993, 1998, 2001), and then the days belonging to anticyclone (AG) and cyclone (CG) situations were identified (see, e.g., *Péczely*, 1961; *Tar*, 2007; *Tar* and *Puskás*, 2010a).

For constructing the model, the average wind speed of every subsequent day has to be known, thus the last day and all days before and after every missing day were deleted from the database. The study period (January 1, 1991 –December 31, 2000) is composed of 3653 days. The number of days taking into consideration varies between 100% (Kékestető, Szeged) and 93.9% (Miskolc) of the 3653 days, because of missing and deleted days. These are called *complete time series* henceforward.

With a few tenth of difference, 67% and 33% of the studied days belong to AG and CG groups, respectively, at the particular stations. Let us consider that AG/AG, when an AG day is followed by another AG day is the conditional event, while CG/AG means a CG day following an AG one. Similarly, CG/CG and AG/CG days can be defined as well. Their conditional relative frequencies are 83%, 17%, 64%, and 36%, respectively. These results are in accordance with the results of our studies covering four years (*Tar* and *Puskás,* 2010b). Days belonging to CG and AG can be followed by any days, therefore, they could be indicated as WE/AG and WE/CG (WE - whatsoever).

3. Statistics of the daily relative change of daily average wind speed

Daily wind speed day by day is characterized by the relative amount of

$$\Delta v_r = \frac{v_n - v_p}{v_p}, \tag{1}$$

where v_p and v_n are wind speeds of the present and the next day respectively. Δv_r is approximately independent of the height of the anemometer. In percentage it shows the change of daily average wind speed compared to that of the previous day.

Since Δv_r is the observed value of a probability variable with special structure, their most important statistical functions are analyzed in detail in relation primarily with situation groups and their transitions.

3.1. Basic statistics of relative change

3.1.1. Average values

Average values of Δv_r in the complete time series and in the various transitions are presented in *Table 1*. It can be seen that the average is always positive, i.e., the average wind speed of the next day is always greater than that of the previous day in a long-term average. Values range between 0.18 (Győr) and 0.08 (Miskolc) with slight orographic differentiation in the complete time series: greater values appear in Western Transdanubia followed by the data of Great Plain and finally by stations in mountains shown in *Fig. 2*. Only Budapest does not fit into this series.

Table 1. Mean values of relative changes Δv_r

	whole period	**WE/AG**	**WE/CG**	**AG/AG**	**CG/AG**	**CG/CG**	**AG/CG**
Szombathely	0.17	0.19	0.12	0.18	0.24	0.16	0.05
Győr	0.18	0.22	0.09	0.23	0.18	0.10	0.07
Pécs	0.11	0.14	0.06	0.15	0.07	0.05	0.08
Budapest	0.09	0.12	0.04	0.11	0.16	0.06	0.02
Kékestető	0.10	0.12	0.06	0.15	0.02	0.03	0.11
Szeged	0.13	0.15	0.07	0.17	0.10	0.07	0.08
Békéscsaba	0.12	0.15	0.07	0.16	0.09	0.06	0.09
Miskolc	0.08	0.10	0.05	0.09	0.14	0.06	0.03
Debrecen	0.13	0.15	0.07	0.17	0.07	0.07	0.08
mean	0.12	0.15	0.07	0.16	0.12	0.07	0.07

Extreme values of Δv_r averages are associated with the transitions. Maximum values appear when the present day belongs to AG. The absolute maximum is 0.24 (Szombathely, CG/AG). Among the subsequent series of maximums, the already mentioned orographic character is somewhat stronger. Minimum values appear when the present day belongs to CG except for Kékestető. The absolute minimum is 0.02 (Budapest, AG/CG and Kékestető, CG/AG). This also indicates that orographic effects cannot be detected in the series of minimums.

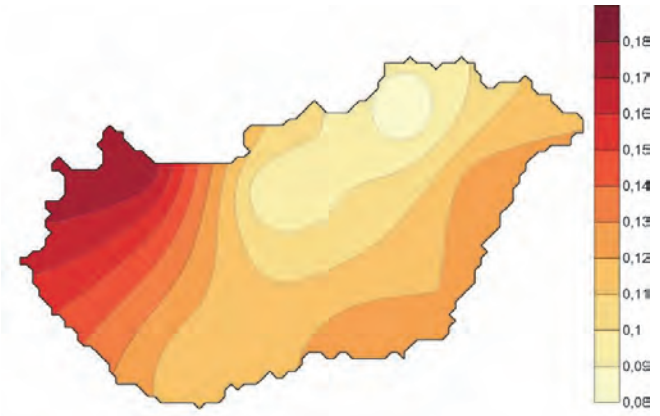

Fig. 2. Spatial differences of average values of Δv_r in the whole time period.

The areal average of Δv_r is also greater in AG/AG, CG/AG, and WE/AG transition. The greatest areal average belongs to the AG/AG transition with a value of 0.16. In the remaining three transitions (CG/CG, AG/CG, WE/CG), the average is the same, 0.07.

3.1.2. Variability

The coefficient of variation (relative standard deviation) is applied to analyze the variability of Δv_r. Its values varying between 30.84 (Budapest, AG/CG) and 3.24 (Szombathely CG/AG) indicating that its statistical characteristics are very variable. Its maximum values occur at CG/CG and AG/CG transitions except for Kékestető, where maximum values appear at either AG/AG or CG/AG transitions. In the series of extreme values according to magnitude, no orographic characteristics can be observed.

3.1.3. Minimum, maximum, scale

It seems like Δv_r is bounded from below, since its minimum values are not lower than –1, varying between –0.94 (Szeged complete time series, WE/CG, CG/CG) and –0.70 (Kékestető and Miskolc, AG/CG). Maximum values vary in a significantly greater interval: 1.91 (Pécs, CG/AG) and 18.71 (Békéscsaba complete time series, WE/AG, AG/AG), i.e., there is almost a tenfold difference in their values. When the frequency distribution was determined (see Section 3.1.6) classification into intervals with a particular width was performed up to $\Delta v_r = 3$. Greater values were classified into the same interval. Their frequency varies between 2.6% and 0.2% with an average of 1%.

3.1.4. Median

Studying the median is important, because its sign yields information on the distribution of Δv_r according to the sign. If the median is 0, half of the sample elements are negative and the other half are positive. If the median is negative, one half of the sample is composed of only negative and the other half is composed of mixed numbers. This means, that negative Δv_r, i.e., decrease of daily average wind speed by the next day has greater probability, while with positive median the opposite occurs.

The absolute value of median is in the range of one hundredth varying between –0.07 and 0.05, except for three cases. The absolute value of median is 0 in 33.3% of the cases, while positive and negative in 23.8% and 42.9% of the cases, respectively. According to these facts, unchanging or increasing average wind speeds in Hungary are more probable (57.1%) than diminishing wind speeds considering the next day. The followings are experienced according to categories: (1) the median is zero everywhere in the complete time series, (2) the median is zero or positive in the cases of WE/AG and AG/AG, while (3) the median is zero or negative in the case of CG/CG. Regarding to stations: zero or positive median occurred in five (four) categories stations Miskolc and Debrecen (Szombathely, Győr, Budapest, Kékestető, and Békéscsaba). It means that Δv_r values are not negative at these stations, i.e., unabating daily average wind speed has greater probability than decreasing. At stations Pécs and Szeged, negative median occurred one time more than positive.

3.1.5. Skewness, kurtosis

Difference of the frequency distribution of Δv_r from normal distribution is shown by the values of skewness and kurtosis coefficients by definition determined from the empirical central momentums (*Dévényi* and *Gulyás*, 1988). Both statistical functions show that the distribution of Δv_r can be very close and also far away from normal distribution, and this is approximately independent of weather and orographic conditions.

3.1.6. Frequency distribution, mode

According to Section 3.1.3, the values of Δv_r were classified into 0.2 wide intervals. Detailed analysis of frequency distributions is not given here, as the primary aim was to determine the empirical value of *mode* ($\langle \Delta v_r \rangle$), defined as the centre of the interval containing the highest number of sample elements. In 90.5% of all cases (64) this interval is (–0.2; 0.0), i.e., the mode of Δv_r is –0.1.

In the rest of the cases, frequencies belonging to mode values are only a few tenth of % greater than that of the intervals containing –0.1. Thus, the most probable value of Δv_r is –0.1 which is independent of weather conditions and their transitions and location, that makes the estimation of the average wind speed of the next day relatively simple.

3.2. Distribution of relative change according to sign

In the estimation of relative changes, the analysis of the distribution of Δv_r according to sign is essential. As we have seen, the average values of Δv_r are positive in all cases, therefore, in the long term, the wind speed of the next day is always greater than that of the previous day. The same was determined when the median was studied. Studying only the weather conditions, the rate becomes the opposite as the rate of negative changes, i.e., decrease is 53.7%.

In *Fig. 3* the appearances of the differences between the positive or 0 and the negative values of Δv_r (d_{pn}, in°%) are presented by categories. For example, 2.4% means that the frequency of $\Delta v_r \geq 0$ values is 51.2%, while that of negative values is 48.8%.

According to *Fig. 3,* the value of d_{pn} at WE/AG and AG/AG transitions is positive at every station in the complete time series, i.e., $\Delta v_r \geq 0$ changes appear with greater probability. The probability of average wind speed of the next day greater than that of the previous day is greatest, 56.2% in Miskolc at CG/AG transition, followed by Kékestető with 55.9% at AG/CG transition. Further order is Budapest with 55.6%, Pécs 54.7%, Debrecen 54.5%, Szeged 54.3%, Győr 54.2%, Békéscsaba 53.2%, and Szombathely 53.1%, all of them at AG/AG transition. Average probability of $\Delta v_r \geq 0$ is greatest at AG/AG with 54.3%, i.e., at this transition, the increase of the wind speed of the next day in Hungary seem to have greatest probability. Smallest probability appears at CG/CG and AG/CG transitions with 48.6% and 48.5%, respectively. Probability of the selected case is greater than 50% in 58.7% of all cases (63).

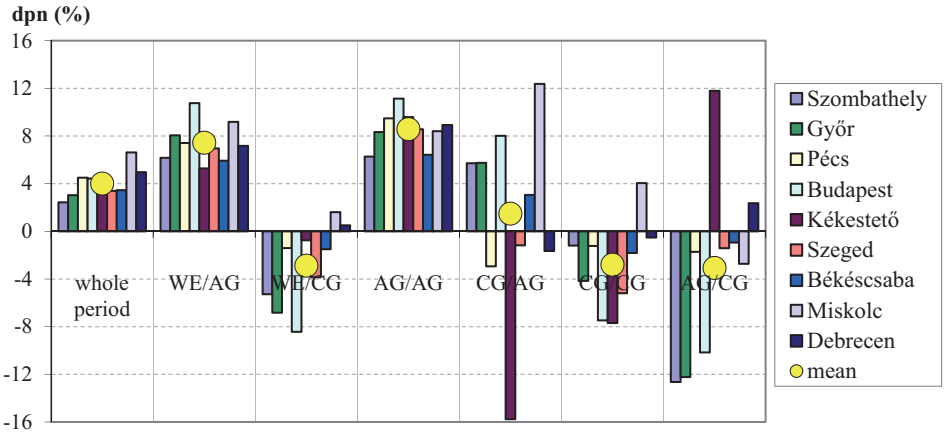

Fig. 3. Ratio of differences between the number of $\Delta v_r \geq 0$ and $\Delta v_r < 0$ cases.

Categories containing only negative d_{pn} values cannot be found. The probability of that the average wind speed of the next day would be smaller than that of the previous day is greatest, 57.9% at CG/AG transition in Kékestető, followed by 56.3% at AG/CG transition in Szombathely, and 56.1 % and 55.1% at AG/CG transition in Győr and Budapest, respectively. The order continues with 52.6% at CG/CG transition in Szeged, 51.5% at CG/AG transition in Pécs, 51.4% at AG/CG transition in Miskolc, 50.9% at CG/CG transition in Békéscsaba, and 50.8% at CG/AG transition in Debrecen.

When values of d_{pn} are studied by stations in the complete time series, it can be observed that they vary in smaller intervals than at the transitions. The range here is 4.2%, while the average is 4%. Consequently, independently of weather conditions in Hungary, the probability of greater and smaller daily average wind speed of the next day than that of the present day is 52% and 48%, respectively. National averages of d_{pn} in the rest of the categories are positive at transitions when the present day is AG, and negative if the present day is CG. The order, shown in *Fig. 3*, is 7.4%, –2.9%, 8.6%, 1.5%, –2.8%, –3.1%.

3.3. Relationship between the sign of relative change and the average wind speed of the present day

According to Eq. (1) Δv_r is in a very complex function with the average wind speed of the present day (v_p) considering that the average wind speed of the next day (v_n) also depends on this. It is reasonable to regard the (v_p,Δv_r) relationship stochastic. Closest correlation was found with logarithmic regression. Values of $i(v_p, \Delta v_r)$ correlation index is presented in *Table 2*.

Values of $i(v_p, \Delta v_r)$ vary between 0.592 (Győr, CG/CG, see *Fig. 4*) and 0.404 (Miskolc, AG/AG). Regarding absolute values, the maximum coefficient can be found in Győr except for AG/CG transition, when it was found in Budapest. Considering minimum values, there are no such strict orographic orders. Considering station orders, maximum values appeared at CG/CG transitions in seven towns, where the exceptions are Szombathely (AG/CG) and Kékestető (CG/AG). This means that except for the latter ones, the maximums of the correlation index belong to the transitions, when the present day is CG.

The regression curve crosses the horizontal, v_p axis in all cases. The zero point is v_{p0}. For the points of the regression curve with (x,y) coordinates, $y > 0$ before the zero point and $y < 0$ after the zero point. As a result, it can be assumed, that the sign of the observed values of Δv_r are in connection with zero points. Zero points can be regarded threshold values regarding the sign of Δv_r. *Table 2* also presents the values of v_{p0}.

Table 2. The correlation index $i(v_p, \Delta v_r)$ of logarithmic regression and the zero point v_{p0} of regression function

		whole period	**WE/AG**	**WE/CG**	**AG/AG**	**CG/AG**	**CG/CG**	**AG/CG**
Szombathely	$i(v_p, \Delta v_r)$	0.458	0.449	0.478	0.446	0.501	0.474	0.508
	v_{p0} (m/s)	3.8	3.6	4.0	3.5	4.3	4.4	3.4
Győr	$i(v_p, \Delta v_r)$	0.534	0.523	0.561	0.526	0.565	0.592	0.540
	v_{p0} (m/s)	2.5	2.4	2.7	2.3	3.0	2.9	2.4
Pécs	$i(v_p, \Delta v_r)$	0.505	0.495	0.525	0.497	0.488	0.536	0.521
	v_{p0} (m/s)	3.1	3.0	3.3	3.0	3.4	3.4	3.0
Budapest	$i(v_p, \Delta v_r)$	0.473	0.435	0.542	0.434	0.532	0.558	0.544
	v_{p0} (m/s)	2.6	2.6	2.7	2.5	3.1	2.9	2.4
Kékestető	$i(v_p, \Delta v_r)$	0.459	0.457	0.456	0.445	0.501	0.481	0.405
	v_{p0} (m/s)	4.2	4.2	4.2	4.2	4.2	4.2	4.4
Szeged	$i(v_p, \Delta v_r)$	0.513	0.495	0.559	0.496	0.526	0.586	0.543
	v_{p0} (m/s)	3.4	3.3	3.6	3.1	3.8	3.8	3.3
Békéscsaba	$i(v_p, \Delta v_r)$	0.479	0.464	0.549	0.472	0.477	0.563	0.534
	v_{p0} (m/s)	3.3	3.1	3.6	2.9	3.8	3.7	3.4
Miskolc	$i(v_p, \Delta v_r)$	0.434	0.405	0.501	0.404	0.456	0.522	0.474
	v_{p0} (m/s)	3.1	3.0	3.1	2.9	3.6	3.2	3.0
Debrecen	$i(v_p, \Delta v_r)$	0.494	0.483	0.524	0.480	0.515	0.553	0.494
	v_{p0} (m/s)	3.0	2.9	3.2	2.8	3.3	3.3	3.0

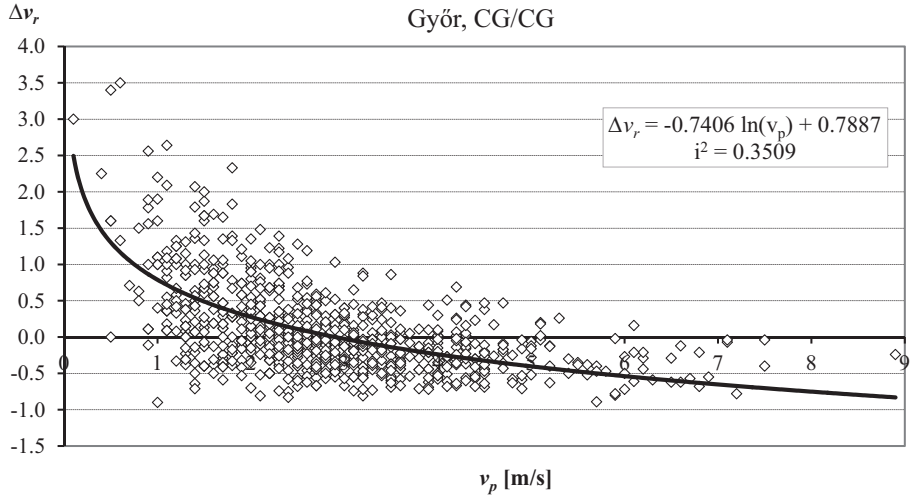

Fig. 4. The closest logarithmic relationship between the present day's average wind speed (v_p) and the next day's relative change (Δv_r).

Fig. 4 shows that most of the *positive or 0 changes* ($\Delta v_r \geq 0$) appear when the average wind speed at 10 m height of the present day is smaller than or equal to the zero point, $v_p \leq v_{p0}$. Maximum and minimum frequency of the event is 48.0% (Miskolc CG/AG) and 29.9% (Kékestető, CG/AG), respectively. Maximums belong to transitions when the present day is AG at the rest of the stations as well, except for Kékestető. In the case of $v_p \leq v_{p0}$, frequencies vary between 15.5% (Kékestető, CG/CG) and 5.5% (Szombathely, CG/AG). Maximums at the rest of the stations also belong to transitions when the present day is CG, except for Pécs. The rate of frequencies belonging to the two conditions is between 8.6 (Szombathely, CG/AG) and 2.0 (Kékestető, CG/CG). Almost 90% of them are between 2 and 6. Frequency of positive changes is 40.4 % when the average wind speed of the present day is smaller than the zero point of the regression curve and 10.2% when it is greater than the zero point.

Frequencies of negative changes ($\Delta v_r < 0$) are between 28.5% (Szombathely, CG/CG, Debrecen, WE/AG) and 17.9% (Pécs, WE/CG) in the case of $v_p \leq v_{p0}$. Maximums belong to transitions when the present day is AG, except for Szombathely and Győr. Greater order is found in the distribution of minimum values: maximums appear at transitions when the present day is CG at every station. Most of the negative changes occur when the average wind speed of the present day is greater than the zero point ($v_p \leq v_{p0}$). In this case, the maximum frequency is 36.5% (Kékestető, CG/AG) while the minimum is 18.8% (Szombathely, WE/AG). Maximums at the rest of the stations belong to transitions when the present day is CG. Minimums appear at transitions WE/AG,

and AG/AG except for Kékestető. Frequency of the two conditions is 1.5 (Szombathely, WE/AG) and 0.5–0.6. Almost 70% of them appear between 0.6 and 1.2. Extreme values are ordered, maximums and minimums appear when the present day is AG and CG, respectively. Probability of negative changes is almost the same on average in the two cases: 23.1% in the case of present day average wind speed smaller than the zero point of the regression curve, and 23% if it is greater.

Average wind speed of the next day, therefore, will probably increase, that is in the case of present day, wind speeds are smaller than the zero point of the regression curve. Smallest probability belongs to the increase of wind speed of the next day when the present daily average wind speed is greater than the zero point. The probability of decrease of the average wind speed of the next day does not differ significantly in the two cases.

The latter statements are independent of location and transitions. If only the sign of Δv_r is to be estimated and the average wind speed of the present day is known, the estimation could be performed with high reliability in comparison to the zero point of the regression curve. Zero points, however, are dependent on location and categories. Since its determination is not simple, it is more sensible to select a statistical parameter as a threshold, which is already known or can be calculated easier.

According to our earlier studies (*Tar,* 2011, 2015; *Lázár,* 2015), the relationship of the simple change of $\Delta v = v_n - v_p$ and the daily average wind speed is described best by linear correlation, and the zero point of the regression line in the complete time series is the same as the average speed of the time period [v]. Based on this result, it was presumed that the average wind speed of the categories could be used instead of zero points because the difference is zero in 12 cases (19%), negative in 6 cases (9.5%) and positive in 45 cases (71.5%). Differences vary between 0.7 m/s (Szombathely, CG/AG) and –0.3 m/s (Kékestető, CG/AG, Szombathely, AG/CG), their average is 0.2 m/s.

Therefore, the conditional relative frequencies of $f(\Delta v_r \geq 0 / v_p \leq [v])$, $f(\Delta v_r \geq 0 / v_p > [v])$, $f(\Delta v_r < 0 / v_p \leq [v])$, $f(\Delta v_r < 0 / v_p > [v])$ were determined, and it is presented in *Fig. 5*. Based on this figure, the following general statements can be made.

It has the greatest probability (33.2% – 43.7%) at every station, except for Kékestető, CG/AG in every category, that Δv_r is positive if the average wind speed of the present day is smaller than the average wind speed of the category. This probability is the second greatest (30.8%) at Kékestető at CG/AG transition after $f(\Delta v_r < 0 / v_p > [v])$ (~35%). The maximum of the frequency $f(\Delta v_r \geq 0 / v_p \leq [v])$ appears always in Szombathely, except for AG/CG situation, thus the absolute maximum is here as well: 43.7% at AG/AG transition. Minimums of the categories split among Békéscsaba, Pécs and Kékestető. The frequency of the event $(\Delta v_r \geq 0 / v_p \leq [v])$ varies between 40.1 % (AG/AG) and 36.2% (CG/CG) on average.

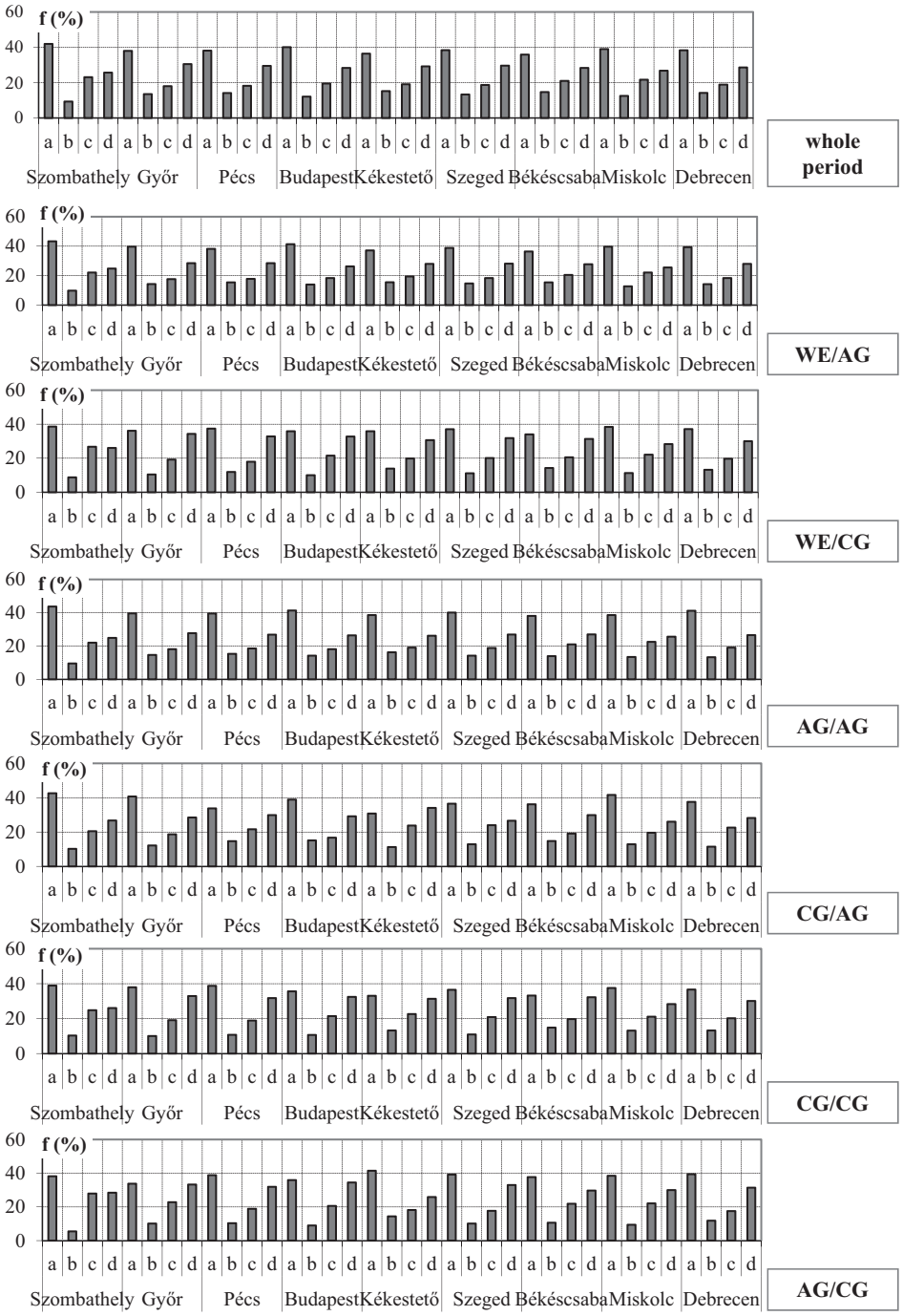

Fig. 5. Conditional relative frequencies of the sign of Δv_r (f, %) referred to the mean wind speed of categories ([v]): a: $f(\Delta v_r \geq 0 / v_p \leq [v])$, b: $f(\Delta v_r \geq 0 / v_p > [v])$ c: $f(\Delta v_r < 0 / v_p \leq [v])$, d: $f(\Delta v_r < 0 / v_p > [v])$

It has the smallest probability (5.5% – 16.2%) in every case, that Δv_r is positive if the average wind speed of the present day is greater than the average wind speed of the category. Smallest $f(\Delta v_r \geq 0 / v_p > [v])$ frequencies appear in Szombathely except for Győr, CG/CG, the absolute minimum is here as well at AG/CG transition. Maximums split among Budapest, Kékestető, and Békéscsaba with the absolute maximum appearing at Kékestető at the AG/AG transition, 16.2%.

The rate of the probability of the two events shows that the probability of positive changes – i.e., increasing average wind speed of the next day compared to the present day is 3.2 times higher on average if the average wind speed of the present day – is smaller than the average wind speed of the present day.

In case of negative changes ($\Delta v_r < 0$), there is no such great difference between the two cases, i.e., between $f(\Delta v_r < 0 / v_p \leq [v])$ and frequencies of the $f(\Delta v_r < 0 / v_p > [v])$. The latter frequencies are always second, i.e., greater than previous frequencies. The exception is Szombathely, WE/CG. Average probability of negative change is 20.3% ($\Delta v_r < 0 / v_p \leq [v]$) and 29.1% ($\Delta v_r < 0 / v_p > [v]$). Their differences are greater than that when the zero point is selected as threshold.

It can be declared that if the average wind speed of the present day is smaller than the average speed of the category, the probability of the increase of the average wind speed of the next day is 1.4 – 2.3 times greater – 1.9 times on average – than the decrease. On the other hand, if daily average wind speed is greater than the average wind speed of the category then the probability of decrease of average wind speed of the next day is 1.6 – 2.5 times – 2.4 times on average – greater than that of increase. Only $[v]$ depends on the weather conditions.

3.4. Estimating the sign of the relative change

Based on the results of the analyses above, the estimation of the sign of average wind speed change for the next day could be attempted using the average wind speeds at 10 m height of the present day and the categories. The algorithm of this estimation is the following: average wind speeds of the present day (v_p) are compared to the average wind speed of the category ($[v]$). If $v_p \leq [v]$ then $\Delta v_r \geq 0$. In the opposite case, $\Delta v_r < 0$ with great probability. Comparing the observed and estimated sign of Δv_r the analyzed time series of the reliability of the model could be tested.

The estimated rate of positive change is above 50% at every station and in every category. The maximum of the estimated values appear in Szombathely in all categories while minimums are variable. The absolute maximum is 66.1% (Szombathely, AG/CG) while the absolute minimum is 53% (Békéscsaba, CG/CG). The rate of positive changes is always overestimated. Differences between the estimated and observed frequencies of $\Delta v_r \geq 0$ cases are presented in *Fig. 6*. It is apparent, that the grade of overestimation is greatest always at Szombathely with the absolute maximum of 22.4% at AG/CG transition. The

maximum of average values is here as well with 10.7%. The location of minimums is variable and the absolute minimum is 1.7% in Budapest at CG/AG transition. The minimum of average values is not here but at WE/AG category with 5.4%, however, the 5.6% value of AG/AG transition is quite close to it.

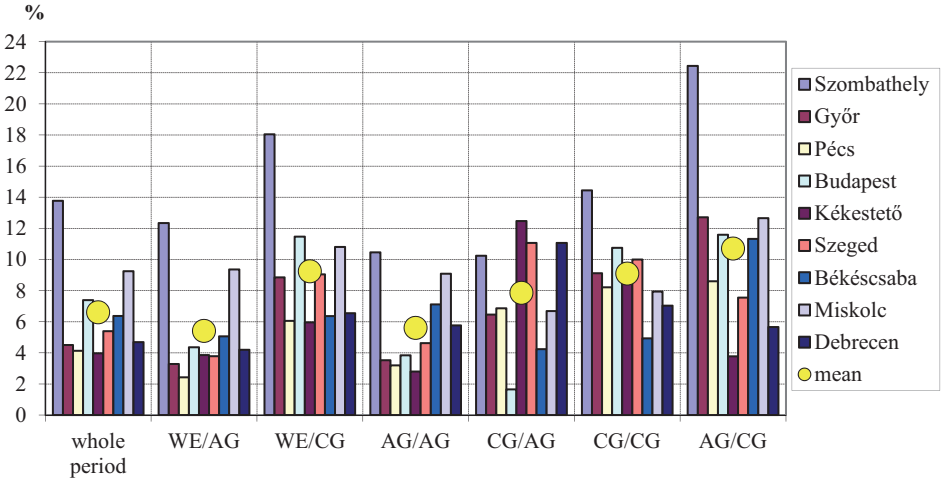

Fig. 6. Differences between the estimated and observed frequencies of $\Delta v_r \geq 0$ cases.

The reliability of the model is indicated by the number of accurate estimations, i.e., when the observed and estimated signs are the same. Rate of these compared to the total number of days in the category is shown in *Fig. 7*. The highest value is 72.2% in Szeged at AG/CG transition but values higher than 70% could be observed in Győr at WE/CG and at CG/CG transitions, and in Pécs at the same and AG/CG transitions and also in Budapest and Debrecen at the same transition. *Our model yields the best results when the present day belongs to a cyclone group*. The absolute minimum can be found in Szeged with 63.1% at CG/AG transition and close values appear in WE/AG and AG/AG categories. *Our model yields the least number of accurate estimations when the present day belongs to an anticyclone group*.

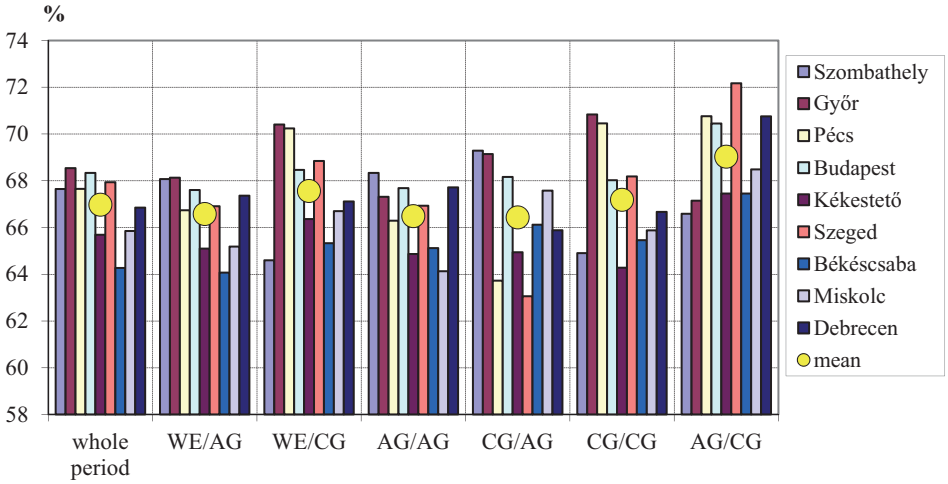

Fig. 7. Rate of accurate estimation of the sign of Δv_r referred to the total number of days in the categories.

It was also studied, how the consideration of macrosynoptic conditions and their transitions modify the number of accurate estimations compared to accurate estimations in the complete time series. *Fig. 8* presents the difference between accurate estimations of six such categories and the complete time series.

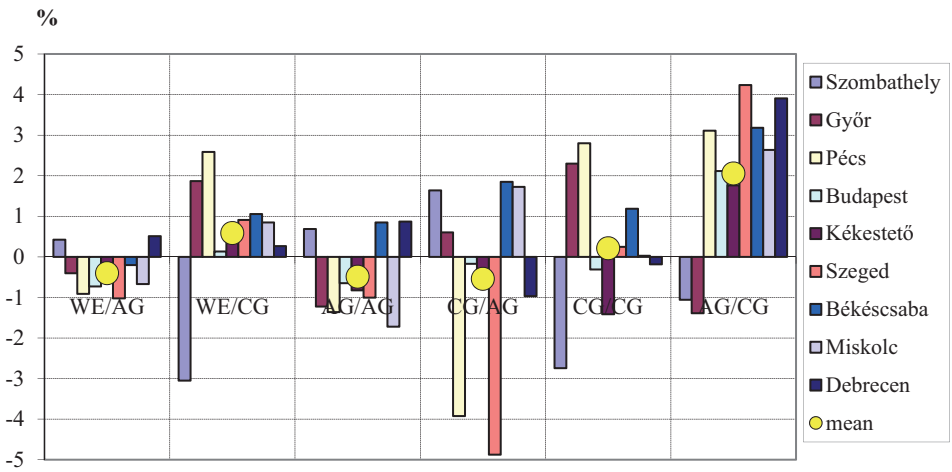

Fig. 8. Differences between the rate of accurate estimations in the macrosynoptic groups and the complete time series.

Differences vary between 4.2% (Szeged, AG/CG) and –4.9% (Szeged, CG/AG). 46.3% (25 cases) are negative, i.e. the number of accurate estimations is smaller than in the complete time series. These appear in categories when the present day belongs to AG in 18 cases. The number of cases when accurate estimations exceed those of the complete time series is 7.4% more (29 cases, 53.7%). These take place in 20 cases in three such categories where the present day is CG. 40.7% of the absolute values of differences are between 2 % and 5%.

The above are reflected by category averages as well: these are negative in the cases of WE/AG, AG/AG, and CG/AG (with values of –0.4, –0.5, –0.5), while positive in the cases of WE/CG and CG/CG, and in the case of AG/CG their values are 0.6, 0.2, and 2.1.

Studying by stations, the number of categories with positive and negative differences is the same in Szombathely, Győr, Pécs, and Szeged (3–3), while the number of negative values is higher in Békéscsaba and Miskolc, and the number of positive values is higher in Békéscsaba, Miskolc, and Debrecen.

As a result, taking into consideration the macrosynoptic conditions and their transitions makes no significant improvement to the accuracy of the estimation. Exceptions could be the 13 cases, when the absolute values of differences reach or exceed 2%. These could be read from *Fig. 8*.

4. Summary and conclusions

The process of constructing a mathematical-statistical model is presented in order to estimate the amount of wind power produced on the next day. The final version of the model is capable of estimating the sign of daily average wind speed change for the next day and the magnitude of average wind speed of the next day from the average wind speed of the present day. The basis of the model is the time series of daily average wind speeds observed in the complete time period and transformed into the height of 10 meters. The analyses were carried out for the complete time series and for the groups of days belonging to the cyclone and anticyclone macrosynoptic conditions (CG and AG) and their transitions (CG/CG, AG/CG, AG/AG, CG/AG).

The average (Δv_r) of the relative amount yielding the change of daily average wind speed day by day, is always positive, i.e., the average wind speed of the next day on average in the long term, is always greater than that of the previous day. The regional average is greater when the next day follows a day belonging to AG.

Values of the variation coefficient applied to analyze the variability of Δv_r show, that this is a very variable statistical character varying between 30.84 and 3.24.

Δv_r can be regarded bottom limited, since its *minimum values* are not below 1. These vary between –0.94 and –0.70. Considering maximums, however, almost tenfold differences are found.

The absolute value of *median* is zero or close to zero except for three cases, between 0.07 and 0.05. In 33.3% of the total number of cases the median is 0, while it is positive in 23.8% and negative in 42.9% of the cases. This also means that the probability of remaining or increasing average wind speed of the next day in national average is greater (57.1%) than that of the decreasing values. Median is zero everywhere in the complete time period.

Skewness and kurtosis coefficients show, that the distribution of Δv_r can be very close to or far away from normal distribution, and this distance is approximately independent of weather and orographic conditions.

Independent, of weather conditions and their transitions and also from location, the most probable value of Δv_r mode is –0.1, that enables us to estimate the average wind speed *value* of the next day relatively simple.

In order to estimate this, the analysis of the *distribution* of Δv_r *according to its sign* is very important. This distribution is characterized in % by d_{pn} showing the differences of negative and greater than, equal to zero values of Δv_r. The probability of greater average wind speed of the next day than that of the previous day is greatest with 56.2% in Miskolc and CG/AG transition and smallest with 53.1% in Szombathely at AG/AG transition. The average probability of the $\Delta v_r \geq 0$ event is greatest in the AG/AG category with 54.3%, so that the increase of average wind speeds of the next day increase at this transition nationwide. Smallest values are found at CG/CG and AG/CG transitions in 48.6% and 48.5%. The probability of the selected event is greater than 50% in 58.7% of the complete series of events (63).

There are no categories containing only negative d_{pn} values. The probability of that the wind speed of the next day is always the same is 57.9% in Kékestető at CG/AG transition.

On national average, independently of weather conditions, the probability of that the average wind speed of the next day is greater/smaller than that of the present day is 52%/48%, respectively.

Δv_r is very complex function of the average wind speed of the present day (v_p) considering that the average wind speed of the next day (v_n) is also dependent on this. Therefore, it is reasonable to regard the (v_p, Δv_r) relationship stochastic. The closest correlation is logarithmic regression.

The regression curve crosses the horizontal v_p the axis. Let us consider this crossing point to be the zero point, v_{p0}. For the points of the regression curve with coordinates (x,y) $y > 0$ before the zero point and $y < 0$ after the zero point. Therefore, the sign of the observed values of $\underline{\Delta v_r}$ could be associated with zero points. Therefore, zero points can be regarded as threshold values in studying the sign of Δv_r. Detailed analyses proved this, however, the determination of these threshold values is not simple, therefore, it is practical to choose a possibly known statistical parameter that can be calculated easier. On the basis of previous

research it was presumed, that the average wind speeds of the categories could be used as threshold values instead of zero points.

Based on the results of related detailed analyses it can be declared, that if the average wind speed of the present day is smaller than the average speed of the category, the probability of the increase of the average wind speed of the next day is 1.4 – 2.3 times higher – 1.9 times on average – than that of its decrease. If the average wind speed of the present day is greater than the average speed of the category, the probability of the decrease of the average wind speed of the next day is 1.6 – 5.2 times higher – 2.4 times on average – than that of the increase. Thus, only [v] depends on weather conditions.

The sign of the change of the next day average wind speed was estimated from the average wind speeds at 10 m of the present day and the categories. The reliability of the presented model was tested by comparing the observed and estimated signs of the analyzed time series of Δv_r.

The reliability of the model is indicated by the number of accurate estimations, i.e., when the observed and estimated signs are the same. They are given as the rate compared to the total number of days in the category. The highest value is 72.2% in Szeged at AG/CG transition but values higher than 70 % could be observed in Győr at WE/CG and CG/CG transitions, in Pécs at the same and at AG/CG transitions, and also in Budapest and Debrecen at the same transitions. *Our model yields the best results when the present day belongs to a cyclone group*. The absolute minimum can be found in Szeged with 63.1% at CG/AG transition. Values lower than 65% were found in 10 cases at 6 stations at various transitions. The average value varies between 69% (AG/CG) and 66.4%. The latter was observed at CG/AG transition, but the values of WE/AG and AG/AG categories are close as well. *Our model yields the least number of accurate estimations when the present day belongs to an anticyclone group*.

Taking into consideration the macrosynoptic conditions and their transitions makes no significant improvement to the accuracy of the estimation.

In order to make the presented model operatively applicable to estimate the sign of the change of the next day average wind speed, the following conditions have to be set:

- The long-term average of the wind speed of the location measured at the height of 10 m has to be known. This can be determined on the basis of wind maps as well.
- The accurate average wind speed of the present day has to be known. This can be determined at the end of the day from, for example, the hourly data. In order to use the estimation for constructing a timetable, this data should be known before the end of the day. As a result, a calculated approximate value, like the so-called (primary) terminus averages have to be used.
- Then these have to be transformed to 10 m based on the height of the anemometer.

Acknowledgements: The authors would like to express their thanks to the Hungarian Meteorological Service for providing data for the analysis.

References

Bremnes, J.B., Villanger, F., and AS, K.V., 2002: Probabilistic forecasts for daily power production. In Proceedings of the Global Wind Power Conference, Paris.

Dévényi, D. and *Gulyás, O.,* 1998: Matematika statisztikai módszerek a meteorológiában. Tankönyvkiadó, Budapest. (In Hungarian)

Kavasseri, R.G. and *Seetharaman, K.,* 2009: Day-ahead wind speed forecasting using f-ARIMA models. *Renew. Energy 34*, 1388–1393. https://doi.org/10.1016/j.renene.2008.09.006

Károssy, Cs., 1993: A Péczely-féle makroszinoptikus tipizálás és a helyzetek katalógusa (1951–1992). In (Ed.: *Nowinszky, L.*) A fénycsapdás rovargyűjtést módosító abiotikus tényezők. OSKAR Kiadó, Szombathely, 113–126. (In Hungarian)

Károssy Cs., 1998: Péczely's classification of macrosynoptic types and catalogue of weather situations (1992–1997). In (Ed.: *Nowinszky, L.*) Light trapping of insects influenced by abiotic factors. Part II, Savaria University Press. 117–130.

Károssy Cs. (2001): Characterisation and catalogue of the Péczely's macrosynoptic weather types (1996–2000). In (Ed.: *Nowinszky, L.*) Light trapping of insects influenced by abiotic factors. Part III. Savaria University Press. 75–86.

Lázár I.(2015): Székelyföld szélklímájának statisztikai vizsgálata. PhD értekezés. Debreceni Egyetem, Földtudományi Doktori Iskola. (In Hungarian)

Mezősi, M. and *Simon, A.,* 1981: A meteorológiai szélmérések elmélete és gyakorlata. *Meteorológiai Tanulmányok*, No. 36.

Péczely, Gy. 1961: Magyarország makroszinoptikus helyzeteinek éghajlati jellemzése. Az Országos Meteorológiai Intézet Kisebb Kiadványai 32. (In Hungarian)

Puskás, J. and *Tar, K., Szepesi, J.,* and *Kovács, E.,* 2014: Statistical Investigation of Subalternation of the Daily Mean Wind Speed on the North-West Region of Carpathian Basin. *In (*Eds*. Kanakidou, M., Mihalopoulos, N., Nastos, P.*) COMECAP 2014 e-book of proceedings. ISBN: 978-960-524-430-9, Vol 3. 85–89.

Shukur, O.B. and *Lee, M.H.,* 2015: Daily wind speed forecasting through hybrid KF-ANN model based on ARIMA. *Renew. Energy* 76, 637–647. https://doi.org/10.1016/j.renene.2014.11.084

Tar, K. and *Puskás, J.,* 2010a: A napi átlagos szélsebesség időbeli megváltozásának függése a frontos és frontnélküli napok váltakozásától. VI. Kárpát-medencei Környezettudományi Konferencia, Nyíregyházi Főiskola, Nyíregyháza. 321–326. (In Hungarian)

Tar, K. and *Puskás, J.,* 2010b: A napi átlagos szélsebesség megváltozásának kapcsolata az időjárási helyzetekkel. *Magyar Energetika 17(3)*, 30–35. (In Hungarian)

Tar, K. and *Puskás, J.,* 2011: Frontok, szélklíma, szélenergia. A Bakonytól Madagaszkárig. Tanulmánykötet a 65 éves Veress Márton tiszteletére. 115–124. (In Hungarian)

Tar, K., 2007: Diurnal course of potential wind power with respect to the synoptic situation. *Időjárás 111,* 261–279.

Tar, K., 2011: A Kárpát-medence szélenergiájáról. VII. Kárpát-medencei Környezettudományi Konferencia, Sapiencia Erdélyi Magyar Tudományegyetem, Kolozsvár. 165–169. (In Hungarian)

Tar, K., 2014a: A napi átlagos szélsebességek egymásra következének statisztikai elemzése az Alföldön. In (Eds.: *Fazekas, I. Szabó, V.*) Környezettudatos energiatermelés és –felhasználás. Meridián Alapítvány. 96–105. (In Hungarian)

Tar, K., 2014b: Statistical structure of the surface layer wind field in Hungary. Direction, speed and energy of the wind. Lambert Academic Publishing.

Tar, K., 2015: A napi átlagos szélsebesség megváltozásának statisztikai szerkezete. *In (Eds.: Kúti, Zs., Puskás, J.*) Tiszteletkötet Károssy Csaba 70. születésnapjára. Szombathely. 47–54. (In Hungarian)

Tar, K., Bíróné Kircsi, A., and *Tóth, T.,* 2016: A szélenergia kutatása a Debreceni Egyetem Meteorológiai Tanszékén (1980–2014). *Légkör 61*, 48-63. (In Hungarian)

Tar, K. and *Lázár, I.,* 2016: Az egymást követő napok átlagos szélsebességeinek statisztikai becslése. In (Ed. *Lázár, I.*) Környezet és energia a mindennapokban, MTA DAB Környezettudományi Szakbizottság. 109–117. (In Hungarian)

Tar, K., Lázár, I., and *Gyarmati, R*.. 2015: Statistical estimation of the next day's average wind speed and wind power. In (Eds.: *Ortiz,W., Somogyvári, M., Varjú, V., Fodor, I., Lechtenböhmer, S.*) Perspectives of Renewable Energy in the Danube Region. 174–191.

Tóth, P. and *Bíróné Kircsi, A.,* 2013: A szélenergia-hasznosítás 2011. évi legújabb eredményei. *Magyar Energetika 20(1)*, 16–21. (In Hungarian).

Tóth, P. and *Bíróné Kircsi, A*., 2014: A szélenergia-hasznosítás 2013. évi eredményei. *Magyar Energetika 21(6)*, 38-41. (In Hungarian).

Tóth, P. and *Bíróné Kircsi, A.,* 2015: A szélenergia hasznosítás legújabb eredményei. *Légkör 60*, 88–91. (In Hungarian)

DOI:10.28974/idojaras.2018.3.5

IDŐJÁRÁS

Quarterly Journal of the Hungarian Meteorological Service
Vol. 122, No. 3, July – September, 2018, pp. 305–320

Application of the crop model WOFOST in grid using meteorological input data from reanalysis and objective analysis

Hristo Chervenkov*, **Valentin Kazandjiev**, and **Veska Gorgieva**

National Institute of Meteorology and Hydrology,
Bulgarian Academy of Sciences
66, Tsarigradsko Shose blvd Sofia 1784, Bulgaria

** Corresponding author Email: Hristo.Tchervenkov@meteo.bg*

(Manuscript received in final form June16, 2017)

Abstract—Meteorological gridded datasets from the reanalysis ERA-Interim of the ECMWF and the objective analysis E-OBSv14.0 of the ECA&D are used to initialize the crop model WOFOST. The data is on daily basis with 0.25° horizontal resolution and the model domain entirely covers southeastern part of Europe. Hence, the general of the authors goal is to investigate the response of the crops system to the averaged weather conditions, rather than of a particular year. For this purpose, multi-year daily averages from the 30-year period of 1981–2010 are considered. This time-span is often treated as "modern climate", and it is frequently used in many evaluation studies. A special, purpose-build software system is designed to perform the simulation, which steers the data flow and the exchange between the different modules. The produced outcome, in form of three-dimensional digital map of the crop production specific variables, shows high spatial and temporal consistency, revealing the relevant features of the geographical and chronological variation of the output parameters at the same time.

Key–words: ERA-Interim, E-OBS, WOFOST, crop simulation in grid

1. Introduction

Continued pressure on agricultural land, food insecurity, and required adaptation to climate change has made integrated assessment and modelling of future agro-ecosystems development increasingly important. Various modelling tools are

used to support the decision making and planning in agriculture, and consequently, many common efforts are dedicated to the problem. Thus, for example, the ACCELERATES project (*Rounsevell et al*., 2006) aimed to assess the vulnerability of European agro-ecosystems to environmental change in support of the conventions of climate change and biological diversity. This was based on a study of the impact of environmental change on land use and biodiversity (for selected species and habitats) in agro-ecosystems. The approach integrated existing models of agricultural land use, species distribution, and habitat fragmentation within a common scenario framework, so that impacts could be synthesized for different global change problems. The results suggest that policy and conservation strategies should not tackle the vulnerability of agriculture and biodiversity independently.

An important component in this is crop modelling. The crop model (CM) simulates or imitates the behavior of a real crop by predicting the growth of its components, such as leaves, roots, stems, and storage organs as a function of the soil and weather conditions and crop-specific parameters. Thus, a CM does not only predict the final state of crop production or harvestable yield, but also contains quantitative information about major processes involved in the growth and development of the crop. Reactions and interactions at the level of tissues and organs are combined to form a picture of the crop's growth processes. In crop growth modelling, current knowledge of plant growth and development from various disciplines, such as crop physiology, agrometeorology, soil science and agronomy, are integrated in a consistent, quantitative, and process-oriented manner (*Oteng-Darko et al*., 2013).

Meteorological conditions are the main abiotic factors for the development of the cultivars, and correspondingly, agriculture is influenced by the prevailing weather and climate. Thus, for example, elevated temperature and humidity affect the biological processes like respiration, photosynthesis, plant growth, reproduction, water use, and other processes. Consequently, the quality and reliability of the meteorological input data for the CMs are of primary importance. The most modern CMs are one dimensional, namely they use the meteorological and soil data measured in certain point of interest. According to the meteorological input, the typical and most widely used source of such information, the time series are collected in the network of the standard measurement stations. Obviously, the resulted CM output is spatially limited also to the vicinity of the location of the point of the information source. An alternative approach is to use meteorological data from reanalysis (RA) and objective analysis (OA) and to run the CM gridcell-by-gridcell independently. The main advantage of the RA and OA is obvious: they provide spatially and temporally the best estimated picture of the state of the atmosphere in form of continuous gridded digital maps. The methods incorporated in every RA model maintain also the dynamical consistency between the variables. The OA, which is, generally speaking, a multistage procedure of error-detecting and removing,

as well as, homogenization and interpolation of the measurements, produces output, which is much more reliable in comparison with the row data. Consequently, such gridded datasets are widely used and will continue to be important for many reasons (see *Haylock et al.*, 2008 for details). The main aim of the presented work is to investigate the principal applicability of RA and OA datasets for initialization of 'state-of-the-art' CM and to analyze the resulted crop model output. For this purpose, a software system is build, which uses data from the current reanalysis of the European Centre for Medium-Range Weather Forecasts (ECMWF) ERA-Interim and from the version 14.0 of the OA data-set E-OBS of the European Climate Assessment&Dataset (ECA&D) for initialization of the version 7.1.7 of the CM WOFOST. Multi-annual daily averages of the input parameters for the time span 1981–2010 are used, and the model domain covers Southeast (SE) Europe entirely.

The aim of the study is to investigate the crop response to the atmospheric conditions, and more specifically, to the climate means, thus, only the meteorological input is altered. All other input settings and parameters of the CM WOFOST are left on their default values. Thus, generally speaking, the work is a preliminary but necessary prerequisite for more realistic simulations.

The article is structured as follows. Section 2. is dedicated to the concise description of the CM WOFOST, the input datasets and the accepted methodology. Section 3. presents the performed calculations and the obtained results. The conclusion and outlook for the further plans are given in the last section.

2. CM WOFOST, input data and methodology

2.1. CM WOFOST

The CM WOFOST (acronym of WOrld FOod STudies) is created by the school of *C.T. De Wit* at the Wageningen University in the Netherlands as a successor of earlier simulators. It is a mechanistic model that explains the growth of annual crops on the basis of the underlying processes, such as photosynthesis, respiration, and how these processes are influenced by environmental conditions. The model is intended to facilitate the computation of the annual crop production, biomass, water use, etc. for a given location and knowledge about soil type, crop type, weather data, and crop management factors, e.g., sowing date, cultivation, and fertilization (*Eitzinger et al.*, 2009).

The major processes are phenological development, CO_2-assimilation, transpiration, respiration, partitioning of assimilates to the various organs, and dry matter formation. Potential production and two levels of limited production (water-limited and nutrient-limited) can be calculated. Potential production represents the absolute production ceiling for a given crop grown in a given area under specific weather conditions, and only this level is considered in the

current study. Production-reducing factors (like weed and pests) have not been taken into account.

Like all mathematical models of agricultural production, WOFOST is a simplification of the reality. Basically, crop yield is a result of the interaction of ecological, technological, and socio-economical factors. In WOFOST, only ecological factors are considered under the assumption that optimum management practices are applied. Crop rotation and soil cultivation effects are not considered.

The key point is, as stated above, that WOFOST is a one-dimensional simulation model, i.e., without reference to any geographic scale. Its application to regions relies on the selection of representative points. Nevertheless, the WOFOST model was calibrated in Bulgaria and used for prediction of crop growing, development, and yields in operational agrometeorological practice in NIMH-BAS (*Kazandjiev* and *Georgieva,* 2006). We are also familiar with other CMs, such as the freely distributed AquaCrop and DSSAT, which is not distributed free of charge. We have adapted one and the other, but we have stopped on WOFOST, because it is the basis of the EC-Crop Growth Monitoring System (CGMS).

In the last two decades, the successive WOFOST versions and their derivatives have been used in many studies around the world including Bulgaria (*Kazandjiev* and *Georgieva,* 2006). WOFOST is a significant component of the BioMA (Biophysical Models Applications) software framework of the MARS (Monitoring Agricultural ResourceS, see https://ec.europa.eu/jrc/en/mars for details) initiative of the EU Joint Research Centre (JRC). Main aim of the initiative is to perform regular crop yield forecasting in order to provide monthly bulletins forecasting crop yields to support the EU's Common Agriculture Policy (CAP). Crop yield forecasts and crop production estimates are necessary at EU and Member State level to provide the EU's CAP decision makers with timely information for rapid decision-making during the growing season. Estimates of crop production are also useful in relation to trade, development policies, and humanitarian assistance linked to food security (*Leo* and *Baruth,* 2013).

Variation in timing of crop production can be taken into account by varying the starting date of the growing season and/or by selecting crop cultivars with different growth durations. WOFOST offers several options for positioning the crop calendar in the year. The start of the simulation can be at a fixed date of crop emergence, at a fixed date of sowing, or at a variable date of sowing. The end of the simulated season is determined by crop maturity or crop death, or set at a fixed end date, e.g., for crops harvested immature.

More in-depth information for the model can be found in the user's guide (*Boogaard et al.,* 1998), which ships together with the free-available distributive.

Crop growth is simulated using daily weather data of many years and different parameters for each relevant soil type within a region. If required for a

particular study, calculated values, e.g., yields, biomasses produced, or water use can be averaged over the simulated years or aggregated over soil types. However, the data needed in this procedure are not always available. The scarcity of the daily weather data is emphasized in the user's guide (*Boogaard et al.*, 1998). It is also stated, that the option included in the model, which uses average (monthly) weather data has to be treated carefully: the use of long-term mean monthly weather data, mean sowing dates, and averaged soil data as model input may lead to a false impression of the agro-ecological potential of a region. This implies that original rather than averaged data must be used as model input, and that if needed, averaging can be done only after the simulation. The temporal and spatial discontinuity of the point measurements is inherent weakness of each dataset, containing such data. Further and very relevant problem is the absence of such a key agrometeorological parameter from the standard (i.e., synoptic) measurements. Usually, to overcome this, empirical and semi-empirical relations between various parameters, for example, sunshine duration, latitude, longitude from one side, and insolation from the other are implemented. Such relations, as a whole, are very schematic, and their suitability in the crop modelling is disputable. This fact was an additional motivator for the authors to implement OA and RA data for the initialization of the CM WOFOST.

2.2. RA ERA-Interim, OA E-OBS, and used methodology

The latest operational RA of the ECMWF ERA-Interim (*Dee et al*., 2011) is the global atmospheric reanalysis from 1979, continuously updated in real time. The data assimilation system used to produce ERA-Interim is based on a 2006 release of the Integrated Forecasting System (IFS) (Cy31r2). The system includes a 4-dimensional variational analysis (4D-Var) with a 12-hour analysis window. The spatial resolution of the dataset is approximately 80 km (T255 spectral) on 60 vertical levels from the surface up to 0.1 hPa. ERA-Interim products are updated once per month with a delay of two months, and are freely available via the ECMWF Public Datasets web interface or from the archiving system.

ERA-Interim-driven crop simulations with WOFOST were performed in the in-depth pan-European study of *de Wit et al.* (2010). In this study, two model setups are considered using two identical model implementations: one uses interpolated observed weather, the other is built from ERA-Interim. Output for both sources was generated for the EU27 and neighboring countries and 14 crops, aggregated to national level and validated using reported crop yields from the European Statistical Office (EUROSTAT). The results indicate that the system performs very similar in terms of crop yield forecasting skill. The other main conclusion of the work is that the ERA-Interim dataset is highly suitable

for regional crop yield forecasting over Europe, and may be used for implementing regional crop forecasting over data-sparse regions.

E-OBS is a land-only daily gridded observational dataset for precipitation amount, minimum, mean, and maximum temperature, and sea level pressure in Europe based on the collected information at ECA&D stations (*Haylock et al.,* 2008). The current version 14.0 covers the period from January 1, 1950 until August 31, 2016. Data is made available on a 0.25 and 0.5° regular latitude-longitude grid, as well as on a 0.22 and 0.44° rotated pole grid, with the North Pole at 39.25N, 162W. In the current implementation, data on the regular 0.25° regular latitude-longitude grid are used. Besides the 'best estimate' values, separate files are provided containing daily standard errors and elevation.

The weather dataset, necessary for the initialization of the CM WOFOST, must contain the time series of the following six variables: irradiation, minimum temperature, maximum temperature, early morning (EM) vapor pressure, mean wind speed at 2 m above ground, and precipitation. The time steps of all variables, except the vapor pressure, have to be one day, and the latter obviously requires sub-daily time resolution. Practically, the only reliable source of such information is the state-of-the-art RA, and this fact, in conjunction with the need for radiation data, was the main reason to use ERA-Interim. Thus, the data for the EM vapor pressure and mean wind speed are taken from ERA-Interim, while the minimum and maximum temperature, as well as the precipitation amount are from E-OBS.

Although WOFOST is supplied with additional MICROSOFT WINDOWS® graphical user interface, it can be executed as stand-alone console application. In the latter case, all initial data have to be in the required format of the crop, soil, and weather files. The fact, that the FORTRAN-77 source code is freely available is of key importance. Alongside other benefits, this allows the model to be recompiled and linked again and integrated in other, purpose-built software projects, as described in detail in the next section.

3. Performed calculations and obtained results

The main aim of the authors was to exploit WOFOST in Unix-like environment, which offers superior opportunities for geophysical modelling. Thus, the model is recompiled and linked under Linux Slackware, using the bash shell script available in the WOFOST distributive. The WOFOST execution, data flow and the linkage between the separate modules are governed from the main, purpose-build program. It is written by the authors in FORTRAN 90/95, and its skeleton is shown as a flow-chart in *Fig. 1*.

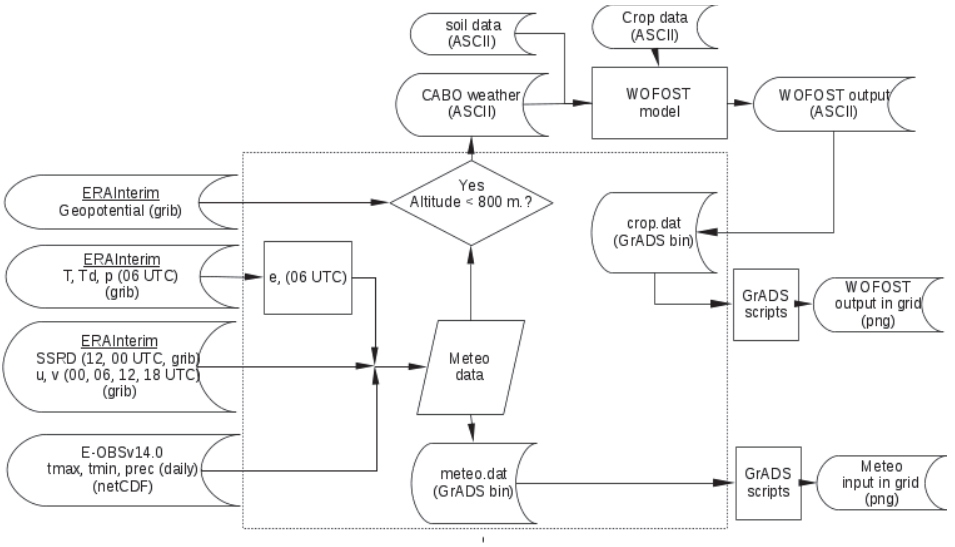

Fig. 1. Building blocks, file formats, and data flow in the simulation system.

The main goal of the authors was to investigate the response of the agricultural system of averaged meteorological conditions rather than of a particular year. Thus, the multi-annual daily averages from the 30-year period 1981–2010 have been considered. All parameters, which are needed for the WOFOST initialization, have been calculated first for every day in the considered period, and the climate averages have been obtained afterward.

The model domain comprises Southeast (SE) Europe and is centered over Bulgaria. It is situated between the 15°and 35° eastern longitudes and the 35° and 50° northern latitudes and consists of 81×61 0.25×0.25° gridcells.

To ensure the spatial conformability between the ERA-Interim and E-OBS, the ERA-Interim datasets are downloaded with 0.25° resolution.

The variables, needed for the calculation of the water vapor pressure, noted in *Fig. 1* with e, namely the temperature T, dew point Td, and surface pressure p, are available in ERA-Interim at 00, 06, 12, and 18 UTC, and thus 06 UTC data are selected as closest to “early morning”. The vapor pressure is obtained with well-known relations, and the results are validated with independent humidity calculators.

From all available ERA-Interim radiation components, the insolation in WOFOST is closest to the surface solar radiation downwards (SSRD, ECMWF grib code 169, table 128), which is available at 12 and 00 UTC of the next day, and the daily sum is the sum of the two terms.

The wind module is calculated from the zonal and meridional components, and the average from the values at 00, 06, 12, and 18 UTC are taken.

The E-OBS datasets are suitable for WOFOST initialization, basically without modification. Additionally, the E-OBS sea-land mask is used to constrain the simulation over the land surface only.

The suitability of a certain place for planting of selected cultivar depends on many factors, but the altitude above the sea level (a.s.l.) is especially relevant. Ultimately, over a certain threshold of altitude, the crop productivity decreases and makes their cultivation senseless. This threshold depends from climatic zone and can vary between 800 and 1000 m. Thus, the lands above the mentioned altitudes have to be excluded beforehand from the simulation. The ERA-Interim surface geopotential field has been used to calculate the altitude, and no calculations have been performed in the regions above 800 m, which is a suitable threshold for the available winter wheat cultivars in the model domain. Generally, all unsuitable grounds have to be excluded, i.e., calculations should not be performed over, for example, forests, internal water sheets, urbanized areas, etc. At the current implementation and grid spacing, however, only the land-sea and elevation criteria are considered.

The physical properties of the soil required by WOFOST are often derived from soil maps. *Boogaart et al.* (1998) emphasizes, that the rules applied to derive these properties from map units are still rather tentative, and only a small number of standard datasets are provided with the model. The absence of "WOFOST-readable" soil inventory in the model grid is the biggest obstacle to maintain the simulation close to the reality. At this stage, the soil type is set to the default one (i.e., as in the model distributive). We have also performed simulations with the most common soils on which winter wheat is grown in Bulgaria, in our case this are the chernozems (phaezems) and vertisols (pelic vertisols) (*Koynov, et al*., 1998). In the later case, the simplest soil geography is assumed: the soils north to the 43rd parallel, which can be defined as the border between Southern and Northern Bulgaria, are set to chernozems, and soils south to the 43rd parallel to vertisols. Such treatment is based on the available soil type measurements. For reasons of brevity, however, these results are not shown here. Simulations were made for the winter wheat crops. As in the supplied example in the distributive, the sowing date is fixed at the first of January. This is also one assumption, which, however, deviates from the agricultural practices Southeast Europe, but it is workable in the considered study.

The work-flow in the modelling system is as follows. The meteorological data are passed from the external files into the main program for the current gridcell. If, at least one variable is missing, or the altitude of the gridcell is above the threshold, the model output is set to undefined value and any other processing is skipped. In the opposite case, the meteorological data are converted and written in WOFOST-readable format and the WOFOST is executed. Afterward the WOFOST-output is intercepted and internally stored.

The WOFOST output includes the following time-depended variables: number of days since emergence, development stage of crop, thermal time since emergence, dry weight of living leaves, dry weight of living stems, dry weight of living storage organs, total above-ground production, leaf area index, transpiration rate, gross assimilation, maintenance respiration rate, and rate of dry matter increase. The process is repeated in a loop for every gridcell in the domain. Finally, the output aggregated for all gridcells is stored in external three-dimensional (in space and time) binary direct access file, which is a very convenient form of storage allowing additional post-processing with powerful instruments like GrADS. The meteorological data for the whole simulation period are also stored in such a file. This makes the further parallel analysis of the meteorological and crop-specific parameters possible. The seasonal average of the insolation, minimum temperature, maximum temperature, EM water vapor pressure, and wind speed ,as well as the precipitation sum for the spring (traditionally accepted as March, April, and May) and the summer (June, July and August), which are the two most relevant seasons to the crop development, are shown in *Fig. 2.*

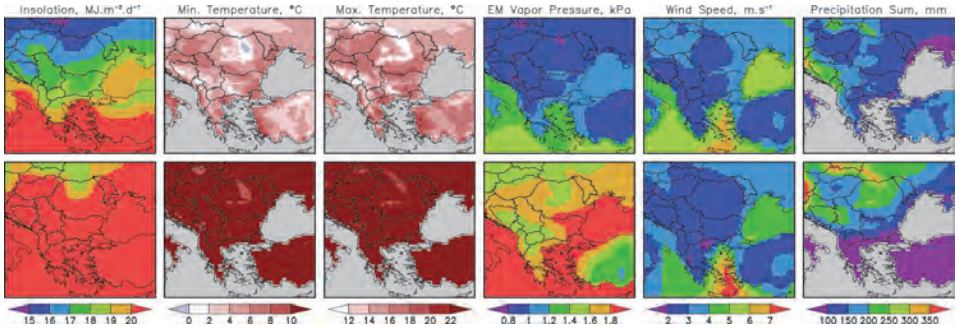

Fig. 2. Seasonal averages of all meteorological parameters, except for precipitation as well as the precipitation sum for the spring (MAM, first row) and summer (JJA, second row).

Figs. 3–6 show the spatial distributions of all 11 WOFOST-output parameters in approximately equidistant time intervals.

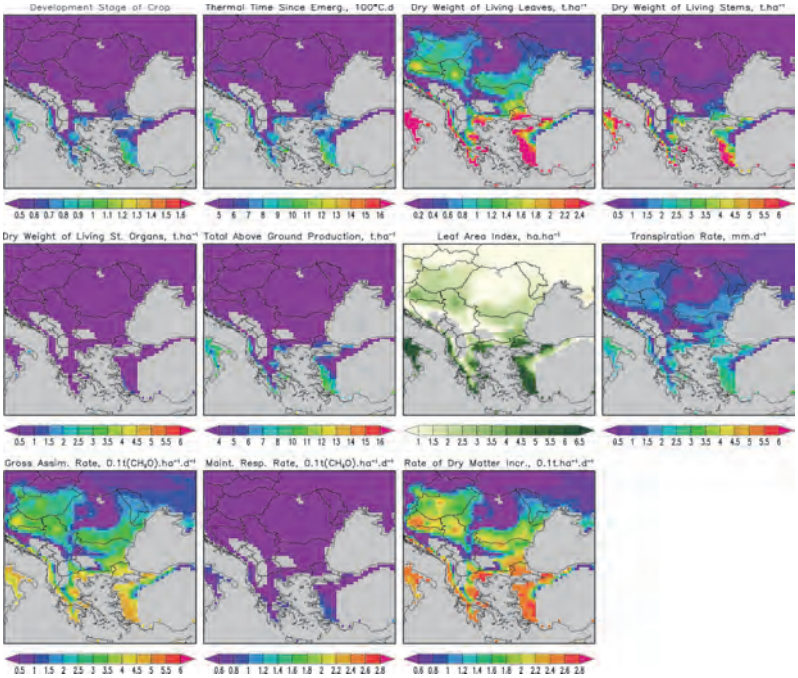

Fig. 3. Distribution of the WOFOST potential crop production output parameters on April 19.

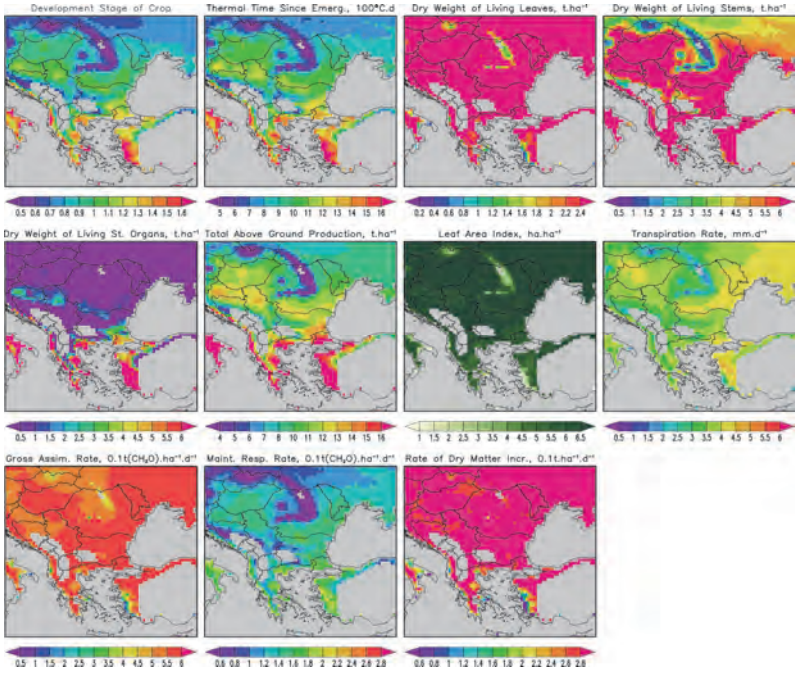

Fig. 4. Same as *Fig. 3*, but for May 29.

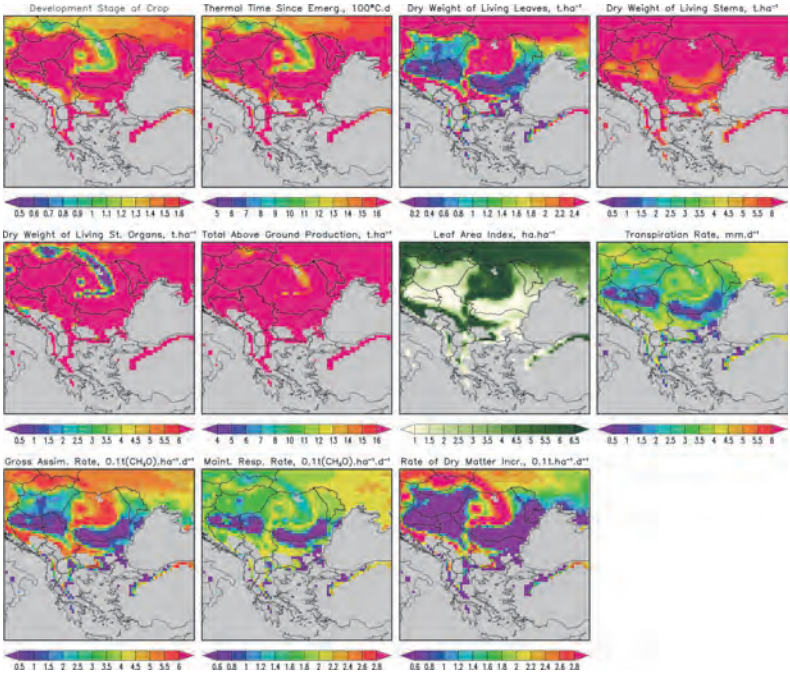

Fig. 5. Same as *Fig. 3*, but for July 8.

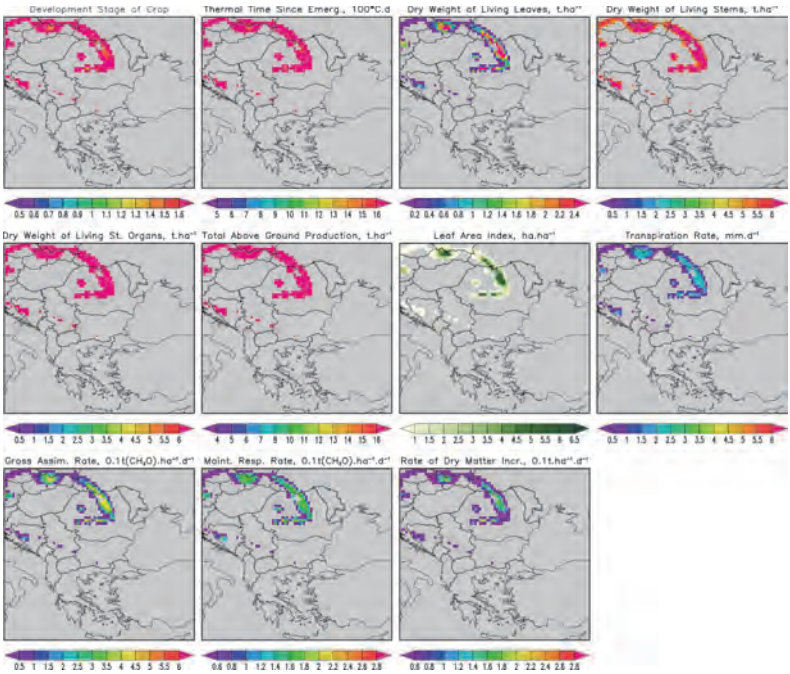

Fig. 6. Same as *Fig. 3*, but for August 17.

The obtained results can be generalized in many directions, but thus far, the main features of the achieved fields of the output variables seem evident. First, these fields are spatially and temporally consistent: the geographical distribution looks realistic, with well reproduced general north-south gradient, elevation, and coastal effects. The last two effects are especially discernible over the main Carpathian ridge and the northwestern coast of Turkey, correspondingly. The timeliness of the simulated crop calendar also seems realistic – the maximum of the dry weight of the storage organs, which is probably the most important parameter from practical point of view, is reached approximately, over the plains in the internal part of the domain, in the second half of June. The model system simulates also the time lag, i.e., the delay of the wheat development of the northern and elevated regions.

It is important, at least from practical point of view, to map the maximum value of, for reasons of brevity, only the 'yield-related' output variables and the day of the simulation (which in our case is equivalent to the day of the year (DOY)), when this maximum is reached. These maps are shown in *Fig. 7*.

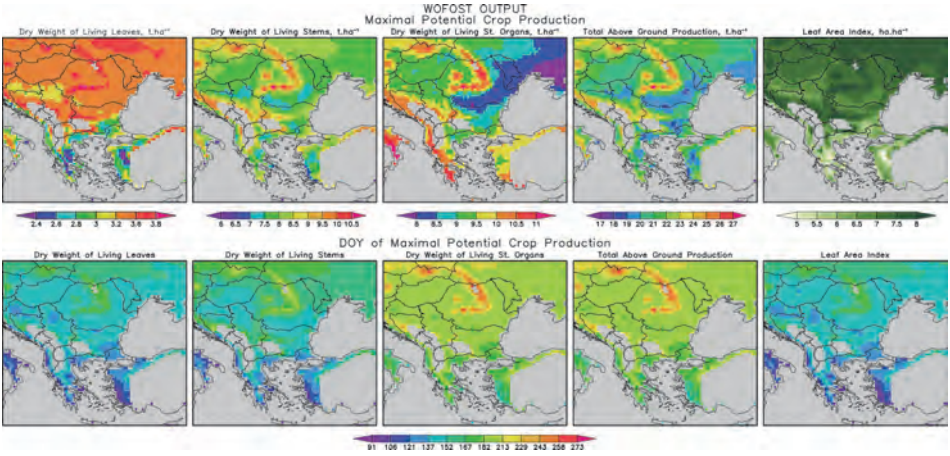

Fig. 7. Maximum value of the yield-related WOFOST output variables and the day of the year, when this maximum is reached.

It is worth mentioning at least two peculiarities of the distributions of the maximums. First is the zone of low productivity, which is elongated from the northeastern corner of the domain to the center. This zone is most clearly expressed in the field of the maximum of dry weight of the storage organs. The reasons for appearance of this zone can be manifold, but most important is perhaps the reduced precipitation in the spring and summer over there, as shown in *Fig. 2*.

The second peculiarity seems at first slightly strange: the productivity over the semi-mountainous regions, which are traditionally not considered as suitable for crop breeding, is bigger than on the plains. This is especially good expressed in the foothill parts of the Carpathians. The plot of the time series of the WOFOST over two gridcells – the first over the Thracian valley in Bulgaria and the second over the Carpathians shows this clearly. In the first gridcell, the maximum is around the end of June and close to 8 t/ha, and in second cell is occurs almost a month later with values near 10 t/ha. In the first case, the main part of the crop development is in June and in the second – in July. Thus, probable explanations for the elevated winter wheat production in the second case are the more favorable weather conditions during the period of yields formation. More specially, the higher yields in more cooler regions are related to a longer growing period (and thus to a longer biomass accumulation period), and that there is a lower drought and heat stress frequency.

The DOY of the maximum of the considered variables and the interrelation between them also look realistic – the distribution of the DOY of the dry weight of leaving leaves and stems, as well as the DOY of the leaf area index are practically identical. The fields of the dry weight of the storage organs and total above-ground production are also identical. Most typical difference between the two groups is the time lag of approximately one month of the second in comparison with the first.

All of the described findings of the performed numerical simulation of the growth and development of winter wheat in Bulgaria and the Balkans, in particular, can be explained with physiological and biological lows of plant organisms. They go through two main stages of development – the vegetative and reproductive stages. During the vegetative stage of growth going on stems, leaves, and roots of the plants, the above descibed findings provide the necessary conditions for the formation and growth of reproductive organs that determines the size of yields. The leaves have the most important function until the moment of physiological maturation of plants. They are the photosynthetic apparatus that ensure the flow of assimilates for the whole plant. After flowering there is no increase of root activity and the root growth is dimishing (in cereals). After formation of reproductive organs, function of leaves gradually decreases and the function of the stems increases that support the growth of these organs. At the same time, a gradual yellowing and dying leaves upwards ensure the flow of assimilates only to the reproductive organs. The whole process is described by logistic or as it is known in biochemistry, autocatalytic functions. This fact justifies the differences in the dates for achieving maximum growth of aboveground parts of plants, as it is shown in *Figs. 8–9*.

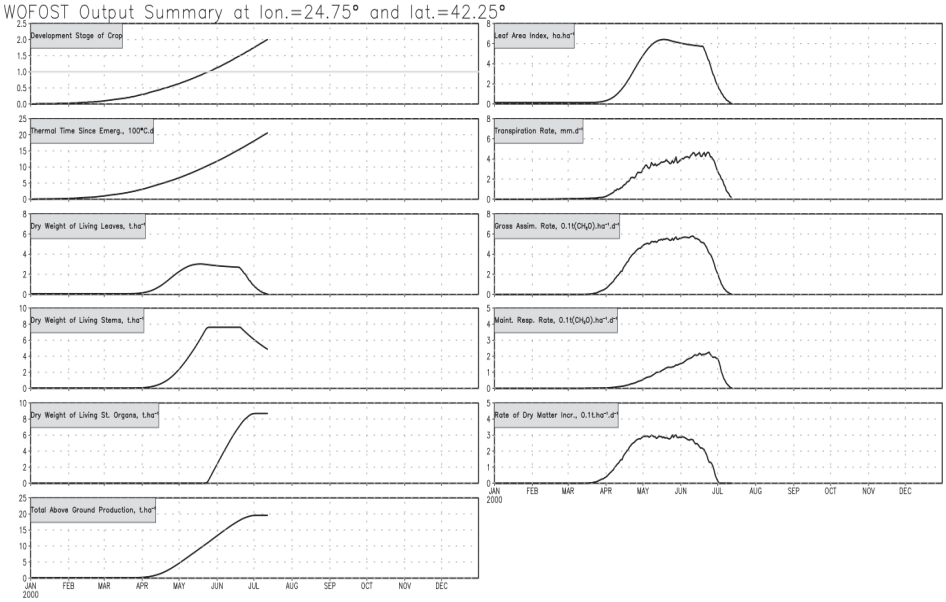

Fig. 8. Time series of the WOFOST potential crop production output parameters for the gridcell in the Thracian valley.

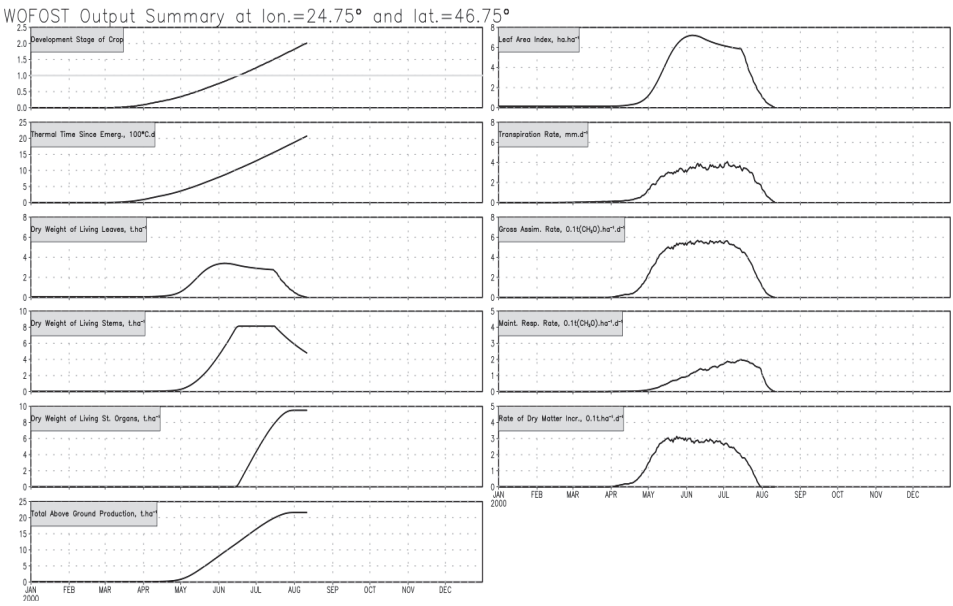

Fig. 9. Same as *Fig. 8*, but for the gridcell in the Carpathian ridge.

4. Conclusion

The most significant outcome of the performed numerical experiment of the application of the crop model WOFOST in grid using meteorological input data from the reanalysis ERA-Interim and the objective analysis E-OBS is the spatial and temporal consistency of the produced output fields. Our study confirms the main conclusion in the work of *de Wit et al*., (2010) regarding the suitability of ERA-Interim for crop modelling. Although such results seem predictable, accounting, first, the spatial and temporal consistency of the input data and, second, the deterministic nature of the CP WOFOST, only the results of such successful simulation can proof this assumption with the necessary rigor. The main limitation of the model system is that only the potential crop production has been taken into consideration so far, which does not allow direct comparison with independent crop yield measurements, therefore, the outcome does not contradict basically with any empirically-derived agrometeorological principles. The produced three-dimensional digital maps of the crop production related parameters offer possibilities of agrometeorological analysis, which would be impossible with the picture derived with meteorological data from limited number (and as rule randomly spread) of stations. Thus, in particular, interesting and significant facts about the spatial and temporal variation of the crop-specific parameters are revealed. The simulation outcome proofs the reliability and suitability of the datasets originated from RA and OA for crop modelling. This is a relevant step ahead in the authors' general plan for preparing more detailed and realistic simulation system. The next step is to include more adequate soil inventory and crop calendar. Later, if implementing seasonal weather forecasting would allow running the system in forecast mode, a futher step will be to predict the future crop production related variables. Such information is of significant importance for wide range of experts and for scientific-based decision-making.

Acknowledgments: We acknowledge the E-OBS data-set from the EU-FP6 project ENSEMBLES (http://ensembles-eu.metoffice.com) and the data providers in the ECA&D project (http://www.ecad.eu). Deep gratitude to the ECMWF for the RA ERA-Interim, and to all other organizations and institutes (IGES/COLA, Unidata, MPI-M and all others) for providing free of charge software and data. Without their innovative data services and tools this study would be not possible. Personal thanks to Dr. Allard de Wit from WUR and Ivan Tzonevsky from ECMWF for the cooperation.

References

Boogaard, H.L., Van Diepen, C.A., Rötter, R.P., Cabrera, J.M.C.A. and *Van Laar, H.H*., 1998: WOFOST 7.1 User's guide for the WOFOST 7.1 crop growth simulation model and WOFOST Control Center 1.5. *Technical Document 52* DLO Winand Staring Centre, Wageningen.

Dee, D.P., Uppala, S.M., Simmons, A.J., Berrisford, P., Poli, P., Kobayashi, S., Andrae, U., Balmaseda, M.A., Balsamo, G., Bauer, P., Bechtold, P., Beljaars, A.C.M., van de Berg, L., Bidlot, J., Bormann, N., Delsol, C., Dragani, R., Fuentes, M., Geer, A.J., Haimberger, L., Healy, S.B., Hersbach, H., Hólm, E. V., Isaksen, L., Kållberg, P., Köhler, M., Matricardi, M., McNally, A.P., Monge-Sanz, B. M., Morcrette, J.-J., Park, B.-K., Peubey, C., de Rosnay, P., Tavolato, C., Thépaut, J.-N. and *Vitart, F*., 2011: The ERA-Interim reanalysis: configuration and performance of the data assimilation system. *Quart. J. Roy. Meteorol. Soc. 137*, 553–597. https://doi.org/10.1002/qj.828

Eitzinger, J., Thaler, S., Orlandini, S., Nejedlik, P., Kazandjiev, V., Håkon Sivertsen, T., and *Mihailovic, D.,* 2009: Applications of agroclimatic indices and process oriented crop simulation models in European agriculture*, Időjárás 113*, 1–12.

Haylock, M.R., Hofstra, N., Klein Tank, A.M.G., Klok, E.J., Jones, P.D., and *New, M.*, 2008: A European daily high-resolution gridded dataset of surface temperature and precipitation for 1950–2006, *J. Geophys. Res. 113*, D20119. https://doi.org/10.1029/2008JD010201

Kazandjiev V. and *Georgieva, V*., 2006: WOFOST Model Calibration for some Cereal Crops in Bulgaria. Proc. of 8th Conference on Meteorology – Climatology and Atmospheric Physics COMECAP 24-26 May 2006, Athens, ISBN 978-960-6806-01-8. 97–102.

Koynov, V., Kabakchiev, I., and *Boneva, V*., 1998: Атлас на почвите в България, Zemizdat, 321. (in Bulgarian)

Leo, O. and *Baruth, B.,* 2013: MARS, the EU Crop monitoring and Yield Forecasting Systems proceeding of the SWF-GEOGLAM. International Meeting on Food Security, Earth Observations and Agricultural Monitoring November 21, 2013, Brussels available online at https://swfound.org/media/126467/10_rtd%20geoglam%20mars%2021%20oct%2013.pdf accessed on the 14.06.2017

Oteng-Darko, P., Yeboah, S., Addy, S.N.T., Amponsah S., and *Owusu Danquah, E*., 2013: Crop modelling: A tool for agricultural research – A review. *E3 Journal of Agricultural Research and Development 2*, 1–6, Available online http://www.e3journals.org

Rounsevell, M.D.A., Berry, P.M., and *Harrison P.A*., 2006: Future environmental change impacts on rural land usebiodiversity: a synthesis of the ACCELERATES project. *Environ. sci. policy 9,* 93–100. https://doi.org/10.1016/j.envsci.2005.11.001

de Wit, A.J.W., Baruth, B., Boogaard, H.L., van Diepen, C.A., van Kraalingen, D.W.G., Micale, F., te Roller, J.A., Supit, I., and *van der Wijngaart, R*., 2010: Using ERA-INTERIM for regional crop yield forecasting in Europe. *Climate Res. 44*, 41–53. https://doi.org/10.3354/cr00872

DOI:10.28974/idojaras.2018.3.6

IDŐJÁRÁS

Quarterly Journal of the Hungarian Meteorological Service
Vol. 122, No. 3, July – September, 2018, pp. 321–343

Bioclimatic and climatic tourism conditions at Zlatibor Mountain (Western Serbia)

Biljana Basarin[1], **Tin Lukić**[1], **Dajana Bjelajac**[1*], **Tanja Micić**[1], **Goran Stojićević**[1], **Igor Stamenković**[1], **Jasmina Đorđević**[1], **Tijana Đorđević**[1], and **Andreas Matzarakis**[2]

[1]*Faculty of Sciences, University of Novi Sad, Department of Geography, Tourism and Hotel Management, Trg Dositeja Obradovića 3, 21000 Novi Sad, Serbia*

[2]*Research Center Human Biometeorology, Deutscher Wetterdienst, Stefan-Meier-Str. 4, 79104 Freiburg, Germany*

Corresponding author Email: dajana.bjelajac92@gmail.com

(Manuscript received in final form May30, 2017)

Abstract— This study presents the climatic and bioclimatic conditions at Zlatibor, as well as their modification and distribution over the year. Zlatibor Mountain is a popular tourist destination in Serbia, and it stands out as a mountain of exquisite natural and anthropogenic values. Information about climate and bioclimate is presented by using physiologically equivalent temperature (*PET*), and universal thermal climate index (*UTCI*) over 10-day periods. The Climate-Tourism/Transfer-Information-Scheme (*CTIS*) was also used as it displays climate and bioclimate information for tourism purposes based on thresholds of relevant parameters and the frequency of occurrence. The weather suitability index (*WSI*) was calculated as well, because it provides synthetic information about suitability of weather for different forms of recreational and tourism activities. The results obtained in this study were used to develop a bioclimatological leaflet for Zlatibor, which could be very useful to the tourism industry and stakeholders in decision-making, but also it will enable tourist to choose the best time for holiday depending on personal preferences and requirements.

Key-words: bioclimate, *PET*, UTCI, CTIS, climatological leaflet, Zlatibor, Serbia

1. Introduction

The environmental resources that are the foundation for tourism/recreation are influenced by weather and climate which also affect the length and quality of tourism and recreation seasons, the health of tourists, and even the quality of tourism experiences (*Scott et al*., 2004; *Katerusha* and *Matzarakis*, 2015; *Stojsavljević et al.,* 2016). Information about climate that is provided to tourists and tourism industry should include not only its general features (mean monthly and annual values of particular climate elements), but also detailed information about thermal comfort as well as aesthetic and physical weather factors (*de Freitas,* 2003). Several studies used bioclimate information and focused on diverse spatial and temporal distributions (*Scott et al.,* 2006; *Scott* and *Lemieux*, 2010; *Matzarakis* and *Amelung*, 2008), but also investigated the ways to incorporate them in tourism sector (*Hall* and *Higham*, 2005; *Matzarakis,* 2006; *Matzarakis* and *de Freitas*, 2001; *Matzarakis et al.,* 2007a; *Amelung et al.,* 2007; *Gössling* and *Hall*, 2006; *Gössling et al*., 2010; *Jopp et al.,* 2010).

During the last three decades, various climate indices for tourism were developed. The widely known and applied is the tourism climate index (*TCI*) (*Mieczkowski,* 1985), which combines seven meteorological parameters but without taking human energy balance into account. From a human-biometeorological point of view, it is necessary to asses the thermo-physiology of human organisms, and consequently their comfort and discomfort, because they are important factors for tourists and their satisfaction during vacations (*Matzarakis,* 2006). Physiologically equivalent temperature (*PET*) is found to be a very useful bioclimatic index for tourism purposes. *PET* uses degree Celsius as a unit, which makes it a good indicator of thermal stress. It also evaluates the thermal conditions in a human physiological manner (*Mayer* and *Höppe,* 1987; *Matzarakis et al.,* 1999; *Höppe*, 1999). Another advantage of *PET* is that it can be applied in different climates and all year round (*Matzarakis et al*., 2007b; *Lin* and *Matzarakis,* 2008; *Zaninović* and *Matzarakis,* 2007; *Gulyás* and *Matzarakis,* 2009; *Çalışkan et al.,* 2011).

PET was used to estimate bioclimatic conditions in different places around the world (e.g., *Gulyas et al*., 2006; *Kovács et al*., 2017; *Thorsson et al*., 2007; *Grigorieva* and *Matzarakis,* 2011). Additionally, *PET* was used to evaluate bioclimatological potential for tourism and recreation in various destinations in different climate zones (e.g., *Matzarakis et al*., 2013; *Katerusha* and *Matzarakis*, 2015; *Çalışkan et al*., 2011; *Brosy et al*., 2014; *Zaninović* and *Matzarakis*, 2009). The first results of biometeorological parameters in Serbia (Vojvodina, northern part of Serbia) were given by *Basarin, et al*., (2014). Respective authors presented a detailed analysis of climate and weather conditions for tourism purposes (for two special nature reserves "Gornje Podunavlje" near

Sombor and "Carska bara" near Zrenjanin), including important parameters such as *PET* and tourism climate index (*TCI*). The latest study based on *PET* analysis in Serbia is published by *Stojićević et al*., (2016), which conducted a detailed bioclimate analysis of Banja Koviljača (Serbia) using *PET* index.

Together, with *PET*, Universal thermal climate index (*UTCI*) (*Jendritzky et al*., 2012) is being used for the assessment of the physiological thermal response of the human body to climatic conditions (*Błazejczyk et al.,* 2012). *UTCI* has been applied in order to determine bioclimatic conditions in cities (e.g., *Idzikowska*, 2010; *Lindner*, 2011), but also to observe the modification of thermal conditions due to the relief features (*Kunert*, 2010). These results are very important for planning different recreational activities, especially at mountain tourism destinations.

The Climate-Tourism/Transfer-Information-Scheme (*CTIS*) (*Matzarakis*, 2007; *Lin* and *Matzarakis,* 2008; *Zaninović* and *Matzarakis,* 2009; *Matzarakis,* 2014) is a recent development in tourism climatology. It displays climate and bioclimate information for tourism purposes based on thresholds of relevant parameters and their frequency of occurrence. Furthermore, it can be adapted to different types of touristic activities. According to *de Freitas* (2003), the three facets of tourism are thermal, physical, and aesthetic, which are combined in *CTIS*. The temporal resolution of *CTIS* is 10 days (*Lin* and *Matzarakis,* 2008). Another index that gives supplementary information about weather suitability for different tourism activities is the weather suitability index (*WSI*) (*Blazejczyk* and *Matzarakis*, 2008). The *WSI* provides information about usefulness of weather for different forms of recreational and tourism activities: passive (sun and air bathing) and active (mild and intensive) (*Blazejczyk* and *Matzarakis*, 2008).

Zaninović and *Matzarakis* (2009) developed a climate leaflet containing climatological and bioclimatological information for tourists. This scheme is valuable for tourists, because it enables them to choose the most suitable time period for holidays depending on personal preferences and requirements. Climate pamphlet is also useful to stakeholders and decision-makers (*Zaninović* and *Matzarakis*, 2009). It includes thermal indices, but also climate facets such as thermal, aesthetical, and physical (*Matzarakis,* 2006), which represent a combination of important factors using mean values and extreme conditions (*Lin* and *Matzarakis,* 2008; *Matzarakis,* 2010).

The bioclimatic analysis in this study concerns Zlatibor Mountain, a popular tourist destination in Western Serbia. Zlatibor Mountain stands out as a mountain of exquisite natural and anthropogenic values, and as such, it is significant for the development of tourism (*Jovanović et al*., 2015). The tourism started to develop at the end of the 19th century and in the beginning of the 20th century, with the substantial increase of tourists since then (*Dragović et al*., 2009). The climate of the investigated area is typical subalpine, with more than 2000 hours of sunshine per year, which makes it one of the most desirable

tourist destinations in Serbia. It is characterized by relatively warm summers and mild winters with abundant snow cover (*Dragović et al.*, 2009; *Stojsavljević et al.,* 2016).

2. Material and methods

2.1. Study area

Zlatibor Mountain is located in Western Serbia. It spreads between 17° 14′ and 17° 28′ E and 43° 36′ and 43° 48′ N. It covers greater parts of the widespread plateau of Starovlaška (*Fig. 1*). The average elevation of Zlatibor is 1000 m. Zlatibor Mountain is often called the "Serbian capital of mountain tourism". The touristic center of Zlatibor is in its central part at an average elevation of 1000 m, and is surrounded by peaks Tornik (1496 m), Čigota (1422 m), and a number of lower ones. Number of tourists during both the summer and winter season, is quite high (*Dragović et al*., 2009; *Stojsavljević et al.,* 2016). Tornik ski resort is located at an elevation of between 1110 – 1490 m, 9 km from the tourist resort of Zlatibor. The total capacity of the ski area is about 5400 skiers per hour. Four runs, Čigota, Tornik, Ribnica, and Zmajevac are covered by an artificial snowing system, so this ski resort no longer depends on snowy weather conditions.

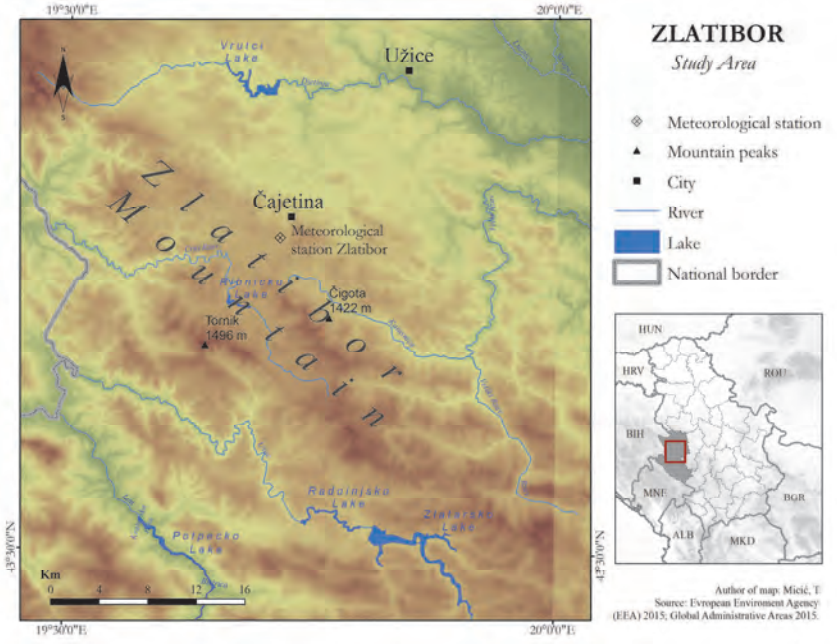

Fig. 1. Physical map of Serbia with the investigated area.

2.2. Data and methods

The climatic and bioclimatic conditions of Zlatibor have been analyzed by using daily data from the Zlatibor meteorological station (43º44'N, 19º43'E, and elevation of 1028 m) during the period between 1992 and 2013. This data is recorded and provided by the Hydrometeorological Service of Serbia in accordance with standards recommended by the World Meteorological Organization (WMO).

Before the calculation of bioclimatological indices, the homogeneity of the meteorological datasets was examined according to the *Alexandersson* (1986) test. The homogeneity analysis indicated that the data for the observed station is homogeneous. There are several methods based on the human energy balance that have been used for the calculation of thermal comfort for tourism (*Matzarkis,* 2006). Commonly used indices that measure the effect of the thermal environment on humans are *PMV* (predicted mean vote) (*Fanger*, 1972), *PET* (physiologically equivalent temperature) (*Mayer* and *Höppe,* 1987; *Höppe,* 1999; *Matzarakis et al*., 1999), *SET* (standard effective temperature) (*Gagge et al*., 1986), *PT* (perceived temperature) (*Staiger et al*., 2012), and *UTCI* (universal thermal climate index) (*Jendritzky et al*., 2012). These thermal indices require input from the same meteorological variables (air temperature, air humidity, vapor pressure, wind speed, short- and long-wave radiation fluxes), but having a detailed thermophysiological basis. *PET* and *UTCI* are seen as preferable to other thermal indices because of their units (°C), which make results more comprehensive (*Matzarakis et al*., 1999).

The *PET* values represent several meteorological parameters that influence the human energy balance such as air temperature, air humidity, wind speed, and short- and long-wave radiation. The calculation of *PET* also considers the heat transfer resistance of clothing and internal heat production (*Matzarakis et al*., 1999; *Lin* and *Matzarakis,* 2008; *Zaninović* and *Matzarakis*, 2009). The RayMan model was used to calculate *PET* (*Matzarakis et al*., 2007b, 2010; *Matzarakis* and *Endler*, 2010). The threshold values for *PET* have been developed in the form of a graded index (*Matzarakis* and *Mayer*, 1996) (*Table 1*). The *PET* (°C) is based on a complete heat budget model of the human body (*Höppe*, 1999), and it provides the equivalent temperature of isothermal reference environment with a water vapor pressure of 12 hPa (50% at 20 °C) and less air (0.1 m/s), at which the heat balance of a reference person is maintained with core and skin temperature equal to those under the conditions being assessed (*Höppe*, 1999). The variables needed and used for calculation include air temperature (*Ta*), vapour pressure (*VP*), wind velocity (*v*), and mean radiant temperature (*Tmrt*). Activity, clothing insulation, height, and weight that are usually standardized in Munich Energy Balance Model for Individuals (*MEMI*) represent human parameters that have a great influence on *PET* values (*Matzarakis et al*., 2011). A typical indoor setting, for the reference person, is selected with work

metabolism of 80 W added to basic metabolism and with clothing insulation of 0.9 clo (*Matzarakis et al.*, 1999; 2007b; *Matzarakis* and *Endler,* 2010). The *PET* values are calculated based on meteorological parameters measured at 7.00 a.m., 2.00 p.m., and 9.00 p.m.

UTCI is defined as the ambient temperature corresponding to a reference environment that provides the same physiological response of a reference person as the actual environment (*Bröde et al*., 2012). The calculation is based on a multi-node model of human thermoregulation (*Fiala et al*., 2001), associated with a clothing model. The meteorological reference frame consists of the mean radiant temperature that is equal to the ambient temperature and the wind speed observed at 10 m above ground set at 0.5 m/s. The reference humidity is set at 50% for ambient temperatures of the reference ≤29 °C and at 20 hPa above. The non-meteorological reference is set at a metabolic rate of 135 W/m^2 and a walking speed of 1.1 m/s. Additionally, by adjusting static clothing insulation to the ambient temperature reflecting seasonal clothing adaptation habits of Europeans, human perception of the outdoor climate is depicted (*Havenith et al*., 2012). The *UTCI* assessment scale is presented in *Table 2*. It is worth mentioning, that while the *PET* scale represents thermal sensations of thermal environment experienced by specific population, the *UTCI* scale was made to represent heat/cold stress intensities regardless the population type. The *UTCI* scale can be applied to a very wide range of temperatures, from –70 to +50 °C (*Bleta et al*., 2014). For the calculations of *UTCI*, the RayMan model was used.

Table 1. Physiological equivalent temperature (*PET*) for different grades of thermal sensation and physiological stress on human beings (*Matzarakis et al.,* 1999)

***PET* (°C)**	**Thermal sensation**	**Physiological stress level**
<4	Very cold	Extreme cold stress
4–8	Cold	Strong cold stress
8–13	Cool	Moderate cold stress
13–18	Slightly cool	Slight cold stress
18–23	Comfortable	No thermal stress
23–29	Slightly warm	Slight heat stress
29–35	Warm	Moderate heat stress
35–41	Hot	Strong heat stress
>41	Very hot	Extreme heat stress

Table 2. UTCI assessment scale: UTCI is categorized in terms of thermal stress (*Bröde et al.*, 2012)

UTCI (°C)	Physiological stress level
< –40	Extreme cold stress
(–40) – (–27)	Very strong cold stress
(–27) – (–13)	Strong cold stress
(–13) – 0	Moderate cold stress
0 – 9	Slight cold stress
9 – 26	No thermal stress
26 – 32	Moderate heat stress
32 – 38	Strong heat stress
38 – 46	Very strong heat stress
> 46	Extreme heat stress

The bioclimatic conditions, *PET* and *UTCI* values are analyzed by means of the annual course of the 10-day mean values of thermal sensation at 7.00 a.m., 2.00 p.m., and 9.00 p.m. during the year. The likelihood of occurrence of mean daily thermal sensation during the year is also included together with the likelihood of occurrences in the morning, afternoon, and evening. This presents a more complete picture of the bioclimatic conditions, and enables everyone to choose the most convenient period for a holiday, considering their personal preferences. The presentation using the temporal resolution of 10 days is very appropriate for tourism, as holidays usually last a week or two, rather than a whole month (*Zaninović* and *Matzarakis*, 2009).

All of the above mentioned parameters are calculated for Zlatibor Mountain, in order to present the climate and bioclimate information to tourists. Furthermore, the results could be presented in a form of bioclimatological leaflet (*Zaninović* and *Matzarakis*, 2009). It is imagined to contain the annual cycle of meteorological variables that are important for tourism and recreation based on 10-day periods (*Zaninović*, 2001; *Lin* and *Matzarakis*, 2008). Parameters that affect tourism on thermal (air temperature, thermal perception), physical (precipitation, snow, wind), and aesthetic dimensions (daylight and clouds) were treated together and were evaluated in a 10-day time resolution (*de Freitas*, 1990; *de Freitas* and *Matzarakis*, 2005). Additionally, annual distribution of mean, mean minimum, and mean maximum temperatures, as well as the number of days with different temperature threshold, representing ice days ($Tmax$<0 °C),

frost days (*Tmin*<0 °C), warm days (*Tmax*≥25 °C), tropical days (*Tmax*≥30 °C) were presented. Cloudiness and the number of clear and overcast days, as well as number of foggy days are included in the aesthetic part of the analysis. Physical factors incorporate the number of days with precipitation, rain, and snow cover. In addition to climatological and bioclimatological parameters, *CTIS* (*Matzarakis,* 2007a, 2007b; *Lin* and *Matzarakis*, 2008; *Zaninović* and *Matzarakis*, 2009; *Matzarakis*, 2014) and *WSI* were used for more successful representation of tourism and recreational conditions in the investigated area (*Zaninović* and *Matzarakis*, 2009; *Blazejczyk* and *Matzarakis*, 2008).

CTIS is very useful in providing information on the frequency of various features of weather in consecutive 10-day periods of the year. Thus, *CTIS* makes the analysis which weather properties would be useful for specific tourism activity very easy. The *CTIS* diagram includes thermal, aesthetic, and physical components of weather as follows:

- Thermal comfort (18.0 °C < *PET* < 29.0 °C);
- Cold stress (*PET* < 0.0 °C);
- Heat stress (*PET* > 35.0 °C);
- Sultriness (*VP* > 18.0 hPa);
- Sunshine days (cloud cover < 4 octas);
- Dry conditions, dry day (precipitation (*RR*) ≤ 1 mm per day);
- Wet conditions, rainy day (*RR* > 5 mm per day);
- Foggy days (relative humidity (*RH*) > 93 %);
- Windy days (*v* > 8 m/s);
- Skiing potential (snow cover > 10 and 30 cm).

For parameters 1, 2, 5, 6, 7, 9, greater probability means less favorable conditions, while for parameters 3, 4, 8, greater probabilities indicates more favorable conditions.

Additionally, *WSI* provides synthetic information about the suitability of weather for different forms of recreational and tourism activities: passive (sun and air bathing) and active (mild and intensive) (*Blazejczyk*, 2007a; 2007b). *WSI* describes weather conditions using seven digits: thermal sensations (due to Subjective temperature – *STI*), radiation stimuli (due to absorbed portion of radiation), physiological strain (due to the physiological strain index – *PhS*), sultriness (due to the heat stress index – *HSI*), daily thermal contrast (due to the temperature amplitude), rain (snow) fall (> 1 mm), and snow cover (> 10 cm) (*Blazejczyk*, 2007a; 2007b).

Every weather condition was assigned a specific code based on particular forms of recreation: sun baths (*SB*), air baths (*AB*), mild recreational activity (e.g., walking, light plays, shopping – *MR*), intensive recreation and summer tourism (e.g., football, biking, climbing, jogging, etc. – *AR*), and ski tourism (*ST*). Every weather condition was estimated using *WSI* as follows: 0 – unfavorable, 1 – favorable with limitations, 3 – favorable without limitations (*Blazejczyk* and *Matzarakis*, 2008). Calculation of all of the above mentioned parameters is adopted from the approach given by *Basarin et al*. (2014).

3. Results

3.1. Air temperature (Ta), humidity (RH), vapor pressure (VP), precipitation (RR), snow, and wind (v)

The frequency distribution of air temperature (*Ta*) for the period from 1992 until 2013 is shown in *Fig. 2*.

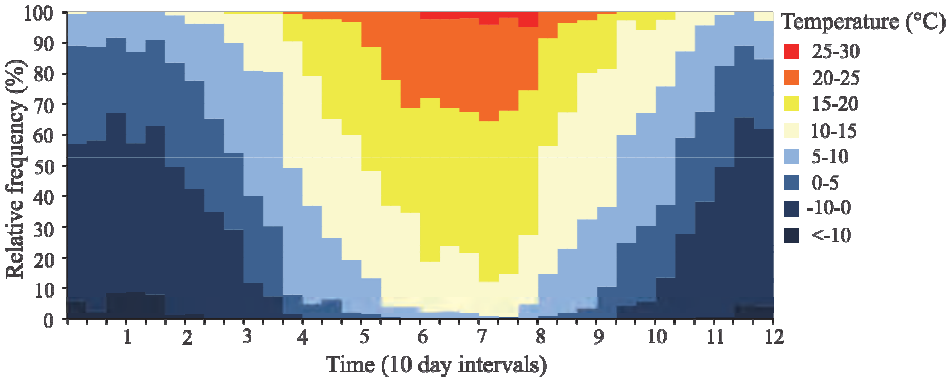

Fig. 2. Relative frequency diagrams of mean daily air temperature for Zlatibor for the period from 1992 to 2013.

Hottest days occur during the summer months with up to 5% of values ranging from 25–30 °C in July and August. The highest percentage was observed in the third period of August. Coldest days can be observed from the second ten-day period in October until the beginning of April. In December and January, more than 50% of days display temperatures ranging between −10.0 and 0.0 °C. Days <−10 °C are rare and show the highest amount (8%) in the third ten-day period in January and February.

Air temperature is also analyzed by means of the annual course of the 10-day mean values measured at 7.00 a.m., 2.00 p.m., and 9.00 p.m. during the year (*Fig. 3*). The mornings and late afternoons are very cold ((–5) – 0 °C) from November until the end of February. From the second ten-day period in April until the third ten-day period in August, mornings and late afternoons are pleasant with temperatures ranging from 10 to 20 °C. During noon in summer months, temperatures could be very high with average values ranging between 20–25 °C.

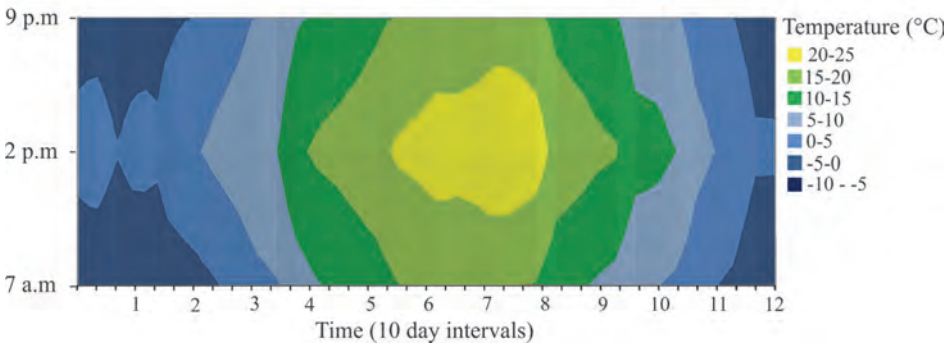

Fig. 3. Annual course of 10-day mean air temperatures at 7 a.m., 2 p.m., and 9 p.m. in Zlatibor for the period from1992 to 2013.

The same kind of frequency diagram was produced for *RH* and *VP* (*Figs. 4* and *5*). Values of *RH* show a high variability with atypical annual cycle. More than 50% of the values in the range between 85 and 95 and above 95% *RH* or even higher are observed during the winter months, December, January, and February. During the same period *RH* between 65% and 85% take up approximately 50% of values. In the summer months, values of *RH* between 45% and 75% occur in approximately 50% of the cases. Values lower than 45% as well as values higher than 85% are rare and take up 10 to 15% of all the cases.

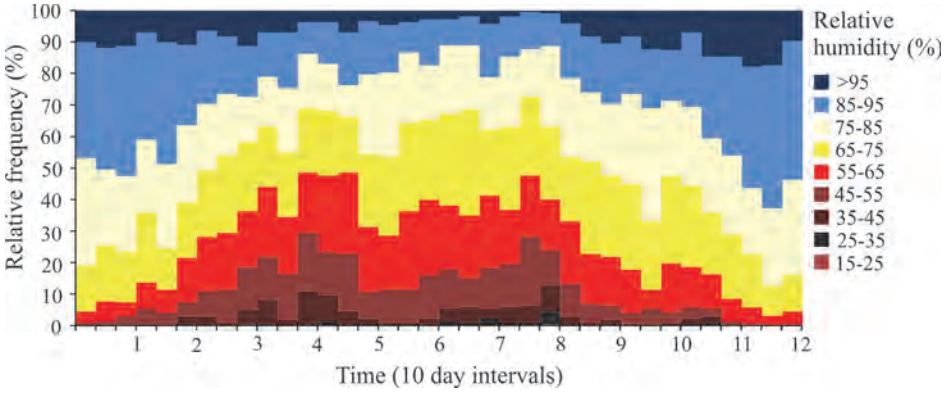

Fig. 4. Relative frequency diagram of relative humidity based on 10-day periods for mean daily values for Zlatibor for the period 1992–2013.

Fig. 5 shows the relative frequency diagram for *VP*. *VP* values equal or higher than 18 hPa, that characterize sultriness, occurs on the average from June until August. The highest amounts occur during July with approximately 10% of the cases. This number makes sultry events very rare at Zlatibor Mountain during the summer months.

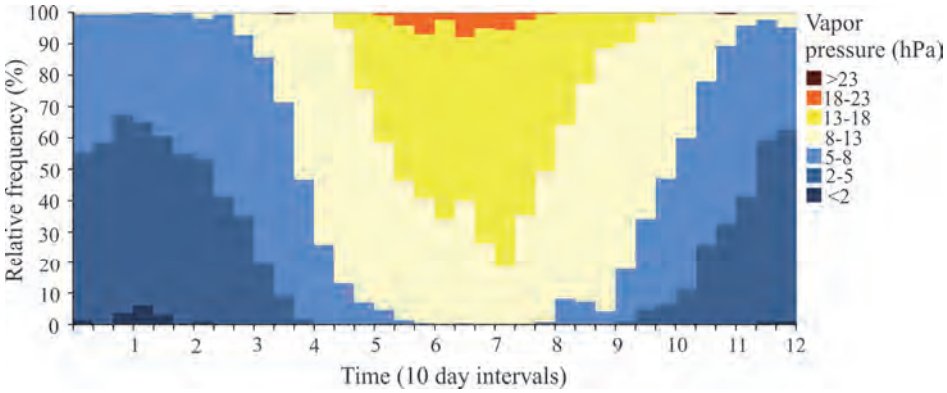

Fig. 5. Relative frequency diagram of vapor pressure based on 10-day periods for mean daily values for Zlatibor for period 1992–2013.

Average number of days with *RR* per year for Zlatibor during the investigated period was 178, days with no rain occur on average for 187 days, while the days with precipitation higher than 5 mm could be observed for 72 days. The frequency distribution of *RR* for Zlatibor was analyzed in order to characterize the rainy periods (*Fig. 6*). Rain events of low intensity (*RR* 0–1 mm) occur all over the year in approximately 5–15% of the cases. Heavy rainfalls also appear throughout the year, but it seems that they are concentrated during late spring and summer months, respectively. The class of most intensive rainfall (*RR* > 20.0 mm per day) was also recorded during the year, but in winter months at only 1–3% of the cases.

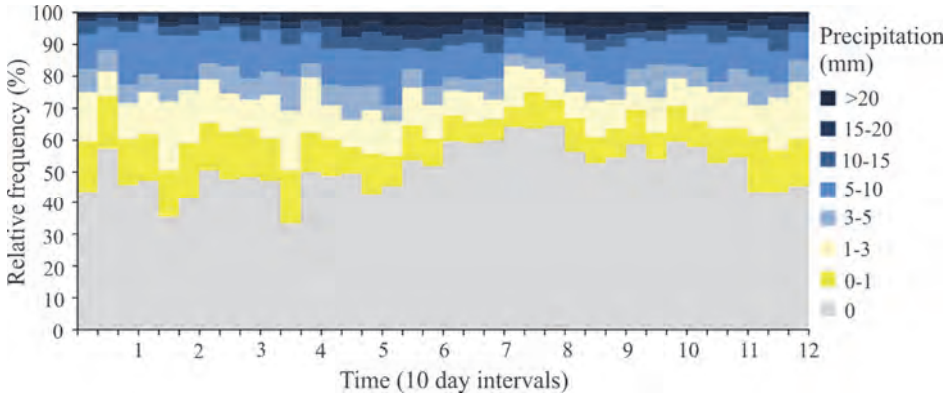

Fig. 6. Frequency diagram of precipitation classes for Zlatibor Mountain for the period 1992–2013.

A snow cover ≥1 cm can be expected at Zlatibor Mountain from the first half of October until the second half of April. Snowy winter lasts on average for more than five months (not with a continuous snow cover). *Fig. 7* depicts the annual course of the mean monthly number of days with snow cover of different depth classes (≥1 cm, ≥10 cm, ≥30 cm, and ≥50 cm). It can be seen that autumn months (September – November), as well as the first part of winter (December) experience a rarer appearance of snow than the second half of the snow season (January and February).

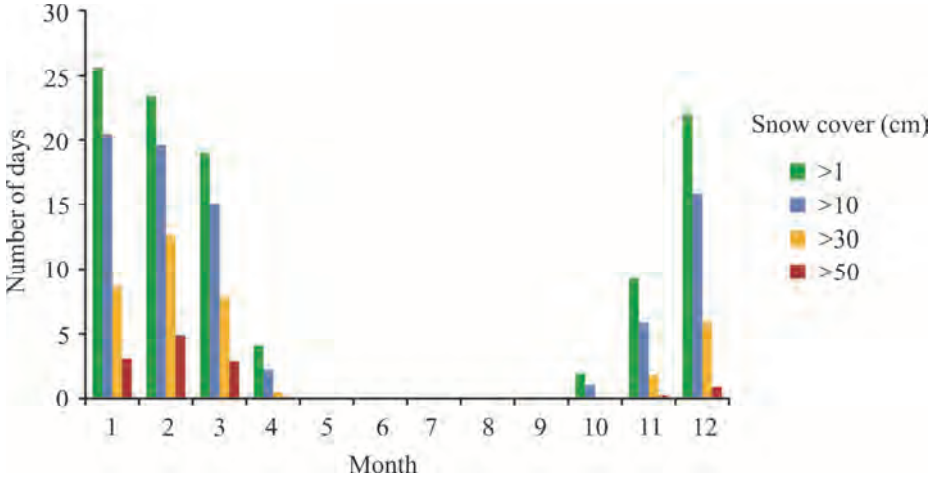

Fig. 7. Annual course of mean monthly number of days with snow cover of different depth classes for Zlatibor Mountain in the period between 1992 and 2013.

Wind direction distribution is visualized by the use of wind charts based on mean values measured daily at 7 a.m., 2 p.m., and 9 p.m. (*Figs. 8a–c*). The prevailing wind directions are SW for all values. During mid-day, the N direction becomes dominant. Wind speeds between 1 and 3 m/s could be observed in approximately 20% of the cases registered at 7 a.m. During noon, the prevailing winds are N and SW with speeds ranging between 0.5–1 m/s in 10% of the cases. In the evening, the dominant winds have speeds in the same range as the ones in the noon (0.5–1 m/s).

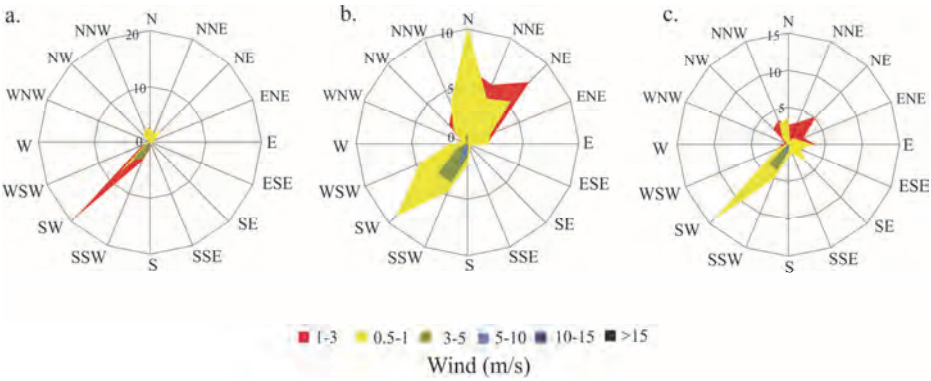

Fig. 8. Wind roses for Zlatibor Mountain based on daily values, for the period from 1992 to 2013 (excluding calms); a) values measured at 7 a.m. (calms=9.7%), b) values measured at 2 p.m. (calms=3.7 %), and c) values measured at 9 p.m. (calms=11.9%).

3.2. Bioclimatological conditions

The different thermal sensations according to *PET* and *UTCI* values at 7 a.m., 2 p.m., and 9 p.m. in ten-day periods are shown in *Fig. 9*. An analysis of Zlatibor's 10-day mean *PET* values between 1992 and 2013 shows, that extreme cold stress may be experienced in morning and evening hours during the colder part of the year (from the end of October through the second ten-day period of March). The extreme cold stress is relatively less observed during afternoons. Better thermal comfort conditions are seen during spring and autumn. The second half of April, May, September, and the first half of October are characterized by *PET* values that seem to be comfortable mostly throughout the day. During summer, June, July, and August experience comfortable thermal conditions in the morning and in late afternoon. During noon in these months, a hot stress can be experienced (*Fig. 9a*). Similar thermal sensations concerning *UTCI* were observed (*Fig. 9b*). The extreme cold stress is observed during whole day in November, December, January, February, and even March. From the second ten-day period in April until July, and from the third ten-day period in August to the end of September, comfortable thermal conditions prevail throughout the day. The heat stress is only present during midday in July and August (*Fig. 9b*).

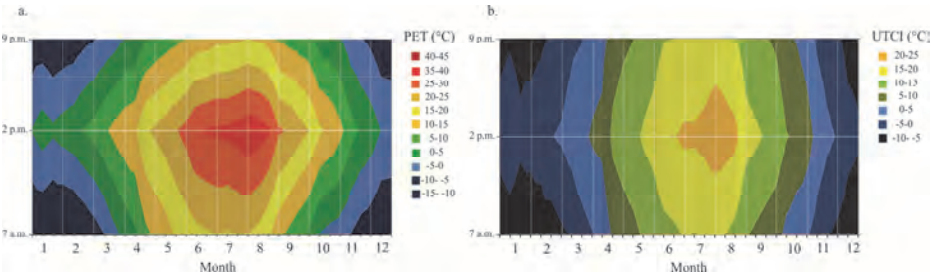

Fig. 9. Annual course of 10-day mean values of thermal sensation a) *PET* b) *UTCI* at 7 a.m., 2 p.m., and 9 p.m. at Zlatibor Mountain for the period 1992–2013.

Relative frequencies for *PET* values divided into 11 classes are presented in *Fig. 10a*. Special thermal conditions are presented by specific class for ten-day intervals at 2 p.m. throughout the year during the period 1992–2013. Similarly, the frequencies of *UTCI* are also shown for ten-day periods at 2 p.m. for the entire year during the investigated period (*Fig. 10b*). Thermal comfort occurs throughout the entire year according to both *PET* and *UTCI*. *PET* values

between 18 and 23 °C with highest probability (>25%) occur in the third ten-day period in April and May, as well as in the end of September and October. Comfortable thermal class of *UTCI* occurs mostly during spring and autumn months with the highest probability of more than 50%. *PET* classes that indicate cold stress (<0 °C) conditions can be observed from October to the end of March, with highest frequencies (~50%) from December until the end of January. During the same period, the *UTCI* values lower than 0 °C can be seen from September to May. The highest frequencies of extreme cold stress (>50%) are present from December until the end of February. Days with strong heat stress, defined as *PET* values >35 °C, can be observed from the third ten-day period in April until the end of September with maximum frequencies (~30%) during June until August. *UTCI* values >26 °C are recorded from the end of May until the end of September with the highest frequencies in the beginning of August (~20%).

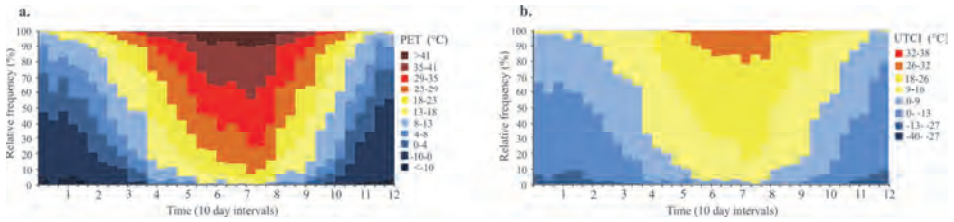

Fig. 10. The probability of occurrence of different thermal sensations a) *PET* and b) *UTCI* at 2 p.m. at Zlatibor Mountain for the period 1992–2013.

3.3. Climate-Tourism Information Scheme (CTIS) and Weather Suitability Index (WSI)

The annual courses of different parameters and factors that are described earlier are summarized clearly in the *CTIS* for Zlatibor Mountain (*Fig. 11*). Following the frequency of thermally unsuitable *PET* classes, the highest percentage of days with cold and heat stress is found in the monthly decades with a high proportion of cold or heat stress. Thus, the months with low percentage of these unfavorable *PET* classes are thermally favorable. The highest amount of thermally comfortable days is found in June, July, and August. When comparing the percentage of days with sunshine duration (>5h) to dry days, it can be seen that all over the year there are positive values. The lack of days with high wind speed contributes to the suitability of Zlatibor's bioclimatological conditions

during summer months. Snow cover, which is an advantage in touristic terms, concentrates mostly at the end of December, during January, and February, which is recognized as the month with the highest occurrence of the days with snow cover higher than 10 cm.

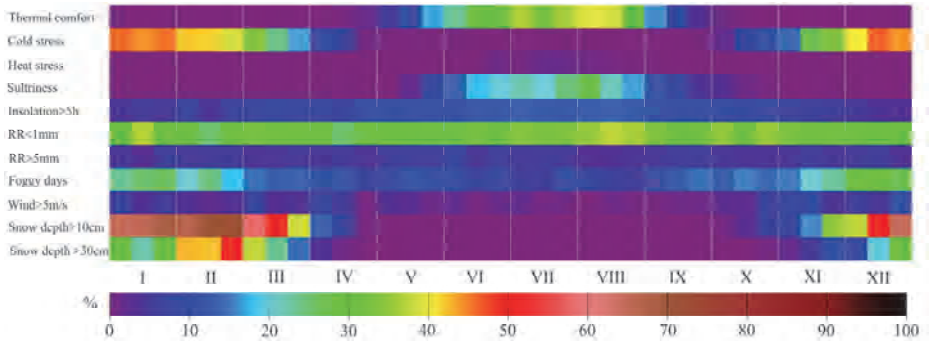

Fig. 11. CTIS for Zlatibor Mountain (frequency of occurrence in the period 1992–2013 in percent).

Weather suitability index (*WSI*) provides another important clue about bioclimatological conditions for tourists and recreationists. It is used to assess the usefulness of particular weather conditions for different forms of activity. *Fig. 12* shows patterns in annual variability of *WSI*. It can be seen that the weather conditions most favorable for passive recreation (sun and air baths, *WSI_SB* and *WSI_AB*) occur during summer months. However, the conditions for mild recreational activity (e.g. walking, light plays, shopping – *WSI_MR*) are best during the warmer part of the year from the 150th day (end of May) until the 300th (end of October) of the year. On the other hand, intensive forms of active recreation (*WSI_AR*) can be practiced throughout the whole year. The weather conditions for ski tourism (*WSI_ST*) are favorable during winter due to the snow cover and snow cover duration. The ski season is prolonged using artificial snowing system installed at Tornik ski resort.

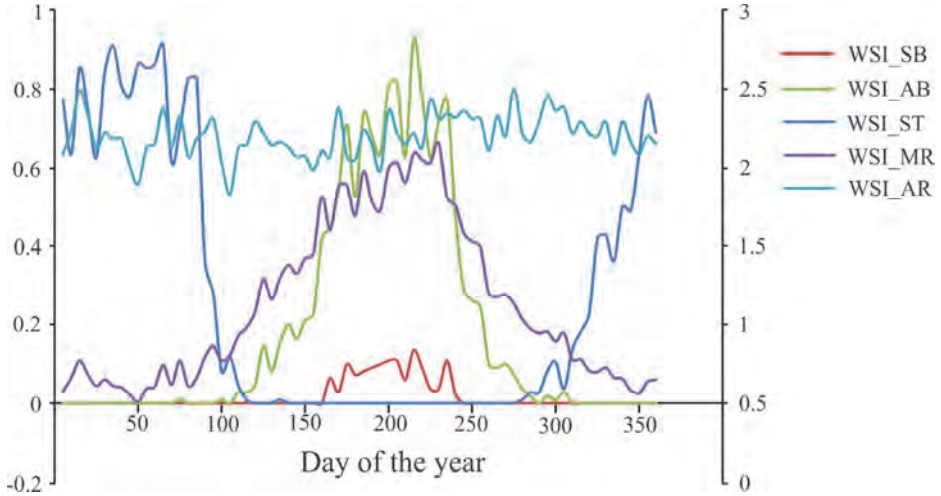

Fig. 12. Annual variations of weather suitability index for Zlatibor Mountain based on five-day intervals for the period between 1992 and 2013. The abbreviations are as follow: WSI_SB - sun baths (right y-axis), *WSI_AB* - air baths (right y-axis), *WSI_ST* - ski tourism (left y-axis), *WSI_MR* - mild recreational activity (left y-axis), *WSI_AR* - intensive recreation and summer tourism(left y-axis); index values refer to 0 – unfavorable, 1 – favorable with limitations, 3 – favorable without limitations.

4. Discussion

Results of the earlier studies showed that bioclimatological indices such as *PET* and *UTCI* reflect the thermal condition better than air temperature, relative humidity, and other individual meteorological elements.

This study assesses the bioclimate potential for tourism of one of the most important tourism destinations in Serbia. Recently, the leaflet as a mean of presenting the climate and bioclimate information for tourists was introduced (*Zaninović* and *Matzarakis*, 2009). Similarly, in this study a climatological and bioclimatological brochure was proposed as a "tool" that could help tourists to learn more about the climate of the destination and choose the best time to travel. It evaluates the aesthetic, physical, and thermal conditions for Zlatibor Mountain in order to reveal its potential for tourism and recreation.

The bioclimatic indexes such as *PET* and *UTCI* are more understandable for people, which use their experience in an indoor environment to assess the outdoor thermal condition. Furthermore, the *PET* and *UTCI* frequencies for 10-day intervals combined with the results of the analysis of aesthetic weather

components, as well as physical variables, display the likelihood of certain perceptions in detail for the whole year (*Lin* and *Matzarakis,* 2008).

Similarly to Bursa's (*Çalışkan et al*., 2012) and Hvar's (*Zaninović* and *Matzarakis*, 2009) bioclimatological leaflet for Zlatibor mountain, in the left hand column, temperature conditions given in annual course of mean, mean minimum, and mean maximum values and annual course of relative humidity could be presented. Days with extreme temperature values suppose to be classified (hot days, tropical days, frost days, and tropical nights), and their annual distribution should be given in 10-day intervals. The components of aesthetic weather conditions such as cloudiness, insolation, as well as the number of clear and overcast days could be presented as well. Thermal parameters must be analyzed using *PET* and *UTCI* values in 10-day intervals. The number of days with precipitation (snow and rain) should also be included, as well as days with different classes of snow depth. In addition, the brochure can also include precise information about the mean wind speed and direction over the year for the investigated area. For tourists that are fond of different recreational activities during their holiday, *WSI* could be included in the leaflet.

Lin and *Matzarakis* (2008) showed that the number of tourists visiting the Sun Moon Lake in Taiwan is not significantly affected by climatic and bioclimatic factors. They argued that the most frequently visited periods are not the best time for visit, as tourists may suffer from cold stress or rainy periods. According to the Statistical Office of the Republic of Serbia, more than 106,000 people, mainly domestic tourists visited The Zlatibor Mountain. As shown by *Stojsavljević et al.* (2016), an increase in the number of tourists can be observed in the period 2001–2014. Using the monthly data about tourist visits for the period between 2000 and 2013 and the average monthly *PET* values for the same period, the correlation coefficient is 0.6, and it is statistically significant ($p < 0.05$) (*Fig. 13*). Comparing the mean monthly *UTCI* values, the Pearson correlation coefficient is even higher, it is 0.7 ($p < 0.05$). It could be seen that the highest number of tourists visit Zlatibor during May, June, August, and September, when the thermal comfort conditions occur on more than 30% of the cases for *PET* and more than 50% for *UTCI*, as the comfort range for *UTCI* scale is considerably higher.

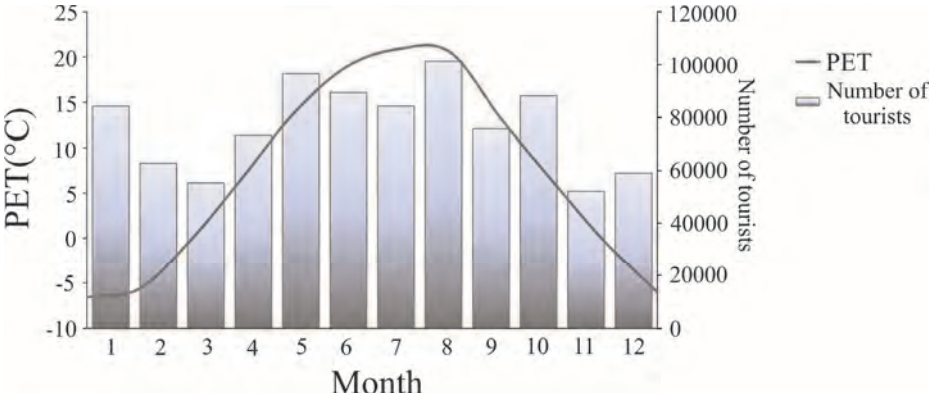

Fig. 13. Annual and seasonal number of tourists who visited Zlatibor during the period between 2000 and 2013.

5. Conclusion

The aim of this study was to analyze Zlatibors's climatic and bioclimatic conditions, as well as their variability and distribution over the year in order to provide substantial information for the tourism and tourism industry in general. The results were the basis for the creation of a bioclimate and tourism climate brochure, which is user-friendly and understandable by everyone. It is produced to be used as part of tourism promotions, and it is very important for the evaluation of various natural resources and alternatives. Since Zlatibor offers thermo physiologically comfortable conditions during spring and autumn, but also during morning and late afternoons in summer, the mountain resort is suitable for different health, recreation, and other tourism activities from May to September. The number of days with snow cover higher than 10 cm enhanced with artificial snowing system enables the continuous ski-season from December until April. One advantage of Zlatibor's climatology is that insolation during the day in summer is higher than 10 hours, which makes it one of the sunniest destinations in Serbia. Snowy winters, thermos-physiologically comfortable spring and autumn, as well as warm summers, provide favorable bioclimatological conditions, thus allowing year-round touristic activities.

Monitoring of detailed bioclimate parameters and their variability on the local, regional, and national level can contribute to the creation of the suitable platform for the strategic planning and adaptation of tourist destinations in Serbia and neighboring countries as well.

Acknowledgements: This research was supported by Project 176020 of the Serbian Ministry of Education, Science and Technological Development and by Project 114-451-2080/2016 of the Provincial Secretariat for Science and Technological Development, Vojvodina Province.

References

Alexandersson, H., 1986: A homogeneity test applied to precipitation data. *J. Climatol. 6,* 661–675. https://doi.org/10.1002/joc.3370060607

Amelung, B., Blazejczyk, K., and *Matzarakis, A*., 2007: Climate change and tourism: assessment and coping strategies. Maastricht–Warsaw– Freiburg. 1–227.

Basarin, B., Kržič, A., Lazić, L., Lukić, T., Đorđević, J., Janićijević Petrović, B., Ćopić, S., Matić, D., Hrnjak, I., and *Matzarakis, A.* 2014: Evaluation of bioclimate conditions in two Special Nature Reserves in Vojvodina (Northern Serbia). *Carpathian J. Earth Environ. Sci. 9 (4),* 93–108.

Błazejczyk, K., Epstein, Y., Jendritzky, G., Staiger, H., and *Tinz, B.,* 2012: Comparison of UTCI to selected thermal indices. *Int. J. Biometeorol. 56,* 515–535. https://doi.org/10.1007/s00484-011-0453-2

Blazejczyk, K., 2007a: Weather limitations for winter and summer tourism in Europe. In (Eds. *Matzarakis, A., de Freitas, C.R.* and *Scott, D*.) Developments in Tourism Climatology. Commission on Climate, Tourism and Recreation, International Society of Biometeorology, Freiburg. 116–121.

Blazejczyk, K., 2007b: Multiannual and seasonal weather fluctuations and tourism in Poland. In (Eds. *Amelung, B., Blazejczyk, K*. and *Matzarakis A*.) Climate Change and Tourism Assessment and Copying Strategies. Albert-Ludwig Universitaet Freiburg, Maastricht – Warsaw – Freiburg. 69–90.

Blazejczyk, K. and *Matzarakis, A.,* 2008: Evaluation of climate from the point of view of recreation and tourism. In (Ed. *Masami, I*.), Proceedings of the 18th International Congress of Biometeorology, Harmony within Nature. CD Hum3-COST-O04, 1–4.

Bleta, A., Nastos, P. T., and *Matzarakis, A.,* 2014: Assessment of bioclimatic conditions on Crete Island, Greece. *Regional Environ. Change 14,* 1967–1981. https://doi.org/10.1007/s10113-013-0530-7

Bröde, P., Fiala, D., Blazejczyk, K., Holmer, I., Jendritzky, G., Kampmann, B., Tinz, B., and *Havenith, G.,* 2012: Deriving the operational procedure for the Universal Thermal Climate Index (UTCI), *Int. J. Biometeorol. 56,* 481–494. https://doi.org/10.1007/s00484-011-0454-1

Brosy, C., Zaninović, K., and *Matzarakis, A.,* 2014: Quantification of climate tourism potential of Croatia based on measured data and regional modeling, *Int. J. Biometeorol. 58,* 1369–1381. https://doi.org/10.1007/s00484-013-0738-8

Çalışkan, O., Çiçek, I., and *Matzarakis, A.,* 2011: The climate and bioclimate of Bursa (Turkey) from the perspective of tourism, *Theor. Appl. Climatol. 107,* 417–425. https://doi.org/10.1007/s00704-011-0489-6

de Freitas C.R., 1990: Recreation climate assessment. *Int. J. Climatol. 10,* 89–103. https://doi.org/10.1002/joc.3370100110

de Freitas C.R., 2003: Tourism climatology: evaluating environmental information for decision making and business planning in the recreation and tourism sector. *Int. J. Biometeorol. 48,* 45–54. https://doi.org/10.1007/s00484-003-0177-z

de Freitas C.R. and *Matzarakis, A.,* 2005: Recent developments in tourism climatology, *Bull. German Meteorol. Soc. 1*, 2–4.

Dragović, R., Filipović, I., and *Nikolić, J.,* 2009: Iskoristivost prirodno-geografskih uslova Zlatibora i Zlatara za razvoj ekoturizma i zdravstvenog turizma. *Bull. Serbian Geogr. Soc. 89*, 115–128. (in Serbian). https://doi.org/10.2298/GSGD0901115D

Fanger P.O., 1972: Thermal comfort: analysis and applications in environmental engineering. McGraw-Hill, New York. 1–244.

Fiala, D., Lomas, K.J., and *Stohrer, M.,* 2001: Computer prediction of human thermoregulatory and temperature responses to a wide range of environmental conditions. *Int. J. Biometeorol. 45,* 143–159. https://doi.org/10.1007/s004840100099

Gagge, A.P., Fobelets, A.P., and *Berglund, L.G.,* 1986: A standard predictive index of human response of the thermal environment, *ASHRAE Trans 92,* 709–731.

Gössling, S. and *Hall, C.M.,* 2006: Uncertainties in predicting tourist travel flows based on models, *Climatic Change 79,* 163–173. https://doi.org/10.1007/s10584-006-9081-y

Gössling, S., Hall, C.M., Peeters, P., and *Scott, D.,* 2010: The future of tourism: a climate change mitigation perspective. *Tourism Recreat. Res. 35,* 119–130. https://doi.org/10.1080/02508281.2010.11081628

Grigorieva, E. and *Matzarakis, A.,* 2011: Physiologically equivalent temperature as a factor for tourism in extreme climate regions in the Russian Far East: preliminary results, *Eur. J. Tourism, Hosp. and Recreation 2,* 127–142.

Gulyás, Á. and *Matzarakis, A.,* 2009: Seasonal and spatial distribution of PET – physiologically equivalent temperature (PET) in Hungary. *Időjárás 113,* 221–231.

Gulyas, A., Unger, J., and *Matzarakis, A.,* 2006: Assessment of the microclimatic and human comfort conditions in a complex urban environment: modelling and measurements, *Build. Environ. 41,* 1713–1722. https://doi.org/10.1016/j.buildenv.2005.07.001

Hall C.M. and *Higham J.,* 2005: Tourism, recreation and climate change (Aspects in tourism). Channel View, Claverdon. 1–328.

Havenith, G., Fiala, D., Błazejczyk, K., Richards, M., Bröde, P., Holmér, I., Rintamaki, H., Benshabat, Y., and *Jendritzky, G.,* 2012: The UTCI clothing model, *Int. J. Biometeorol. 56,* 461–470. https://doi.org/10.1007/s00484-011-0451-4

Höppe, P., 1999: The physiological equivalent temperature- a universal index for the biometeorological assessment of the thermal environment, *Int. J. Biometeorol. 43,* 71–75. https://doi.org/10.1007/s004840050118

Idzikowska, D., 2010: Differences in bioclimatic conditions in four European cities: Budapest, Paris, Rome and Warsaw. In (Eds. *Matzarakis, A., Mayer, H.* and *Chmielewski, F.M.*) Proceedings of the 7th Conference on Biometeorology. 201–206.

Jendritzky, G., de Dear, R., Havenith, G., 2012: UTCI—Why another thermal index?, *Int. J. Biometeorol. 56,* 421–428. https://doi.org/10.1007/s00484-011-0513-7

Jopp, R., DeLacy, T., and *Mair, J.,* 2010: Developing a framework for regional destination adaptation to climate change, *Curr. Iss. Tourism 13,* 591–605. https://doi.org/10.1080/13683501003653379

Jovanović, D., Govedarica, M., Sabo, F., Bugarinović, Ž., Novović, O., Beker, T., and *Lauter, M.,* 2015: Land Cover change detection by using Remote Sensing – A Case Study of Zlatibor (Serbia). *Geographica Pannonica 19,* 162–173. https://doi.org/10.5937/GeoPan1504162J

Katerusha, O. and *Matzarakis, A.,* 2015: Thermal Bioclimate and Climate Tourism Analysis for Odessa. *Geografiska Annaler: Series A, Physical Geography 97,* 671–679. https://doi.org/10.1111/geoa.12107

Kovács, A., Németh, A., Unger, J., and *Kántor, N*. 2017: Tourism climatic conditions of Hungary – present situation and assessment of future changes. *Időjárás 121,* 79–99.

Kunert, A., 2010: Modeling of UTCI index in various types of landscape. In ((Eds. *Matzarakis, A., Mayer, H*. and *Chmielewski, F.M.*,), Proceedings of the 7th Conference on Biometeorology. 302–307.

Lin, T.P. and *Matzarakis, A.,* 2008: Tourism climate and thermal comfort in Sun Moon Lake, Taiwan, *Int. J. Biometeorol. 52,* 281–290. https://doi.org/10.1007/s00484-007-0122-7

Lindner, K., 2011: Assessment of sensible climate in Warsaw using UTCI, *Prace i Studia Geograficzne 47*, 285–291.

Matzarakis, A., 2006: Weather and climate related information for tourism, *Tourism Hospital. Plan. Develop. 3,* 99–115.

Matzarakis, A., 2007: Assessment method for climate and tourism based on daily data. In (Eds. *Matzarakis, A., de Freitas C.R*. and *Scott D*.), Developments in tourism climatology. Commission on Climate, Tourism and Recreation, International Society of Biometeorology, Freiburg. 52–58.

Matzarakis, A., 2010: Climate change: temporal and spatial dimension of adaptation possibilities at regional and local scale. In (Ed. *Schott, C.*), Tourism and the implications of climate change: issues and actions (Bridging tourism theory and practice vol. 3). Emerald Group Publishing, Bingley. 237–259.

Matzarakis, A., 2014: Transfer of climate data for tourism applications – The Climate-Tourism/Transfer-Information-Scheme. *Sust. Environ. Res. 24,* 273–280.

Matzarakis, A. and *Mayer, H.,* 1996: Another kind of environmental stress: thermal stress. *WHO Newsletter 18*, 7–10.

Matzarakis, A., Mayer, H., and *Iziomon, M.G.,* 1999: Applications of a universal thermal index: physiological equivalent temperature, *Int. J. Biometeorol. 43,* 76–84. https://doi.org/10.1007/s004840050119

Matzarakis, A. and *de Freitas, C.R.,* 2001: Proceedings of the first international workshop on climate, tourism and recreation. International Society of Biometeorology, Commission on Climate Tourism and Recreation, Freiburg. 1–270.

Matzarakis, A. and *Amelung, B.,* 2008: Physiologically equivalent temperature as indicator for impacts of climate change on thermal comfort of humans. In (Eds. *Thomson, M.C., Garcia-Herrera, R.* and *Beniston, M.*) Seasonal Forecasts, Climatic Change and Human Health. Advances in Global Change Research, vol. 30. Springer Sciences and Business Media, Berlin. 161–172. https://doi.org/10.1007/978-1-4020-6877-5_10

Matzarakis, A., de Freitas, C. R., and *Scott, D.,* 2007a: Developments in tourism climatology. Commission on Climate, Tourism and Recreation, International Society of Biometeorology, Freiburg. 1–289.

Matzarakis, A., Rutz, F., and *Mayer, H.,* 2007b: Modelling Radiation fluxes in simple and complex environments – application of the RayMan model. *Int. J. Biometeorol. 51,* 323–334. https://doi.org/10.1007/s00484-006-0061-8

Matzarakis, A. and *Endler, C.,* 2010: Climate change and thermal bioclimate in cities: impacts and options for adaptation in Freiburg, Germany. *Int. J. Biometeorol. 54,* 479–483. https://doi.org/10.1007/s00484-009-0296-2

Matzarakis, A., Rutz, F., and *Mayer H.,* 2010: Modelling Radiation fluxes in simple and complex environments – Basics of the RayMan model. *Int. J. Biometeorol. 54,* 131–139. https://doi.org/10.1007/s00484-009-0261-0

Matzarakis, A., Muthers, S., and *Koch, E.,* 2011: Human biometeorological evaluation of heat-related mortality in Vienna. *Theor. Appl. Climatol. 105,* 1–10. https://doi.org/10.1007/s00704-010-0372-x

Matzarakis, A., Rammelberg, J., and *Junk, J.,* 2013: Assessment of thermal bioclimate and tourism climate potential for central Europe—the example of Luxembourg. *Theor. Appl. Climatol. 114,* 193–202. https://doi.org/10.1007/s00704-013-0835-y

Mayer, H. and *Höppe, P.,* 1987: Thermal comfort of man in different urban environments, *Theor. Appl. Climatol. 38,* 43–49. https://doi.org/10.1007/BF00866252

Mieczkowski, Z., 1985: The tourism climate index: a method for evaluating world climates for tourism. *Canadian Geographer 29,* 220–233. https://doi.org/10.1111/j.1541-0064.1985.tb00365.x

Scott, D. and *Lemieux, C.,* 2010: Weather and climate information for tourism, *Procedia Environ. Sci. 1,* 146–183. https://doi.org/10.1016/j.proenv.2010.09.011

Scott, D., McBoyle, G., and *Schwartzentruber, M.,* 2004: Climate change and the distribution of climatic resources for tourism in North America, *Climate res. 27,* 105–117. https://doi.org/10.3354/cr027105

Scott, D., McBoyle, G., Minogue, A., and *Mills, B.,* 2006: Climate change and the sustainability of ski-based tourism in Eastern North America: a reassessment, *J. Leisure Res. 14,* 376–398. https://doi.org/10.2167/jost550.0

Staiger, H., Laschewski, G., and *Grätz, A.,* 2012: The Perceived Temperature – A versatile index for the assessment of the human thermal environment. Scientific Basics. Part A, *Int. J. Biometeorol. 56,* 165–176.

Stojićević, G., Basarin, B., and *Lukić, T.* 2016: Detailed bioclimate analysis of Banja Koviljača (Serbia). *Geographica Pannonica 20,* 127–135.

Stojsavljević, R., Božić, S., Kovačević, M., Bubalo Živković, M., and *Miljković, Đ.* 2016: Influence of selected climate parameters on tourist traffic of Kopaonik and Zlatibor mountains (Republic of Serbia). *Geographica Pannonica 20*, 208–219.

Thorsson, S., Honjo, T., Lindberg, F., Eliasson, I., and *Lim, E.,* 2007: Thermal comfort and outdoor activity in Japanese Urban Public Places, *Environ. Behavior 39,* 1–25.

Zaninović, K., 2001: The bioclimatic potential of Croatian Adriatic coast. In (Eds. *Matzarakis A.* and *de Freitas, C.R.*), Proceedings of the First International Workshop on Climate, Tourism and Recreation. 257–265.

Zaninović, K. and *Matzarakis, A.,* 2007: Climatic changes in thermal comfort at the Adriatic coast. In (Eds. *Amelung, B., Blazejczyk, K.* and *Matzarakis, A.*) Climate Change and Tourism: Assessment and Coping Strategies. 155–164.

Zaninović, K. and *Matzarakis, A.,* 2009: The bioclimatological leaflet as a means conveying climatological information to tourists and the tourism industry, *Int. J. Biometeorol. 53,* 369–374.

DOI:10.28974/idojaras.2018.3.7

IDŐJÁRÁS

Quarterly Journal of the Hungarian Meteorological Service
Vol. 122, No. 3, July – September, 2018, pp. 345–360

A dynamic data-driven forecast prediction methodology for photovoltaic power systems

Zoltán Kapros

Szent István University, Faculty of Mechanical Engineering,
Institute of Environmental Systems, Department of Physics and Process Control,
Páter Károly u. 1., Gödöllő, H-2103, Hungary,
E-mail: zkapros@t-online.hu

(Manuscript received in final form July 31, 2017)

Abstract—At present, the capacity of the new photovoltaic (PV) systems are growing rapidly in Hungary. The limit to growth can be estimated, but it is influenced by several things. Even a realistic goal for the next 20–30 years can be to reach the 20–25% variable renewable energy ratio in the electricity consumption. The main barrier is the variability of these systems, thus the grid integration is a huge challenge in the near future. A new dynamic data-driven forecasting methodology is worked out and tested by examining the Budapest District Heating Co. Ltd. top installed solar systems. The tested prediction method was only for 5 minutes ahead in the expected average performance in a 15-minute period. The main elements of the tested methodology and some main results will be presented in this article.

Key-words: small scale photovoltaic systems, genetic algorithm, dynamic data driven forecast, equivalent peak load hour, power prediction

1. Introduction

The aim of the Hungarian National Energy Strategy is that the annual final energy consumption school dot exceed 692 PJ by 2030 compared to the 677 PJ/year in 2012 (Parliamentary Decision 77/2011). According to the National Environmental Programme, in the field of renewable energy sources in Hungary, it is desirable to put greater emphasis on decentralized, local

applications, in particular in relation to solar energy (Parliamentary Decision 27/2015). In addition, the main national energy target is also fixed in this Decision by 2020. Therefore, the targeted share of renewable energy sources is 14.65%, and the total reached energy savings could be 10% with environmental considerations. However, our national commitment towards the European Union is 'only' 13% share (Directive 2009/28/EC). In Hungary, the share of renewable energy has already reached 9.51% in 2014 (*Szabó,* 2016). For the 13% share in the period in 2015–2020 we have already reached 37% increase from the 2014 level, but for the national target are still need 49% growing, if the country's gross energy consumption will not increase until 2020.

The individual Member States data of the renewable energy utilization can be traced from the Eurostat public databases (Eurostat Database, 2017). At the end of 2014, the renewable energy ratio was found to be 9.5% of the total energy consumption. *Fig. 1* shows the changes in the renewable energy consumption achieved in Hungary compared to the 2009 data. Overall, we can see that near 10% gross inland renewable energy consumption growth is achieved in the previous six years. Now it seems, that at least nearly 30% surplus could be needed over the next five years. The obligated amount depends on the final energy consumption (FEC) in 2020. If it would be only 15% higher than it was in 2014, we would need near 40% growing until 2020. Moreover, the national target is higher than the EU obligation. All in all, this seems a serious challenge.

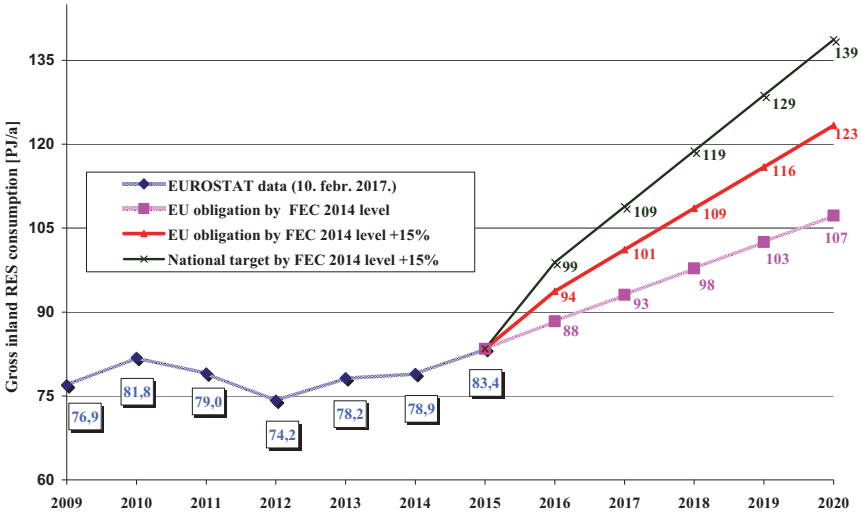

Fig. 1. Changes in renewable energy consumption in Hungary.

However, it is important to point out that the share of the renewable energy in Hungary has been significantly modified from March 14, 2017, after the domestic energy methodologies update (Eurostat Database, 2017). Thus, the official share of renewable energies has increased to 14.6% in 2014 from the earlier presented 9.51%. Therefore, it seems presently, that Hungary was able to reach the renewable target without serious progress or greater emphasis on decentralized, local applications.

Although, in 2015, the volume of electricity in the Hungarian feeding tariff system increased only by 1.1% (reaching the 25 MW PV capacity), due to the support system restructuring, significant growth is expected in 2016–2017 by the PV systems. Thus, more than 1.5 GW PV capacity is possible until 2018 due to new local applications. More weather-dependent power plants (variable energy resources) and complex development are needed. By the mitigation of the growing development and operational costs because of the larger variable energy production, one of the key elements is the predictability.

It is important to see that there are huge differences between the different types of variable energy resources. Solar energy utilization is fundamentally governed by planetary conditions. Thus, a theoretically expected solar power curve as a guideline can be specified. However, the actual differences in meteorological conditions can cause significant differences in the power outputs from the PV systems. Besides the intensity of the light, the actual spectral composition of the sunshine also determines the actual power generation capacity of the solar cells. In case of small rooftop systems these effects are not measurable cost-effectively because of the relative very small produced energy amounts, and the real time data management also would be relatively expensive by one or more small PV systems. At the same time, unexpectable changes in the spectral composition and other important effects (e.g., air temperature) give information, if we have a god theoretical reference curve. So the light also could be an information carrier.

In clear weather, with the greatest direct radiation ratio, the largest part of the intensity of the global radiation could produce electricity with photovoltaic effect, so this situation is more or less predictable. In cloudy weather, the indirect (diffuse) radiation component increases the spectral characteristics of the radiation changes, and the predictability declines. The differences in meteorological effects (the ratio between the direct and indirect components and spectral characteristics in the solar radiation or temperature conditions) from the expected values in the near past could give information for the near future. In this case, the main task of meteorological measurements can be to sign the huge changes in circumstances. Therefore, this could indicate if the information in the light from the near past is not or only partly applicable to predict the near future.

2. Assessment

The latest generation of prediction methods works with a number of meteorological, temporal, and geographic parameters, such as temperature, relative humidity, wind speed, sunshine duration (SSD), day of the year, and location (latitude, longitude, and altitude) that affect the global radiation modeling values. A recent prediction method is generally based on artificial neural networks, where the expected net global radiation could be predicted by the values of these parameters (*Hussain* and *Al-Alili*, 2015). So the predictions are generally based on the experienced data and local knowledge. The so-called typical meteorological year is built of many time series parameters. The resulting values give a good approach in terms of long-term durability, but in terms of a given year, there may be significant inaccuracies. A further disadvantage is that the global and local environmental changes are not built into the calculations. Thus, analysis of trends and outline additional parameters are also required. These are very expensive methods.

As a new direction, the typical meteorological year is determined only from easily and cheaply available data, but this simplified data set can only be treated as a first approximation, and the forecast can be based on the variation of this data set and some dynamically measured parameters (actual whether parameters). In the University of Leeds, the global radiation quantity with one minute dividing was predicted in this way (*Bright at al*, 2015). Developing the conditions for determining the accurate prediction of solar power systems considered to be a key factor contributing to the integration to the electricity network (*Lorenz* and *Heinemann*, 2012). By the optimal grid control and balancing activities, the relative error of short-term forecasting of energy production should be below 10% (*Wu* and *Xia*, 2015). A reliable network operation requires different forecast horizons (*Kostylev* and *Pavloski*, 2011). These aims can be categorized as follows:

1. planning, optimization, network assessment, cost-benefit analysis, evaluation of alternatives, verification by supports;
2. 15 minutes schedule giving an electricity trader;
3. clarification of the planned schedule before the beginning of the relevant period;
4. clarification of the planned schedule within the relevant 15-minute-long period;
5. prediction for a very short (balancing) forecast, for example only 1 minute ahead.

The demand for forecasts for shorter periods first appeared by the larger photovoltaic power generation systems. For larger PV plants, the cloud migration and its impact on the intensity changes can be followed. The average

intensity in an area can be estimated with moving averages of the radiation profiles (spatial smoothing effect) (*Longhetto et al*., 1989). The solar energy prediction by the high PV power plants can be managed by a wavelet variability model which uses 25 radiometer sensors around the plant (*Dyreson at al.,* 2014). Solutions like the wavelet variability model, which are acceptable for multi-megawatt power plants (*Lave et al*., 2013) even often do not provide cost effective solution for small scale sizes. This paper examines the possibilities suggested by the last two points and illustrates some of the results (*Kapros*, 2017).

3. Methods

3.1. Individual prediction of PV systems

Modeling the PV predictions could be based on stochastic assessments. However, the variability of PV generation does not follow any well described distribution. The stochastic models, which use standard or other type distributions, can be used for several hours, several days, or even longer period. Furthermore, it is not enough to know of the average external temperature conditions, because the PV system efficiency is determined also by other external parameters (e.g., spectral light irradiation, temporary cloud effects, etc.), and by the individual characteristics of the PV systems. For these reasons, the genetic algorithm method was applied in this study.

A genetic algorithm approach is based on the observed mathematical regularities of genetic populations. Accordingly, the knowledge on the observed capabilities (as genetically determined values) in the starting position can determine the possibilities of the future capabilities in the probability space. Therefore, performance, which has the highest probability within a given set of possibilities, can be precisely defined.

The genetic method was performed with an encoding process in the sampling period and a decoding process in the predicted period based on deviations between the typically expected and the measured real performance values. Thus, the fundamental part of this methodology was the developing of the expected typical performances for every minute in the examined period with physically based forecasts achievable free of charge. For getting the expected typical data some well-known equations for calculating the amount o electricity with relatively few required information and some free public databases were used. Therefore, for every minute of a year, the expected performance values were determined in a reproducible manner. The amount of electricity, generated by a photovoltaic system, is expressed by the following equation based on the effective global radiation (*Earthscan*, 2008):

$$q_{el} = H_{\alpha,\beta} \times \eta_M \times A_{PV}\,, \tag{1}$$

where q_{el} is the photovoltaic power generation capacity [W], $H_{\alpha\beta}$ is the effective radiation with α tilt angle and β orientation of the PV modules[W/m^2], η_M is the PV module efficiency [%], and A_{pv} is the useful photovoltaic solar surface [m^2].

The aim of this study was to find results which are independent from the PV generators. For this reason, the equivalent peak load hours were calculated. Therefore, the codes which are used in the genetic algorithms were developed from the expected equivalent peak load hours based on physical modeling by typical conditions. The equivalent peak load hours *(Sharma* and *Tiwari,* 2012) are characterized by the energy-generating capacity in a given moment. It means that, if the same amount of power will produce in one year, the equivalent peak load hours are equal to the traditional peak load hours:

$$h_{ekv} = \frac{\zeta_{real}}{P_P}. \tag{2}$$

The dimension of the equivalent peak load hour (h_{ekv}) could be kWh/kW or hour. This is the ratio of a typical solar electricity generating capacity of a given t period *(*ξ_{real} [kWh]) and the nominal capacity of the PV system (P_p [kW$_p$]. If the performance is expressed as an equivalent peak load hour, the expected value can be written as follows:

$$h_{ekv,t}(t) = \frac{(G_{PV}(t) \times \eta(t) \times A_{PV})}{P_P}, \tag{3}$$

where G_{pv} [W/m^2] is the sum of the effective global radiation (effective direct normal to the plain) and diffuse solar radiation by south orientation. The equivalent peak load hours show a reachable capacity at a given moment. If the system is functioning at a given time at specific equivalent peak load hours, then in an imagined year with equal continuous output power, the same value would result for the peak load hours for that year. This value represents an actual capacity of the PV power plant, which is clear, meaningful, and comparable. Therefore, in every minute, we can get the expected equivalent peak load hours according to the following equation:

$$h_{ekv,AC}(t) = \frac{P_{AC}(t)}{(P_p \times 1000)} \times 8760. \tag{4}$$

Therefore, it is enough to make a physically based model for the PV generator' expected alternating current performance at a given time (P_{AC} [W]), and this is easy to express this value in equivalent peak load hours. The invented

new method is a data-driven determination system, where expected values are physically modeled as in the forecasted time (t_0), ehen they are dynamically and continuously changing depending on the sets of measured data in the monitoring period before t_0 with Δt_1, Δt_2, ..., Δt_n durations. This continuous changing is guided by the encoded metered data contents of the sampling period, which express also the currently unique and determinative effects for the electricity production. Therefore, the coding system is capable to capture the slightly or seriously unexpected behavior (the differences) in the sampling period as genetically deterministic properties. In this coding system, there are stock defined unique properties, and this gives the approximately parental genetic material. Thus, the code most likely and valid in the following short time can be determined.

All in all, the probability of any next value can be calculated within the range which is designated by the recorded code set in the sampling period. This makes it possible to join different probabilities for different amounts of the future performances. However, the chances still remain for the decisive changes in extreme weather conditions. These effects are considered as genetic mutation effects. The mutation gives a performance, which has zero probability based on the genetic material of the sampling period. The above is determined by the differences between the observed (measured) and expected equivalent peak load hours according to the next equation:

$$H_i(t) = \frac{(h_i^*(t) - h_i(t))}{h_i^*(t)}, \tag{5}$$

where the expected equivalent peak load hours (h^*_i) are determined by the physical-based modeling and analysis. The real equivalent peak load hours (h_i) can be calculated from the measured performance values. The difference between these two values is the physically based prediction error, from which the specific error (H_i) was expressed. The past series of this specific error may also be defined in accordance with the Eq. (6) in the sampling period (before t time moment, between n and m time moments). From these, the average dH/dt change can be determined. In the following equation, the time is in seconds units according to the SI system:

$$\frac{dH_i}{dt} \approx \frac{\Delta H_i}{\Delta t} = 60\frac{(H_i - H_{i-1}) + (H_{i-1} - H_{i-2}) + ... + (H_{m+1} + H_m)}{\Delta t_{n-m}}. \tag{6}$$

In Eq. (6), the length of the periods between H_i *and* H_m are the same according to the following equation:

$$t_i - t_{i-1} = t_{i-1} - t_{i-2} = ... = t_{m+1} - t_m. \tag{7}$$

Thus, the error factor prediction is described as follows:

$$H_t = H_{t-1}(1+\frac{dH}{dt}) \approx H_i(1+\frac{dH_i}{dt})^{\frac{\Delta t_{t-n}}{60}} \approx H_i(1+\frac{\Delta H_i}{\Delta t})^{0,4\frac{\Delta t_{t-n}}{60}}. \quad (8)$$

The 0.4 multiplier exponent was the most favorable during the test of Eq. (8). The reason is that the *H* specific errors during the sampling period are not fully independent from each other. Behind the variations of these specific error values, more stochastic processes can be assumed in the sampling period. Changing of the specific errors between the predicted and measured values in the period between *m* and *n* is made only partly by those natural effects, which occurs similarly after the *t-n* period in *t* time. Thus, the predicted equivalent peak load hours (κ_t) for *t* time at *n* time can be calculated by the following equation:

$$\kappa_t = h_t^* + H_t \times h_t^* = h_t^* \times (1 + H_t). \quad (9)$$

In the research, the duration of the predicted period was 1 minute, the *n* exponent was 5 minutes, and the *m* exponent was 15 minutes. Therefore, during the measurement and analysis, the series of κ_t was available 5 minutes before time t. This gave the opportunity to give a different forecast for the average performance in every 15 minutes with 5 minutes before the end of the period. During the test, the prediction for average performance (equivalent peak load hours) in 15-minute periods based on 5 minutes measured data and 10 minutes predicted data from this presented method. Thus, the predicted 15-minute average data of the average equivalent peak load hours in the given Δt period (κ_q [h]) is illustrated with the following equations:

$$h_{q1} = h_{(t-14)} + h_{(t-13)} + h_{(t-12)} + h_{(t-11)} + h_{(t-10)}. \quad (10)$$

$$h_{q2} = \kappa_{(t-9)} + \kappa_{(t-8)} + \kappa_{(t-7)} + \kappa_{(t-6)} + \kappa_{(t-5)} + \kappa_{(t-4)} + \kappa_{(t-3)} + \kappa_{(t-2)} + \kappa_{(t-1)} + \kappa_t. \quad (11)$$

$$\kappa_q(t) = \frac{h_{q1}(t) + h_{q2}(t)}{15}. \quad (12)$$

The significance of the error factor is stronger in these times when the radiation is more intensive, so the period between 10:00 and 16:00 in local time were also separately analyzed.

3.2. Virtual PV systems group prediction

The second part of this research examined the prediction possibilities for the virtual groups based on the former methodology. The prediction is based on

only one real-time monitored photovoltaic (VP) power plant, but the predicted performances were made related to the whole virtual PV power system. This methodology could be useful for some very small (micro) domestic PV systems which are built in a small region. In view of the methodology, the forecasting error between the analytical prediction and the real energy production in a 15 minutes period by a monitored plan could correlate to this error by the other power plant. This correlation is determined by the following equation:

$$\kappa_{q1}(t) \approx \frac{h^*_{q1}(t)}{1 - \dfrac{\kappa_{qt}(t) - h^*_{qt}(t)}{\kappa_{qt}(t)}}. \tag{13}$$

In the case of virtual a generator built by *w+1* number of PV systems, the forecasts can be calculated with the weighted (as rated power) predictions by systems. So the virtual-group level forecast could be given by the following equation:

$$\mathrm{K}_{qt}(t) = \frac{I_{P0}\kappa_{qt}(t) + I_{P1}\kappa_{q1}(t) + I_{P2}\kappa_{q2}(t) + \ldots + I_{Pw}\kappa_{qw}(t)}{I_{P0} + I_{P1} + I_{P2} + \ldots + I_{Pw}}, \tag{14}$$

where the I_{P0} is the rated power of that reference PV power system, which is alone monitored directly and in real time by the whole virtual group.

3.3. Measurement

The test system was the solar power system of the FŐTÁV Ltd., which is built on the top of its central office building by 150 pieces of PV panels with 250 W_P nominal rated capacities per units and eight inverters, which connect it to the public grid. The maximum output capacity of one inverter is 5 kW, and in six cases there are a ten solar panels formed string and a nine solar panels formed string parallel connected, and in two cases there are two parallel connected nine panel formed sting behind an inverter. Based on the measurement data of these eight inverters we could evaluate eight independent systems. The types of PV modules are AS-250 W 60P ECO polycrystalline silicon solar cells. The orientations of PV modules are +10.7 degrees (SSW), and their tilt angles are 20 degrees. The nominal connection capacity of the whole PV plants to the grid is 40 kW. The research examined a reference power plant owned by the Budapest District Heating Co. Ltd. The PV plant is located in the company's headquarter in Budapest on the top of the 'D' building. The research analyzed data from seven different days which was randomly selected (*Table 1*).

Table 1. The test days and characteristics

No.	Dates	The serial number of the day	Sunrise in local time	Sunset in local time	Azimuth at sunrise	Azimuth at sunset	Potential sunshine duration [h]
1.	Apr 1, 2014	91	6:23:09	19:13:13	-97.58°	97.89 °	12.84
2.	Apr 20, 2014	110	5:46:32	19:39:56	-108.07 °	108.37 °	13.89
3.	May 1, 2014	121	5:27:32	19:55:15	-113.55 °	113.89 °	14.16
4.	May 20, 201.	140	5:01:25	20:20:01	-121.36 °	121.58°	15.31
5.	Jun 1, 2014	152	4:50:58	20:32:51	-124.80°	124.96°	15.69
6.	Jun14, 2014	165	4:46:12	20:42:09	-126.86°	126.91°	15.93
7.	Jul 20, 2014	201	5:07:10	20:32:34	-122.58°	122.38°	15.42

The reference power plant was considered only one part of the whole system (one inverter part Eq. (8)). With the same orientation and the same angle, 19 panel units have a single inverter. The main data of the plant are:

- Latitude: 47.4584°N, Longitude: 19.045°E;
- PV module type: AS-60P 250 W ECO;
- Rated power of a panel: 250 W_P;
- The number of solar panels installed: 150;
- Position: +10.7 degrees (SSW) (determined by measuring from map);
- Angle of inclination: 20 degrees;
- The PV power plant nominal connection capacity: 40 kW.

The group forecast is based on the measurement and forecast data of a single system. Two PV generator groups with different characters were made virtually. The homogeneous group was the photovoltaic system of the FŐTÁV in the Kalotaszeg street as a whole (eight independent and measured inverter units). The heterogeneous group was built partly from the homogeneous virtual group. It contained the number 1, the number 3 (both 4750 W_P), and the number 7 (4500 W_P) inverters, but partly it was consisted of two other small scale PV systems with different locations and products (both 2160 W_P). *Table 2* shows the main data.

Table 2. The homogeneous and the heterogeneous groups

Homo-geneous group	Place	Rated power	Hetero-geneous group	Place	Rated power
Inv. 1.	Kalotaszeg str.	4750 W_P	Inv. 1.	Kalotaszeg str.	4750 W_P
Inv. 2.	Kalotaszeg str.	4750 W_P	Inv. 3.	Kalotaszeg str.	4750 W_P
Inv. 3.	Kalotaszeg str.	4750 W_P	Inv. 7.	Kalotaszeg str.	4500 W_P
Inv. 4.	Kalotaszeg str.	4750 W_P	HADR	Hadriánusz str.	2160 W_P
Inv. 5.	Kalotaszeg str.	4750 W_P	LEIB	Leibstück str.	2160 W_P
Inv. 6.	Kalotaszeg str.	4750 W_P			
Inv. 7.	Kalotaszeg str.	4500 W_P			
Inv. 8	Kalotaszeg str.	4500 W_P			
Total rated power		**37 500 W_P**	**Total rated power**		**18 320 W_P**

4. Measured data and statistical analysis

The results of the forecast by a clear sky are demonstrated in *Fig. 2*. The numerical error of the forecast is also important. The uncertainty effects are characterized, which are caused by the PV system in the network's stability (*Fig. 2.*). The dynamic forecast error in most cases is below 500 hours, and only one case was more than 2000 hours with a short oscillation. It seems that if the effect which caused the error and its length would be known, the forecast could be more accurate by attenuating the errors caused by oscillatio.

April 1, 2014 was the second least volatile day from the seven tested days, which was slightly cloudy, basically sunny, and there were stable light conditions. Predictability is difficult for these types of weather, because the bell curve is not clearly outlined, and significant differences may occur compared to the expected values. However, the changes in the lighting conditions are less dynamic, which is favorable in view of the developed genetic algorithm methodology. So the relative errors of the prediction between 10 and 16 hours were only typically below 5%. Furthermore, we noticed that some major faults, which caused by short-acting dynamic changes, can incorporate into the forecast. and later can cause an opposite distortion. In *Fig. 2* the measured values and the experienced prediction errors of the equivalent peak load hours also are shown. The forecast distortion and oscillations are well-observed. For the oscillation damping. it may be sufficient to use some real-time measurement, of the typical conditions (light intensity, wind speed, spectral conditions), because the real-time tracking could be useful to filter the mutations effects out of their following there lifetime.

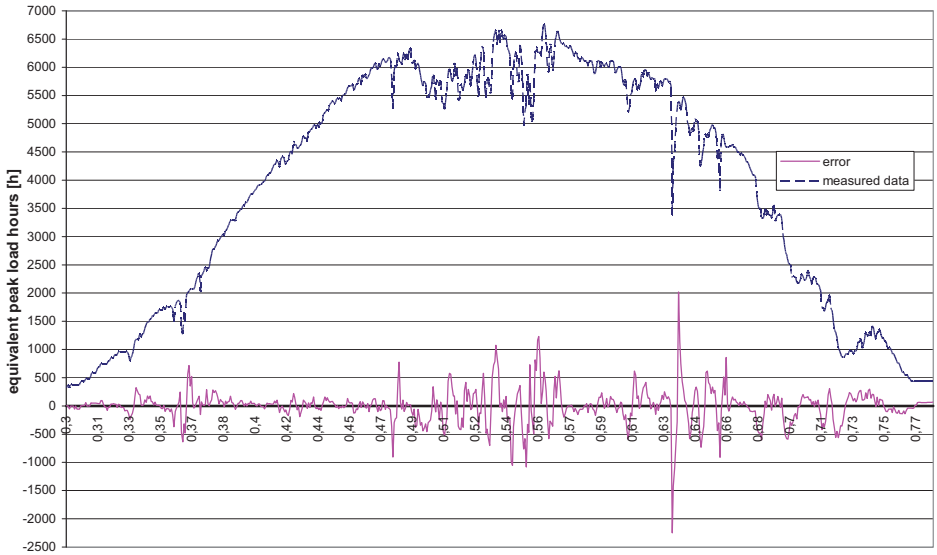

Fig. 2. AC error of the forecast, calculated by Eq. (9) on April 1, 2014.

Figs. 3 and *4* show the relative error according to the prediction calculated by Eq. (12), where the forecast is for a 15 minutes average equivalent peak load hour and it was made also 5 minutes earlier, than the end of the period. In a highly volatile day, the method was also tested. Even in this case, the forecast accuracy was an average of around 9% (*Fig. 5*.)

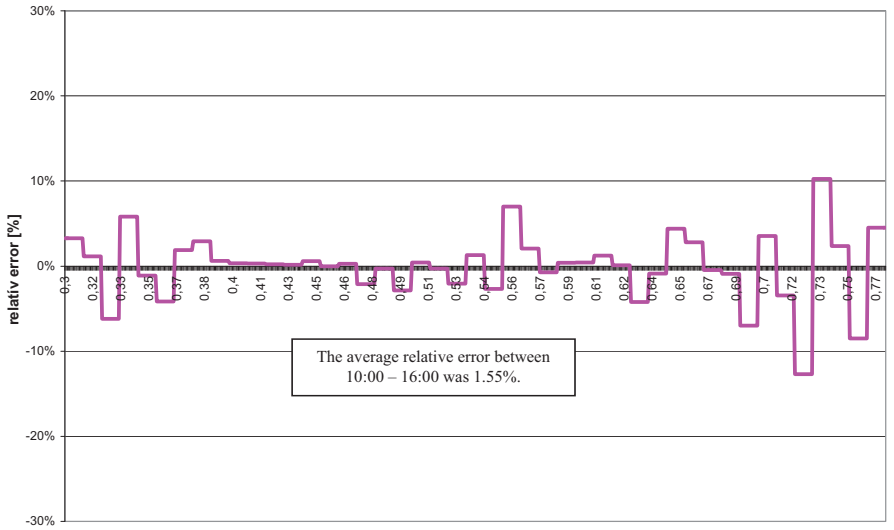

Fig. 3. AC relative error of the forecast, calculated by Eq. (12) on April 1, 2014.

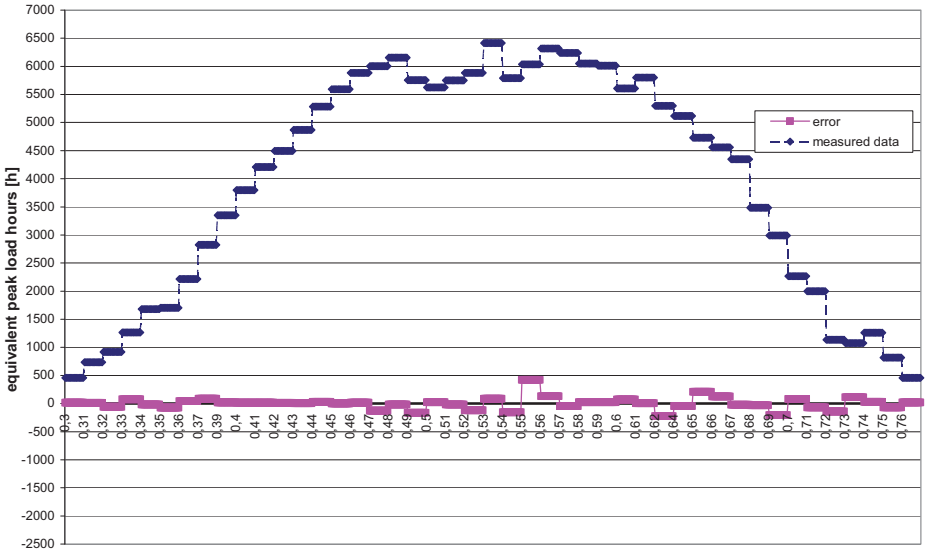

Fig. 4. AC error of the forecast, calculated by Eq. (12) on April 1, 2014.

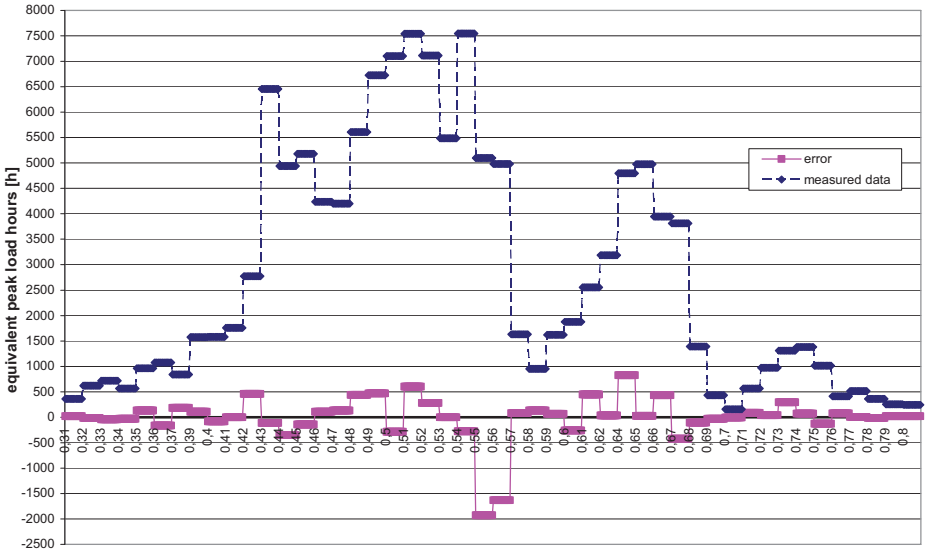

Fig. 5. AC error of the forecast, calculated by Eq. (12) on June 1, 2014.

Considering the researched seven days, the average relative error was below 6%. In three days of seven, all errors by each period between 10 and

16 hours were below 10%. On average of these seven days, the prediction errors remain below 5% with 65% probability.

Based on the differences between the predicted values and the measurement data, the absolute and relative errors for each minutes were determined with the following equations. The results of the prediction are shown in *Tables 3* and *4*. The results of the forecast for virtual group in the tested day are shown in *Table 5*.

$$\Delta h_t = \left| h_{ekv,t} - h_t^{**} \right|. \tag{15}$$

$$h_h = 100 \times \frac{\Delta h_t}{h_{ekv,t}}. \tag{16}$$

Table 3. 1-minute forecast performance data between 10:00 and 16:00 hours

	Errors (equivalent peak load hour)				Relative errors				
Date	**Average error**	**Above 200 hour**	**Between 100 and 200 hour**	**Under 100 hour**	**Average error**	**Above 15%**	**Between 10% and 15%**	**Between 5% and 10%**	**Under 5%**
Apr 1.	**235**	37.95%	20.22%	41.83%	**4.34%**	4.43%	5.26%	19.11%	71.19%
Apr 20.	**885**	55.68%	13.85%	30.47%	**20.68%**	30.47%	13.02%	16.07%	40.44%
May 1.	**693**	55.40%	24.38%	20.22%	**17.18%**	26.59%	12.47%	22.71%	38.23%
May 20.	**798**	29.64%	17.73%	52.63%	**34.56%**	15.51%	0.55%	4.16%	79.78%
Jun 1.	**1 203**	80.33%	9.97%	9.70%	**28.74%**	54.85%	12.19%	13.57%	19.39%
Jun 16.	**1 880**	72.58%	13.02%	14.40%	**55.75%**	47.92%	5.54%	12.47%	34.07%
Jul 20.	**175**	12.19%	16.90%	70.91%	**3.87%**	3.60%	1.39%	4.99%	90.03%

Table 4. 15-minute forecast performance data between 10:00 and 16:00 hours (5 minutes before the end of the period)

	Absolute errors (equivalent peak load hour)				Relative errors				
Date	**Average error**	**Above 200 hour**	**Between 100 and 200 hour**	**Under 100 hour**	**Average error**	**Above 15%**	**Between 10% and 15%**	**Between 5% and 10%**	**Under 5%**
Apr 1	**87**	12.50%	25.00%	62.50%	**1.55%**	0.00%	0.00%	4.17%	95.83%
Apr 20	**302**	37.50%	16.67%	45.83%	**6.63%**	12.50%	0.00%	29.17%	58.33%
May 1	**256**	37.50%	29.17%	33.33%	**5.92%**	12.50%	8.33%	25.00%	54.17%
May 20	**260**	29.17%	8.33%	62.50%	**4.36%**	8.33%	8.33%	4.17%	79.17%
Jun 1	**397**	58.33%	20.83%	20.83%	**9.29%**	20.83%	12.50%	20.83%	45.83%
Jun 16	**694**	75.00%	8.33%	16.67%	**13.09%**	37.50%	12.50%	16.67%	33.33%
Jul 20	**56**	8.33%	4.17%	87.50%	**0.93%**	0.00%	0.00%	8.33%	91.67%

Table 5. 15-minute forecast performance data for a virtual power plan (5 minutes before the end of the period)

Date 2014	Evaluated periods	Absolute errors (equivalent peak load hour)		Relative errors	
		Homo-geneous	Hetero-geneous	Homo-geneous	Hetero-geneous
Apr 1	7:08-18:36	79	89	3.01%	3.42%
	10:00-16:00	90	102	1.60%	1.77%
May 20	6:25-19:09	473	331	9.78%	9.51%
	10:00-16:00	665	466	9.65%	7.67%
Jun 1	7:34-19:14	273	429	11.28%	19.55%
	10:00-16:00	402	567	8.94%	14.81%
Jul 20	6:32-19:14	61	161	1.86%	4.78%
	10:00-16:00	80	214	1.31%	3.47%
Average	**whole daytime**	**222**	**253**	**6.48%**	**9.32%**
	10:00-16:00	**309**	**337**	**5.38**	**6.93**

5. Conclusions

The overall conclusion is that the developed dynamic prediction method appears to be an applicable method in case of the small-scale solar systems. It is verified that the prediction for each 15-minute period within five minutes before the end has a good accuracy even under strongly variable weather. Although the measurements were made by a relatively small system, the results get special actuality by the expected huge increases of the almost 500 kW_P domestic photovoltaic systems. Thus, the applicability of this dynamic forecasting method for the individual larger system would be useful to test.

The presented group-level prediction method for the micro PV systems could be an essential tool for the so-called aggregator services, because they would be able to use this information with their demand side management activities for the timetable of the virtual smart grid.

The presented method is a good example for the less costly dynamic forecasting solution demonstrating, that the active measures with reasonable accuracy in most cases would be ensured.

References

Bright, J., Crook, R., and *Taylor, P.G.*, 2015: Methodology to stochastically generate synthetic 1-minute irradiance time-series derived from mean hourly weather observational data. Proceedings of the ISES Solar World Congress 2015, Daegu, Korea, 08-12. November, 2015, 142–151.

Dyreson, A.R., Morgan, E.R., Monger, S.H., and *Acker T.L.*, 2014: Modeling solar irradiance smoothing for large PV power plants using a 45-sensor network and Wavelet Variability Model. *Solar Energy 110*, 482–495.

Directive 2009/28/EC of the European Parliament and of the Council of 23 April 2009 on the promotion of the use of energy from renewable sources and amending and subsequently. Annex I. National overall targets for the share of energy from renewable sources in gross final consumption of energy in 2020 repealing Directives 2001/77/EC and 2003/30/EC,

Earthscan, 2008: Planning and installing photovoltaic systems. A guide for installers, architects and engineers. Earthscan Publications Ltd.

Eurostat Database, Complete energy balances - annual data (nrg_110a). Downloading is on 10. February 2017. http://appsso.eurostat.ec.europa.eu/nui/show.do?dataset=nrg_110a&lang=en

Eurostat Database, Share of energy from renewable sources (nrg_ind_335a). Downloading is on 2. May 2017. http://appsso.eurostat.ec.europa.eu/nui/show.do?dataset=nrg_ind_335a&lang=en

Eurostat Database, Supply, transformation and consumption of renewable energies - annual data. Downloading is on 10. February 2017. http://appsso.eurostat.ec.europa.eu/nui/show.do?dataset=nrg_107a&lang=en

Hussain, S. and *Al-Alili, A*., 2015: Selection of relevant input parameters for solar radiation, ISES Solar World Congress, 8-12. November 2015, Daegu, Korea, 2 p. Downloading is on 10. December 2015. http://swc2015.org/index.php?g_page=program&m_page=program11

Kapros, Z., 2017: Autonomous and grid collaborative photovoltaic system optimization. PhD thesis, Szent István University, Gödöllő.

Kostylev, V. and *Pavlovski, A.,* 2011: Solar power forecasting performance towards industry standards. Proceedings of the 1st International Workshop on the Integration of Solar Power into Power Systems, 24. October 2011, Aarhus, Denmark, 8 p. Downloading is on 28. December 2015.https://ams.confex.com/ams/92Annual/webprogram/Manuscript/Paper203131/AMS_VK_%20AP_Paper%202011%20submitted.pdf

Lave, M., Kleissl, J. and *Stein, J.S.* 2013: A wavelet-based variability model (WVM) for solar PV power Plants, IEEE Trans. Sustain Energy 4, 501–509.

Longhetto, A., Elisei, G. and *Giraud, C.*, 1989: Effect of correlations in time and spatial extent on performance of very large solar conversion systems, *Solar Energy 43,* 77–84.

Lorenz, E., and *Heinemann, D.,* 2012: Prediction of solar irradiance and photovoltaic power. Compr. Renew. Energy. 239–292.

Parliamentary Decision 77/2011 (X. 14.) about the implementation of the National Energy Strategy

Parliamentary Decision 27/2015 (VI. 17.) about the National Environmental Programme for 2015-2020

Sharma, R. and *Tiwari, G.N.,* 2012: Technical performance evaluation of stand-alone photovoltaic array for outdoor field conditions of New Delhi. *Applied Energy 92,* 644–652.

Szabó, Zs., 2016: A megújuló energia termelés Magyarországon, A megújuló villamosenergia-támogatási rendszer (METÁR) jövőbeni keretei Magyarországon. REKK Energiapolitikai Fórum, 2016. június 9. Budapest. (In Hungarian). Downloading is on 15. December 2016. http://rekk.hu/downloads/events/Sz.Zs._REKK_20160609_final.pdf

Wu, Z. and *Xia, X.,* 2015: Optimal switching renewable energy system for demand side management. *Solar Energy 114*, 278–288.

INSTRUCTIONS TO AUTHORS OF *IDŐJÁRÁS*

The purpose of the journal is to publish papers in any field of meteorology and atmosphere related scientific areas. These may be

- research papers on new results of scientific investigations,
- critical review articles summarizing the current state of art of a certain topic,
- short contributions dealing with a particular question.

Some issues contain "News" and "Book review", therefore, such contributions are also welcome. The papers must be in American English and should be checked by a native speaker if necessary.

Authors are requested to send their manuscripts to

Editor-in Chief of IDŐJÁRÁS
P.O. Box 38, H-1525 Budapest, Hungary
E-mail: journal.idojaras@met.hu

including all illustrations. MS Word format is preferred in electronic submission. Papers will then be reviewed normally by two independent referees, who remain unidentified for the author(s). The Editor-in-Chief will inform the author(s) whether or not the paper is acceptable for publication, and what modifications, if any, are necessary.

Please, follow the order given below when typing manuscripts.

Title page should consist of the title, the name(s) of the author(s), their affiliation(s) including full postal and e-mail address(es). In case of more than one author, the corresponding author must be identified.

Abstract: should contain the purpose, the applied data and methods as well as the basic conclusion(s) of the paper.

Key-words: must be included (from 5 to 10) to help to classify the topic.

Text: has to be typed in single spacing on an A4 size paper using 14 pt Times New Roman font if possible. Use of S.I. units are expected, and the use of negative exponent is preferred to fractional sign. Mathematical formulae are expected to be as simple as possible and numbered in parentheses at the right margin.

All publications cited in the text should be presented in the *list of references*, arranged in alphabetical order. For an article: name(s) of author(s) in Italics, year, title of article, name of journal, volume, number (the latter two in Italics) and pages. E.g., *Nathan, K.K.*, 1986: A note on the relationship between photosynthetically active radiation and cloud amount. *Időjárás 90*, 10–13. For a book: name(s) of author(s), year, title of the book (all in Italics except the year), publisher and place of publication. E.g., *Junge, C.E.*, 1963: *Air Chemistry and Radioactivity*. Academic Press, New York and London. Reference in the text should contain the name(s) of the author(s) in Italics and year of publication. E.g., in the case of one author: *Miller* (1989); in the case of two authors: *Gamov* and *Cleveland* (1973); and if there are more than two authors: *Smith et al.* (1990). If the name of the author cannot be fitted into the text: *(Miller*, 1989); etc. When referring papers published in the same year by the same author, letters a, b, c, etc. should follow the year of publication. DOI numbers of references should be provided if applicable.

Tables should be marked by Arabic numbers and printed in separate sheets with their numbers and legends given below them. Avoid too lengthy or complicated tables, or tables duplicating results given in other form in the manuscript (e.g., graphs). *Figures* should also be marked with Arabic numbers and printed in black and white or color (under special arrangement) in separate sheets with their numbers and captions given below them. JPG, TIF, GIF, BMP or PNG formats should be used for electronic artwork submission.

More information for authors is available: journal.idojaras@met.hu

Published by the Hungarian Meteorological Service

Budapest, Hungary

INDEX 26 361

HU ISSN 0324-6329